INVESTIGATION OF ERRORS OBTAINED WITH REFLECTION-PLANE MOUNTED MODELS DUE TO END PLATE TARES

Thesis by

Herman Miller

In Partial Fulfillment of the Requirements

For the Degree of

Aeronautical Engineer

California Institute of Technology

Pasadena, California

1948

ACKNOWLEDGEMENT

The author wishes to express his appreciation for the assistance given him by Dr. Clark B. Millikan under whose direction this research investigation was carried out. He also extends thanks to Elmer Ward for his work in designing the mechanical components used to carry out the investigations, to Josiah E. Smith, Richard W. Bell, and Louis V. Schmidt for their assistance on technical problems, and to Nell Kindig for her work on the figures.

ABSTRACT

Because of the great interest in and emphasis on high-speed wind-tunnel tests, it has become increasingly important to provide a support system which affects the tunnel flow and the flow over the model as little as possible. One type of support which is being used a great deal at the present time is the so-called reflection-plane mount. This mount derives its name from the fact that the model consists of only half of the prototype wing or airplane, mounted on its plane of symmetry. Ordinarily the model is mounted next to one of the tunnel walls, but many variations of mounting have been used. A circular end plate may or may not be mounted as a metrical portion of the installation.

The purpose of the tests, described in this report, was to determine the interference effects of the tunnel wall or end plate on the model, the interference effects of the model on the end plate, and the true forces acting on the model and end plate. It was also desired to determine the forces acting on the portion of the model in the boundary layer and to determine the effects of gaps between the wing and end plate and between the end plate and tunnel wall.

TABLE OF CONTENTS

TABLE OF CONTENTS (Cont'd)

INDEX OF FIGURES

INDEX OF FIGURES (Cont'd)

INDEX OF FIGURES (Cont'd)

INDEX OF FIGURES (Cont'd)

INDEX OF FIGURES (Cont'd)

INDEX OF FIGURES (Cont'd)

TEST NOTATION

α	Angle of attack of wing chord line relative to tunnel axis (α is positive when the wing leading edge is raised, trailing edge lowered; direction defined as the pilot sees it.)
C_L	Lift coefficient determined from balance data with no corrections applied = $\frac{\text{lift}}{qS}$ (C_L is positive when it tends to lift the wing)
C_n	Normal force coefficient determined from integrated pressure data (cf. Sec. IV-C)
C_{D_u}	Drag coefficient determined from balance data with no corrections applied = $\frac{\text{drag}}{qS}$
C_{D_o}	Profile drag coefficient (C_{D_o} is determined from wake survey data, (cf. Sec. IV-B)
$C_{m_{c/4}}$	Pitching moment coefficient about the 0.25 chord determined from balance data, no corrections have been applied with the exception of those which were made to transfer the moments about the trunnion axis (0.50 chord) to the 0.25 chord, $C_m = \frac{\text{pitching moment}}{qSc}$ (C_m is positive when it tends to raise the nose)
C_{m_o}	Pitching moment coefficient about the 0.25 chord determined from integrated pressure data (cf. Sec. IV-C)
$\delta(\ )$	Increment of ( ) due to change in configuration, used for denoting increment of C_L, C_D or C_m
R	Reynolds number = $\frac{\rho c V}{\mu}$
$\frac{P}{q}$	$\frac{\text{Static pressure measured-tunnel free stream static pressure}}{q}$
$\frac{H}{q}$	$\frac{\text{Total pressure measured-tunnel free stream static pressure}}{q}$

For the foregoing coefficients:

S	Projected wing panel area
c	Length of airfoil chord
b	Span of wing panel
q	Dynamic pressure averaged over model span = $\frac{\rho V^2}{2}$

TEST NOTATION (Cont'd)

V	Average windstream velocity
ρ	Mass density of air (Note: A correction is applied in the tunnel airspeed calibration so that in the above formulae ρ is to be taken as the free air density unaffected by compressibility.)
μ	Absolute viscosity of air = $3.93 \times 10^{-7} \left(\frac{T}{308}\right)^{0.78}$ $\frac{\text{lbwt sec}}{\text{ft}^2}$
T	Temperature in degrees Kelvin of the equivalent free air stream
s	Distance from end plate surface in inches
$\frac{x}{c}$	Ratio of distance from leading edge of wing (x) to wing chord (c); positive when downstream

MODEL NOTATION

$( )_B$ ~ Mounted on balance system

$( )_G$ ~ Supported from ground

W Two dimensional wing section; superscript F indicates wing is fixed at $\alpha = 0^\circ$

P^1 Right-hand end plate aligned flush with tunnel wall; superscript R indicates end plate rotated 180° from normal orientation

P^2 Left-hand end plate aligned flush with tunnel wall; superscript R indicates end plate rotated 180° from normal orientation

G Gap around end plates; subscript s indicates gap sealed

G^0 indicates both end plates 0.10 inch out of tunnel

G^I " " " " 0.05 " in to "

G^{I-1} " " " " 0.04 " " " "

G^{I-2} " right-hand end plate in 0.05 inch at top, 0 inches at bottom; left-hand end plate flush

G^{I-3} indicates right-hand end plate in 0.05 inch at front, 0 inches at rear; left-hand end plate flush

G^{I-4} indicates right-hand end plate in 0.05 inch at rear, 0 inches at front; left-hand end plate flush

W_1 Airfoil section template with 0.44 inch span mounted on right-hand end plate

W_2 Airfoil section template with 0.69 inch span mounted on right-hand end plate

T_r Roughness strips on tunnel wall 2.25 inches ahead of end plates; these strips are made of a 1/8 inch diameter rod soldered to a flat metal strip 1/16 inch thick, 1 inch wide and 42 inches long; Scotch Cellophane tape was used to fasten these strips to the wall

R_2 Total head drag rake mounted 12 inches from right-hand end plate

R_2' Total head drag rake mounted 14 inches from right-hand end plate

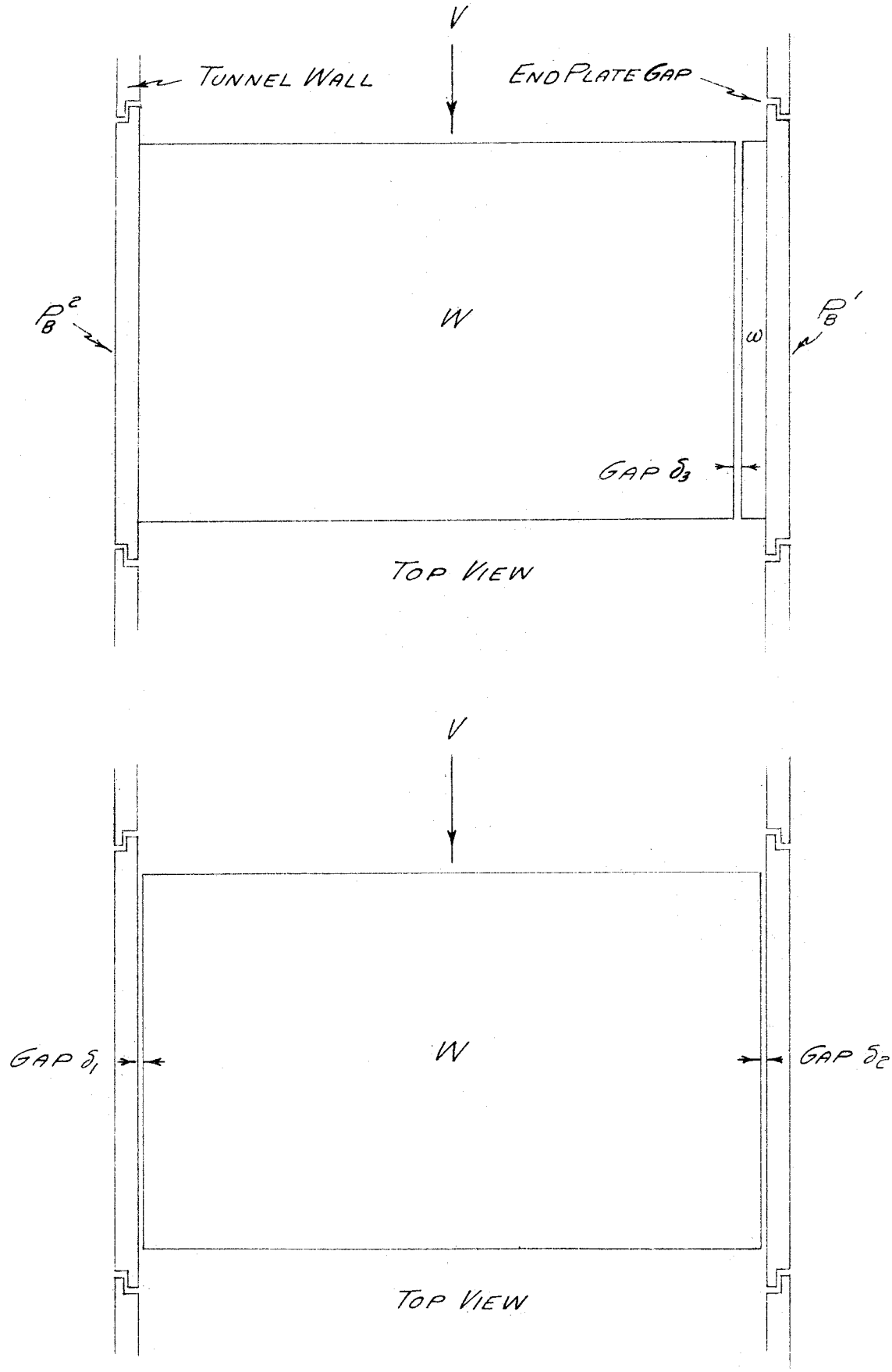

Fig. 1. Sketch showing model configuration components

MODEL DATA

Wing Panel

Chord = 2 ft

Span = 3 ft

Area = 6 ft^2

Airfoil Section = NACA 0012-64 modified by the inclusion of straight line elements to the trailing edge. The modifications also reduced the thickness ratio of the test section to 10.71 percent of the actual chord length

I. INTRODUCTION

This report contains the results obtained during investigations carried out at the GALCIT* ten-foot wind tunnel during the month of March 1948. These investigations were made to determine the aerodynamic characteristics of a wing-end plate installation, the magnitude of the wing-end plate interference forces, and the possibilities of alternate methods of mounting. From the results, it was hoped that it would be possible to determine the errors which might be present when making tests on reflection-plane mounted models and to determine the magnitude of these errors. The investigations were carried out using a two-dimensional wing section in order to restrict the tests to the more fundamental parameters.

The tests were made at two tunnel operating conditions; one at a dynamic pressure of 40 lb/ft^2 (V = 130 mph) and the other at q = 80 lb/ft^2 (V = 185 mph). The corresponding Reynolds numbers, based on the wing chord, were 2.24×10^6 and 2.98×10^6.

The organization of the report is indicated in the Table of Contents. Most of the experimental results are presented in plotted form on Figs. 11 to 77. The points on these Figures represent actual experimental data with no fairing corrections applied. These Figures are presented in groups immediately following the discussion of the results indicated by the corresponding group of Figures. A complete list of the Figures and their location in the report is given on the Index of Figures. The test notation, model notation and model data are given on the pages following the Index of Figures.

---

* Guggenheim Aeronautical Laboratory, California Institute of Technology.

II. DESCRIPTION OF EXPERIMENTAL SETUP

A. The Two-Dimensional Test Section of the GALCIT Ten-Foot Wind Tunnel

All of the experiments were conducted in a two-dimensional test section which was installed in the normal closed working section of the GALCIT ten-foot wind tunnel.[1)2)] On Fig. 2 is shown a sketch of the two-dimensional installation. The test section was three feet wide, ten feet long and eight and one-half feet high. For a normal installation, the model was mounted horizontally across the three foot span of the tunnel between turntables or end plates which were suspended from the normal six-component balance system. These turntables were flat circular plates, 41 inches in diameter and were aligned flush with the wall. For purposes of the test described herein, static pressure orifices were installed in the end plates as shown on Fig. 3. The end plates were separated from the walls by a 1/8 inch notched gap around their periphery, this made it possible to rotate the model in pitch and also to measure the forces on the model and end plates with the normal balance system. The model was rotated in pitch by means of stings attached to the end plates outside the tunnel walls.

A wake survey rake was mounted on supports at the downstream end of the working section. The position of the rake could be varied both vertically and horizontally and the survey plane could be adjusted fore and aft behind the wing.

The turbulence level in the two-dimensional section was greatly reduced by installing five 30 x 30 mesh, phosphor-bronze, wire screens across the tunnel section upstream of the normal tunnel contraction section. The contraction ratio of the two-dimensional tunnel was a little less than 12$\frac{1}{2}$ to 1.

The combined effects of the large contraction ratio and the screens produced a very low turbulence. Tests with a hot-wire anemometer indicated that the turbulence level in the two-dimensional section was 0.08% ($\sqrt{(\frac{u'}{U})^2} = 0.0008$) parallel and 0.12% perpendicular to the flow direction.

B. Model and Special Installations

The model was constructed of laminated wood built around a metal core. The metal core consisted of a hollow circular steel shaft which extended spanwise from one metal template to another. These templates were cut to the profile of the wing and were welded to the steel shaft. The steel shaft extended several inches beyond each end of the wing and passed through holes in the end plates. A chordwise row of static pressure orifices was installed in the wing at the mid-span position; the pressure leads for these orifices were brought out through the hollow shaft in the wing. The main portion of the wing was 35 1/8 inches in span. A wooden spacer block or steel shims cut to the profile of the wing were used to increase the span of the wing to 36 inches, or less, as desired. For all installations, the model was mounted with the 50% chord at the trunnion axis (the axis about which the balance measured pitching moment).

For the normal model installation, the wing was supported by the end plates as previously described. In order to mount the wing in this way, it was necessary to rotate the end plates 180° with respect to their normal orientation. The wing fitted flush against the end plates and the steel shaft through the center of the wing extended outside the tunnel through the end plates. The end plates were bolted rigidly to the wing and the angle of

attack of the wing was varied by rotating the end plates. The wing and end plates are shown on Photo 3.

When testing the wing "live", end plate "grounded" configuration ($W_B P_G^1 P_G^2$), the wing was supported independently of the end plates. The end plates were fastened to the walls of the two dimensional section and the wing was supported by the balance system. The balance system was connected directly to the wing shaft outside the tunnel in the same way it was normally connected to the end plates. The gap between the wing shaft and the hole in the end plate through which the shaft passed was sealed by a thin rubber diaphragm. The diaphragm was mounted at one end in a fixed position on the end plate while the other end was fastened on a brass ring which was free to rotate on the wing shaft.

For the wing "grounded", end plate "live" configuration ($W_G P_B^1 P_B^2$), the end plates were supported from the balance system in the normal way. The "grounded" wing was supported by two horizontal spindles, one at each end, pinned to the ends of the wing shaft. Stings were also attached to the wing shaft at each end and rods connected these stings to the tunnel image system pitching mechanism. This installation can be seen in Photos 5 and 6. The angle of attack of the model was set with this image system pitching mechanism.

Steel spacer blocks or "templates" were cut to match the wing contour. The templates were made in several thicknesses and could be fastened either to the wing or the end plate. These templates were used for the gap investigations and also to measure the forces on the portion of the wing in the boundary layer (cf. Sec. V-B). One of these templates is shown on Photo 4.

A rubber seal made of thin dental dam was installed around the periphery of both end plates to seal the gap between the end plate and wall. This seal

was fastened solidly to the end plate at one end; the other end was inserted between a rubber pad and an adjustable ring attached to the tunnel wall (cf. Photo 7). Sufficient slack was allowed in the seal to prevent the introduction of forces through the seal. When the seal was not used to prevent airflow through the gap, the outer end of the seal was removed from under the ring and taped to the end plate.

The roughness strips (Tr) which were used to change the thickness of the boundary layer on the end plates were made by soldering a 1/8 inch diameter rod 42 inches long to a 1/16 inch by 1 inch flat metal strip. One of these strips was mounted 2 1/4 inches upstream of each end plate. Photo 2 shows one of these strips.

The same total head rake was used to measure the total head distribution at the center of the end plate and the total head loss in the wing wake. This rake was fastened to the tunnel wall in a fixed position as shown on Photo 1 when the boundary layer measurements were made. When measuring the total head loss in the wing wake, the rake was mounted on a carriage which could be utilized to change the position of the rake. The rake itself was made up of about 80 hypodermic needles which were flattened at the ends and mounted on a long tube. Fairing plates were mounted aft of these tubes to streamline the rake. The tubes were spaced 0.10 inch apart and all total head tubes were in a common plane.

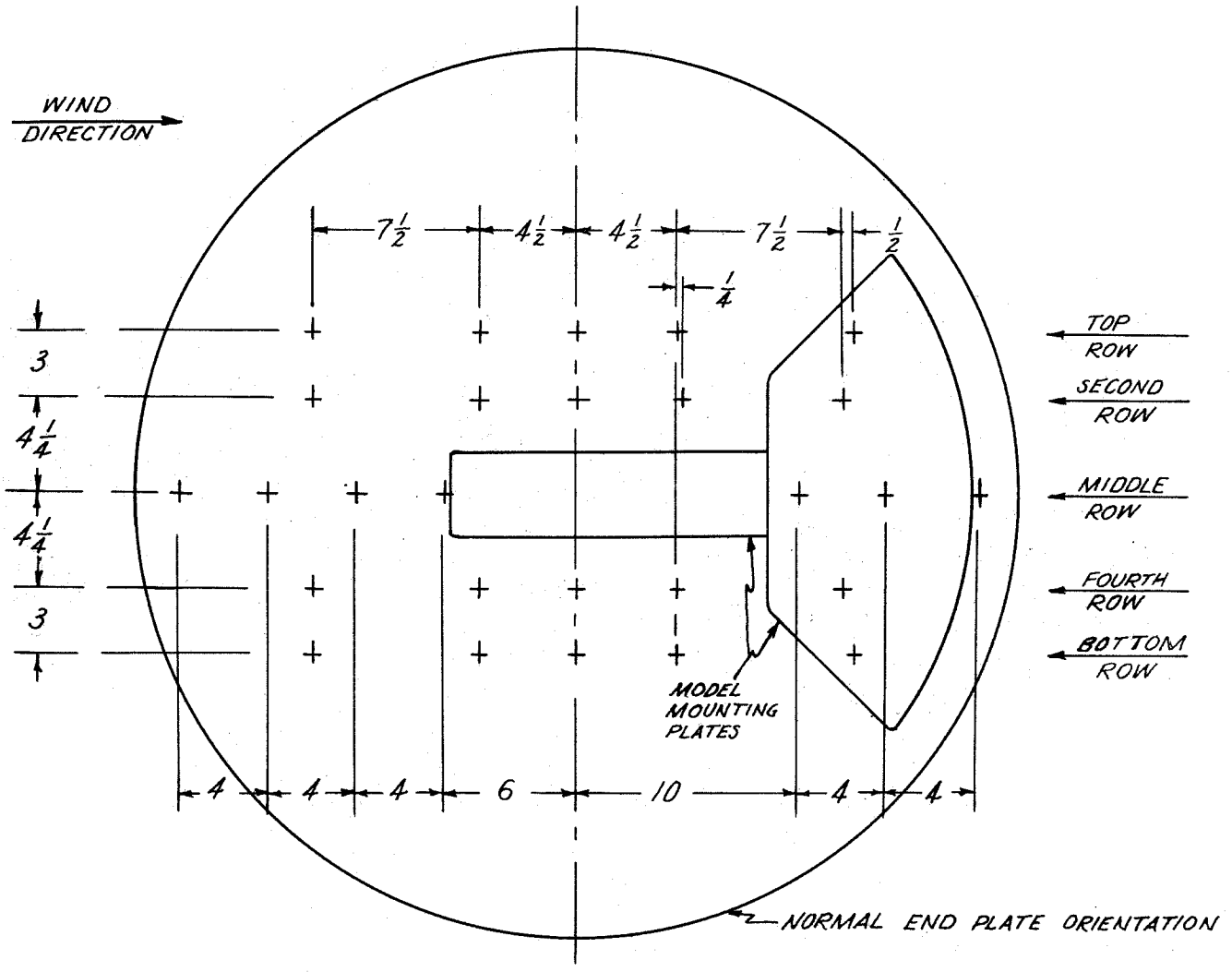

DIMENSIONS IN INCHES
WING CHORD LIES IN PLANE OF MIDDLE ROW
+ ~ ORIFICE

Fig. 3. Sketch showing location of end plate static pressure orifices

III. TUNNEL CALIBRATION AND METHOD OF SETTING DYNAMIC PRESSURE

The dynamic pressure in the two-dimensional test section was determined during the tunnel calibration by mounting a standard Prandtl pitot-static tube on the tunnel centerline at the trunnion axis. At the same time the dynamic pressure was determined, the pressure difference between the static pressure in the 20-foot entrance section and the static pressure at the entrance to the two-dimensional test section was determined. These "calibrated" static pressure differences were used to set the dynamic pressure on all tests. The dynamic pressures were corrected so that the air density may be considered as the free air density unaffected by compressibility.

When the model was installed in the tunnel, the dynamic pressure was corrected for the blockage effect of the model. This correction was based on the perfect fluid theory for a Rankine oval, and was not considered as variable with angle of attack. The correction amounts to a 1% increase in dynamic pressure for a 2-foot chord wing of a thickness equal to 20% chord.

A check was made to determine the effect on dynamic pressure of moving the end plates into or out of the tunnel. For any of the end plate configurations tested the variation in dynamic pressure was less than 3/4% and for most cases was within 1/4%.

Vertical and horizontal traverses with the pitot-static tube revealed negligible variations in the dynamic pressure from the centerline value throughout most of the working section. The total head distribution on the left-hand end plate at the trunnion centerline is shown on Figs. 4-7. These Figures also show the change in distribution due to the transition strips and end plate alignment, with the end plate gap open and sealed.

A static pressure survey indicated that the static pressure along the tunnel axis was constant from a point 17 inches upstream from the trunnion axis to a point 25 inches downstream from the trunnion axis.

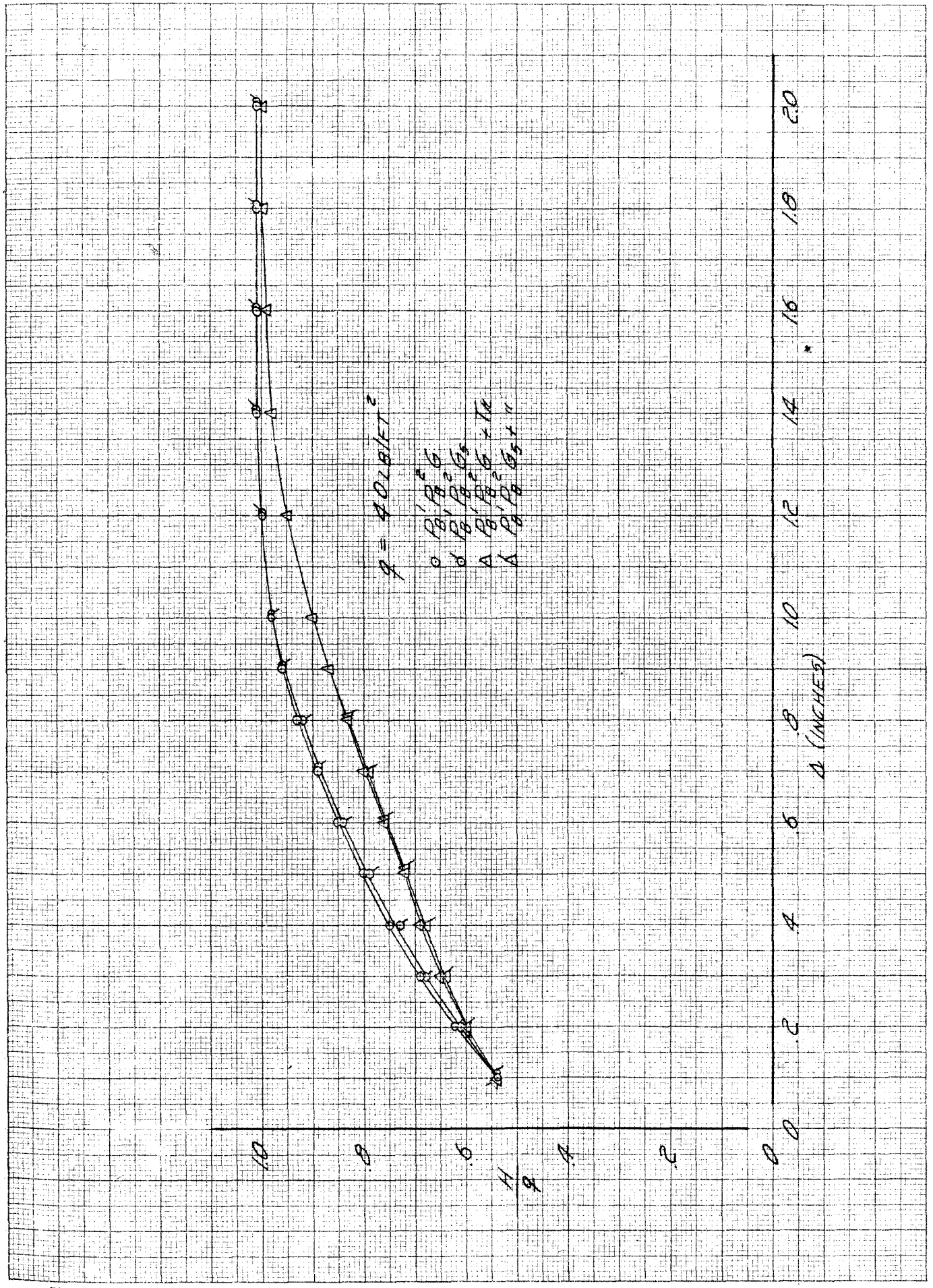

Fig. 4. Effect of roughness strips on boundary layer thickness with end plate gap open and sealed, q = 40 lb/ft^2

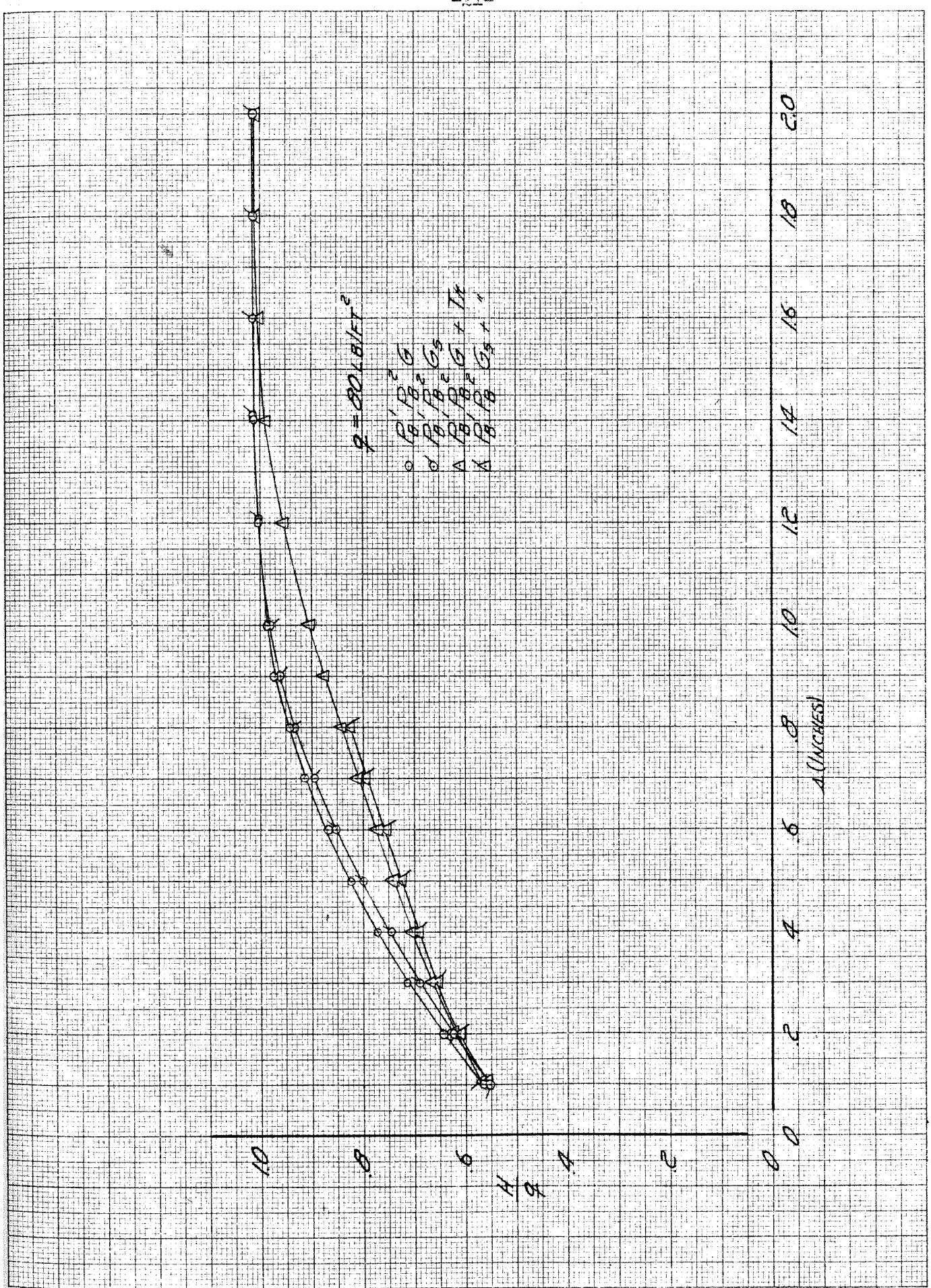

Fig. 5. Effect of roughness strips on boundary layer thickness with end plate gap open and sealed, q = 80 lb/ft^2

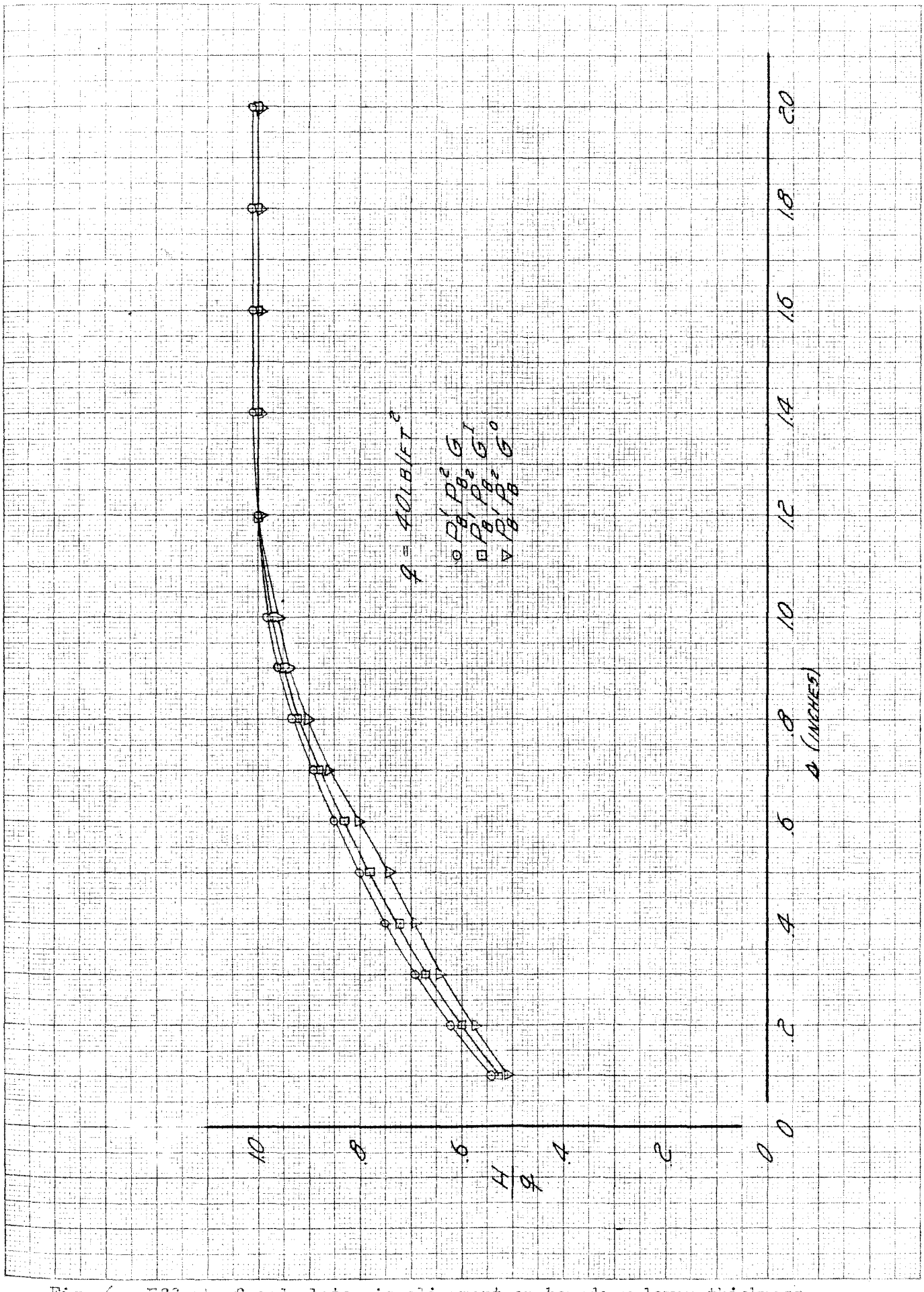

Fig. 6. Effect of end plate mis-alignment on boundary layer thickness, $q = 40$ lb/ft^2

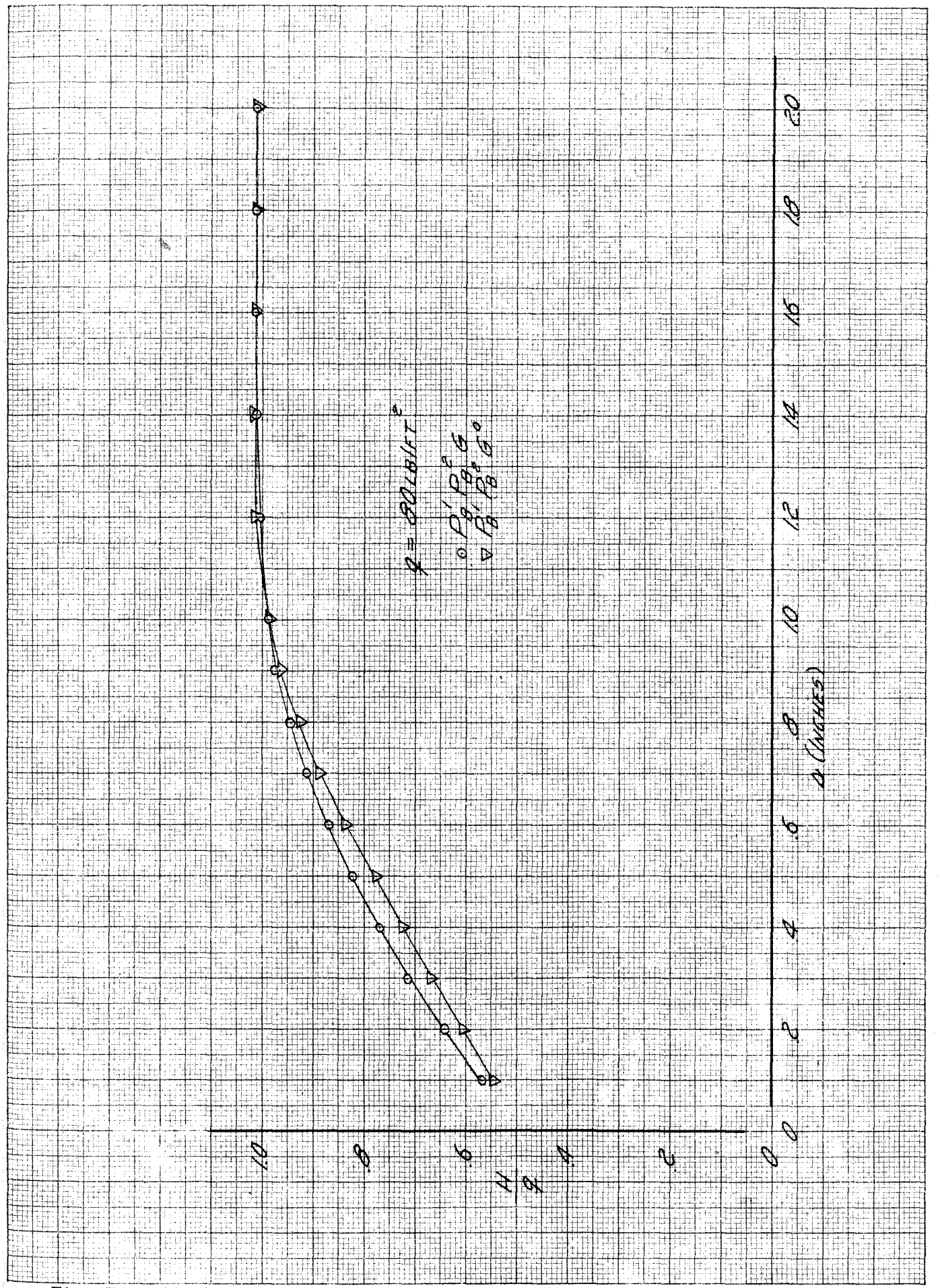

Fig. 7. Effect of end plate mis-alignment on boundary layer thickness, $q = 80$ lb/ft^2

IV. METHOD OF REDUCING DATA

A. Balance Data

The forces on the various configurations were measured on the normal six-component balance system. These balance readings were converted into coefficient form basing the coefficients on the wing panel dimensions. The values of dynamic pressure used were obtained from the calibration previously described. Pitching moments were measured about the 0.50 chord position and transferred to the 0.25 chord position.

The angle of attack plotted on all curves was the angle indicated by the selsyn indicator attached to the pitching mechanism. This selsyn indicated the angle between the tunnel axis and the wing chord. Since there was no flow inclination, this angle requires no windstream inclination correction. The "wall interference" effect of the tunnel floor and ceiling (such that curved flow is induced near a wing developing lift, thus changing the effective camber of the wing) was small in the present case and was neglected.

B. Integrated Wake Drags

Profile drag data were obtained by measuring the total head loss in the wake. The rake used to measure the total head loss in the wake (cf. Sec. II-B) was located 0.50 chord aft of the trailing edge of the wing. The variation of static pressure along the tunnel axis is negligible from a point three-quarters of a chord length ahead of the wing to a point slightly more than one chord length aft of the trailing edge of the wing.

The wake pressure measurements were converted into the loss in momentum in the wake according to the simple momentum theory of B. M. Jones.[3] The static pressure at the rake position was so nearly equal to the free stream

static pressure (tunnel pressure with no model present) that no static pressure gradient correction was necessary. The following equation was applied to obtain the drag coefficient.

$$C_{D_{o_{un}}} = 2 \int_{\text{Wake}} \left[\sqrt{\frac{P_{o_w}-P}{P_o-P}} - \frac{P_{o_w}-P}{P_o-P} \right] d(y/c)$$

where: $C_{D_{o_{un}}}$ = profile drag coefficient, uncorrected for tube displacement or compressibility effects

P_{o_w} = total head measured in wake

P_o = free stream total head

P = free stream static pressure

y = position of measurement across wake

c = wing chord

A correction to the total head readings, called the tube displacement correction, was applied to the profile drag data. This correction arises from the presence of the rake tubes in the turbulent wake, and from the presence of the tubes in a large pressure gradient. It is assumed (and has been verified experimentally [4]) that under these conditions the total head registered by the tubes is too high. The tubes of the total head rake used in these tests were very small and the tube displacement correction never exceeded a C_{D_o} of 0.0002. The final profile drag coefficient was determined from the following equations.

$$C_{D_o} = f \, (C_{D_{o_{un}}} + \Delta C_{D_o})$$

where: ΔC_D = tube displacement error

f = compressibility correction factor

= 0.98 at q = 30 lb/ft^2

= 0.99 at q = 40 lb/ft^2

} GALCIT values

Figure 8 shows the method used to calculate the profile drag on a typical point.

C. Integrated Lift and Pitching Moment

The wing chordwise pressure distribution data were reduced in terms of the pressure coefficient P/q, defined in the Test Notation section. This coefficient is referred to the free stream static pressure in the tunnel, with no model present, and is based on the tunnel dynamic pressure corrected for compressibility effects.

These pressure distributions were plotted against chordwise position as shown on Fig. 9. The normal force is obtained by determining the area under this curve since

$$C_n = -\int_{\text{Chord}} \left[\frac{P_u - P_L}{q}\right] d\left(\frac{x}{c}\right)$$

where: $(\ )_u$ Upper Surface

$(\ )_L$ Lower Surface

Since the direction and magnitude of the force on the airfoil perpendicular to the normal force cannot be determined from pressure measurements, the lift coefficient cannot be explicitly determined. The value of C_L will lie somewhere between the value of $C_n / \cos\alpha$ and $C_n \cos\alpha$.

For $\alpha = 10^\circ$, $\cos\alpha = 0.985$; so the difference between normal force and lift can be no greater than 1.5% at this angle.

In order to determine the pitching moments, the wing static pressure distribution data were modified by computing the quantity

$$\frac{x}{c} \cdot \frac{P_L - P_u}{q}$$

using faired values obtained from the pressure distribution curve. This quantity is plotted against x/c as shown on Fig. 10. The pitching moment is then determined by the following equation:

$$C_{m_{c/4}} = -\int_{Chord}\left[\frac{x}{c}\cdot\frac{P_L-P_u}{q}\right] d\left(\frac{x}{c}\right) + \frac{C_n}{4}$$

D. End Plate Static Pressure Distribution

Static pressure distributions over the end plates were reduced in terms of the pressure coefficient P/q. These end plate static pressures were plotted against the ratio of the pressure orifice station to the wing chord (x/c). The orifices upstream of the wing leading edge were plotted as negative values of x/c. Each horizontal row of orifices on the end plates was plotted on a separate axis; Fig. 3 shows the location of these rows of orifices.

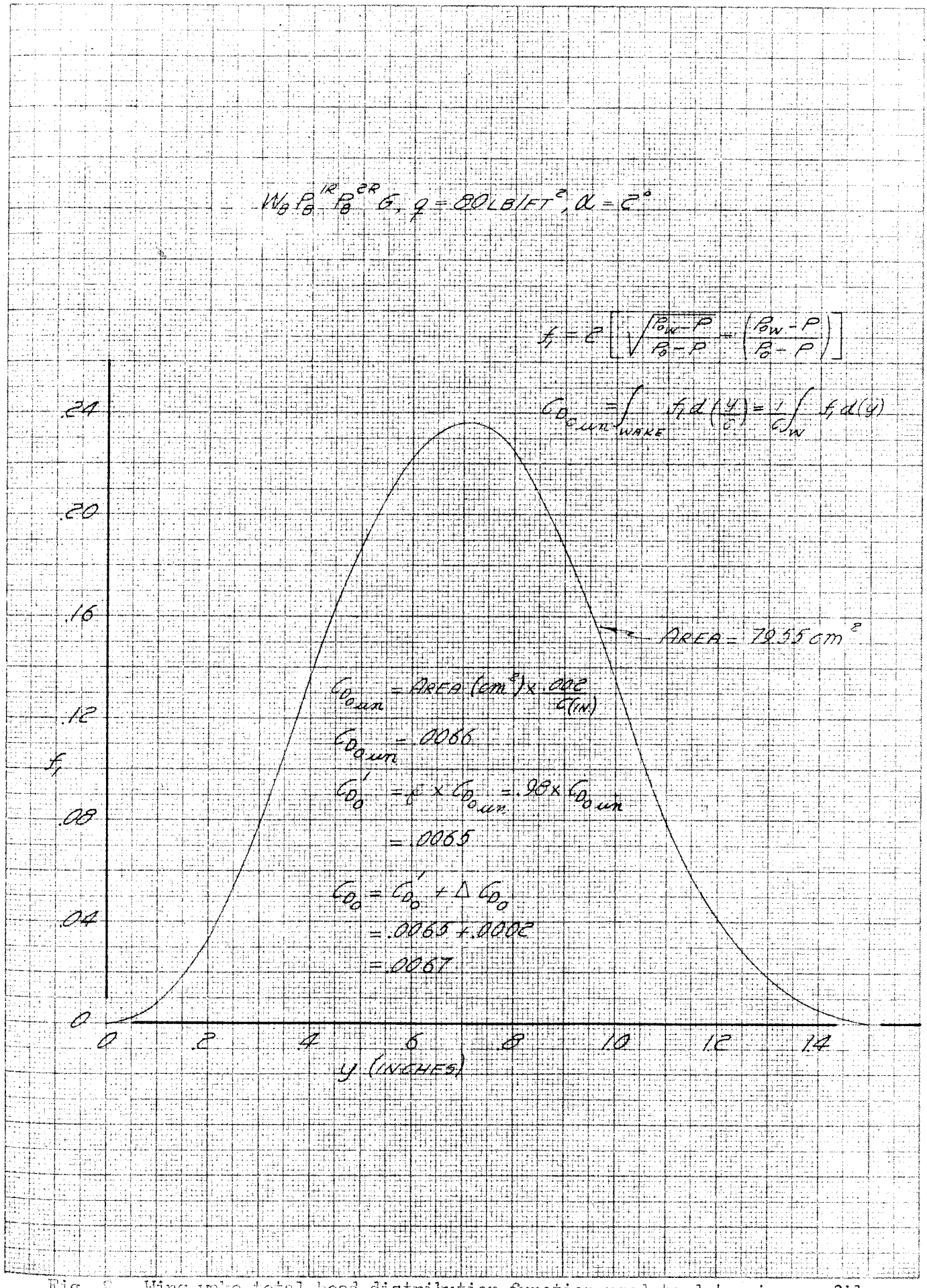

Fig. 8. Wing wake total head distribution function used to determine profile drag at $\alpha = 2^\circ$, q = 80 lb/ft^2

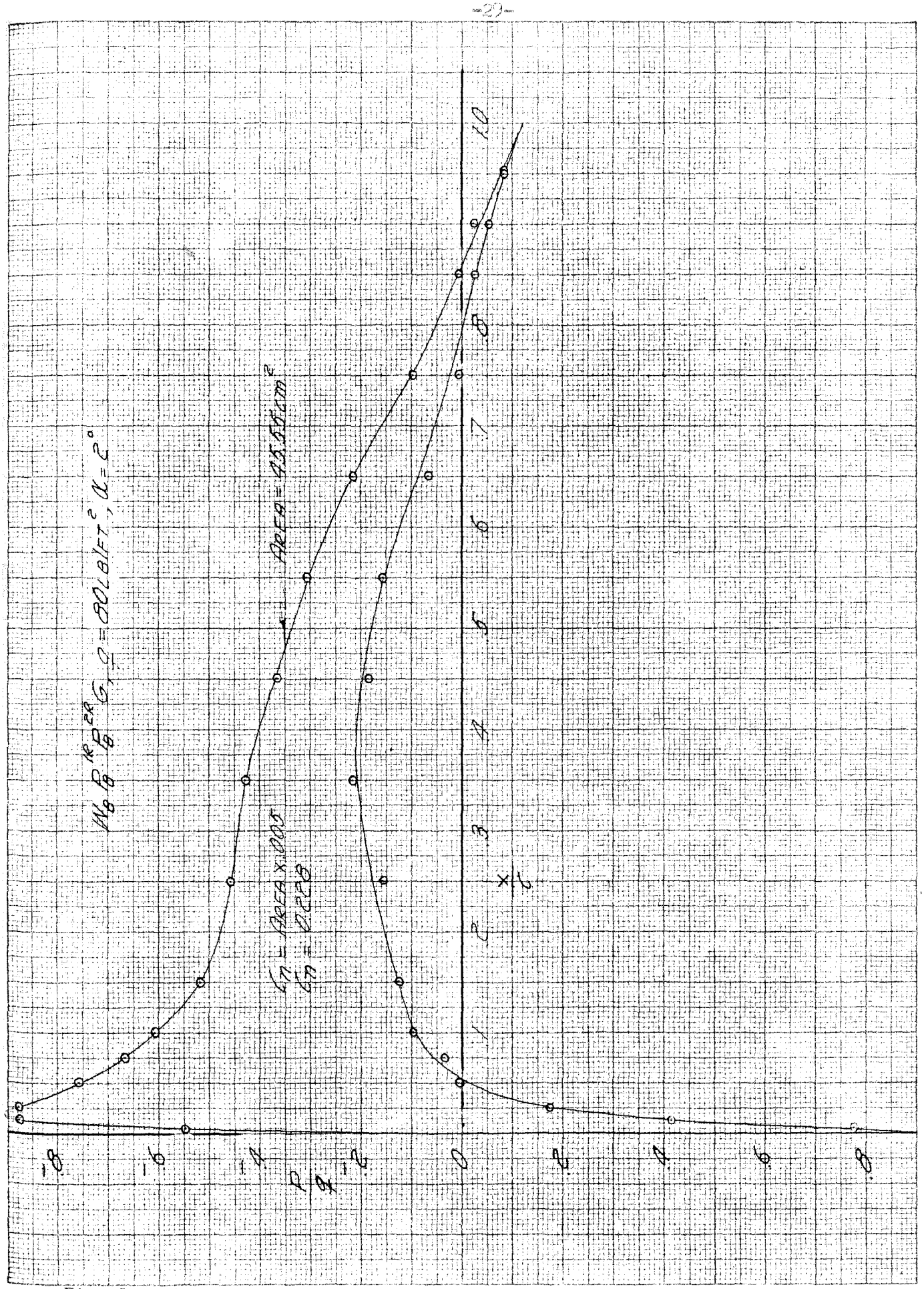

Fig. 9. Wing pressure distribution data used to determine normal force at $\alpha = 2^{\circ}$, $q = 80$ lb/ft^2

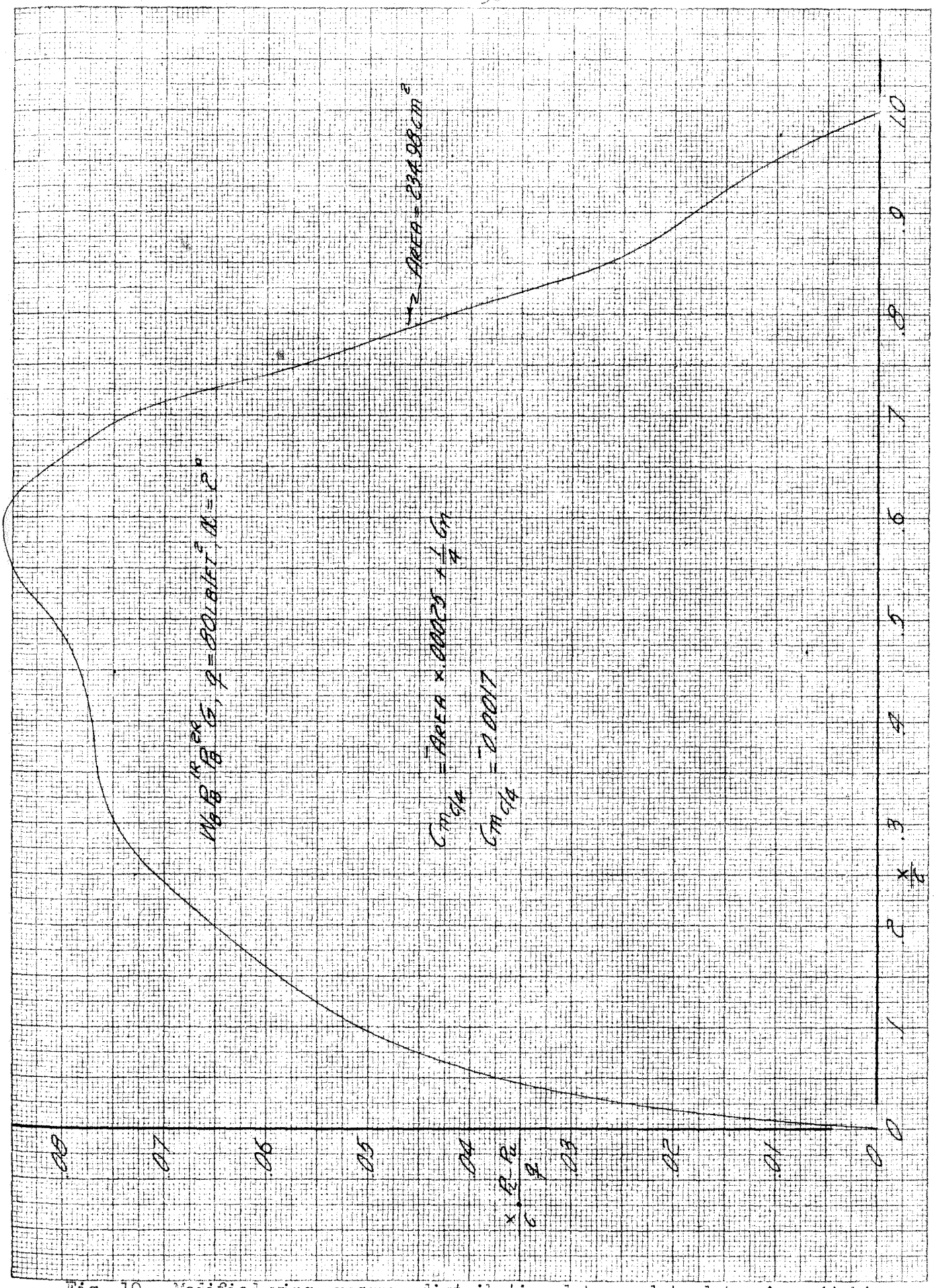

Fig. 10. Modified wing pressure distribution data used to determine pitching moment at $\alpha = 2°$, q = 80 lb/ft^2

V. EXPERIMENTAL RESULTS

A. Wing Results and Effects of End Plate Gap Seal

The force data results obtained with the wing are shown on Figs. 11-21. The first three Figures of this group show the comparison between the balance data results and the results obtained from integrated pressure data. The agreement between the lift force determined from balance readings, and normal force, determined from integrated pressure data, is within the expected accuracy of 1.5% (cf. Sec. IV-D). Pitching moments obtained by the two different methods agree within 1% in stability. When the balance drag results obtained for the wing and end plates were corrected for the end plate drag, the results agreed fairly well with the integrated wake drags. The same is true, to a lesser degree, of balance drag results obtained for the wing in the presence of the end plates when these results were corrected for the effects of the wing-end plate gaps. (The end plate drags and wing-end plate gap effects are described in later sections.) With the end plate drag correction applied to the wing and end plate results, a maximum difference of about five drag points was obtained between the integrated wake pressure results and the balance results. This difference decreases at the higher lifts. When the wing-end plate gap correction was applied to the results obtained for the wing in the presence of the end plates, the results differed from the integrated wake pressure results by as much as ten drag points. The drags obtained from the integrated pressure data were higher than either of the corrected balance drags which indicates that the balance results were over corrected.

In order to determine the consistency of the wing profile, wake measurements were taken at two different spanwise positions of the wing.

It was also desired to determine what effect the end plate gap would have on the integrated wake drag results. Figures 14 and 15 contain the results of these tests and indicate that the wing was uniform at the two positions tested and that the end plate gap has no effect on the integrated wake drag results.

The effects of sealing the end plate gap are shown on Fig. 16-21. It was very difficult to obtain data with the end plate gap sealed when the forces on the end plate were to be measured. The difficulty arose from the great care which had to be taken to install the seal so that it imposed no forces on the end plates. Since the seal had to be re-adjusted for each angle of attack, it can be seen that great difficulty was encountered in obtaining the data. In fact, it took two full days to obtain the data for this configuration at the two dynamic pressures. A great number of points was taken on these runs since the forces appeared to vary even though the tunnel speed was held constant.

With the wing and end plate mounted on the balance system, sealing the end plate gap increases the lift curve slope very slightly and changes the stability by about two percent. With the wing mounted on the balance system in the presence of the grounded end plates, sealing the end plate gap increases the lift curve slope very slightly but produces no change in pitching moment. The change in stability noted for the wing and end plate must therefore be due to a change in force on the end plates due to the end plate gap seal. Visual observations of the seal indicated that with the wing present the pressure was above atmospheric in the portions of the gap

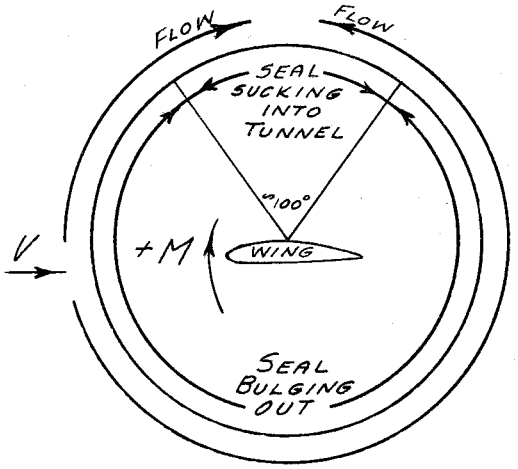

View of End Plate Seal Showing Pressure Distribution in Gap with Wing Present

below the lower surface of the wing and below atmospheric in the portion of the gap above the upper surface of the wing as shown on the accompanying sketch. If the flow in the end plate gap is similar to that indicated in this sketch, then it is possible for flow through the gap to produce an increasingly negative pitching moment with increasing lift. As the wing develops lift, the pressure difference between the top and bottom of the end plate becomes larger and the flow velocity in the gap would increase. Since the longest flow path is in the direction which would produce negative pitching moment, an increasingly negative pitching moment would accompany an increase in lift.

When the drag forces on the wing were measured with the end plates grounded, sealing the end plate gap caused a decrease in drag. The decrease in drag grew larger with increasing lift. This decrease in drag is about one-half as large as the drag increment due to the wing-end plate gaps $\delta_1 = .07, \delta_2 = .05$ (cf. Sec. V-C1). It is felt, therefore, that the end plate gap seal decreases the wing-end plate gap drag.

The drag forces measured for the wing and end plates indicate no corresponding decrease in drag due to sealing the end plate gap. The forces which were measured were very erratic, as was previously mentioned. Since there was no gap between the wing and end plate there could be no reduction in drag such as that described above. Any reduction in the induced drag of

the entire installation due to sealing the end plate gap was either too small to measure or was counterbalanced by an increase in drag due to the flow along the end plate gap.

The static pressure developed by the wing decays rapidly as is shown on Figs. 22-24. The data on these Figures were obtained from the wing static pressure orifices and the static pressure orifices on the end plates. Effects of the end plate shaft seal and other modifications on the end plate static pressure distribution are shown on Figs. 25-27. The end plate gap seal has no effect on the end plate static pressure distribution when there is no gap between the wing and end plate. When the main portion of the wing is held fixed at $\alpha = 0^{\circ}$ and the spacer block template is varied through the angle of attack range, the end plate pressures remain virtually unchanged. See the following section for more details about spacer block template results.

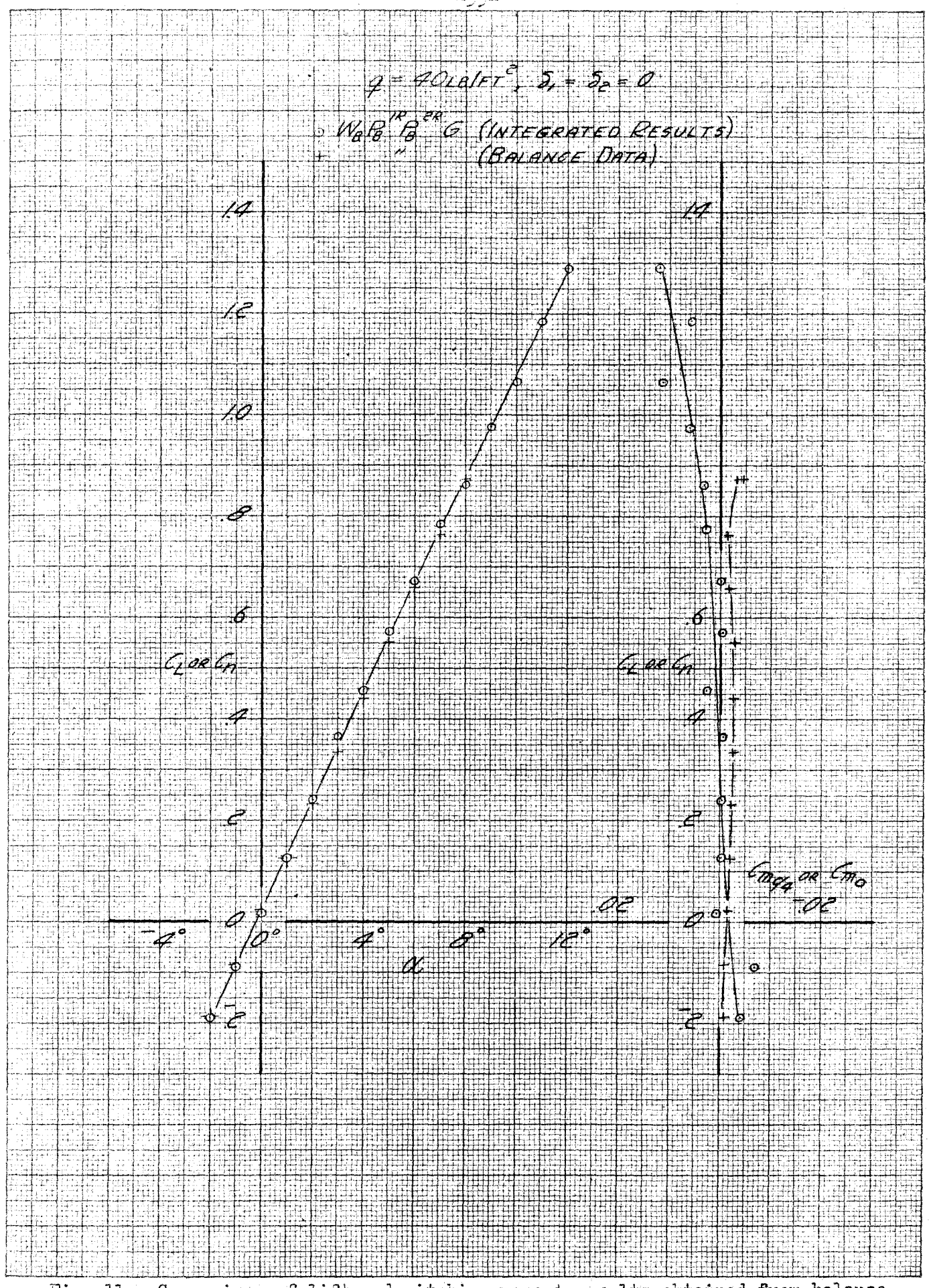

Fig. 11. Comparison of lift and pitching moment results obtained from balance data and from integrated pressure data, q = 40 lb/ft^2

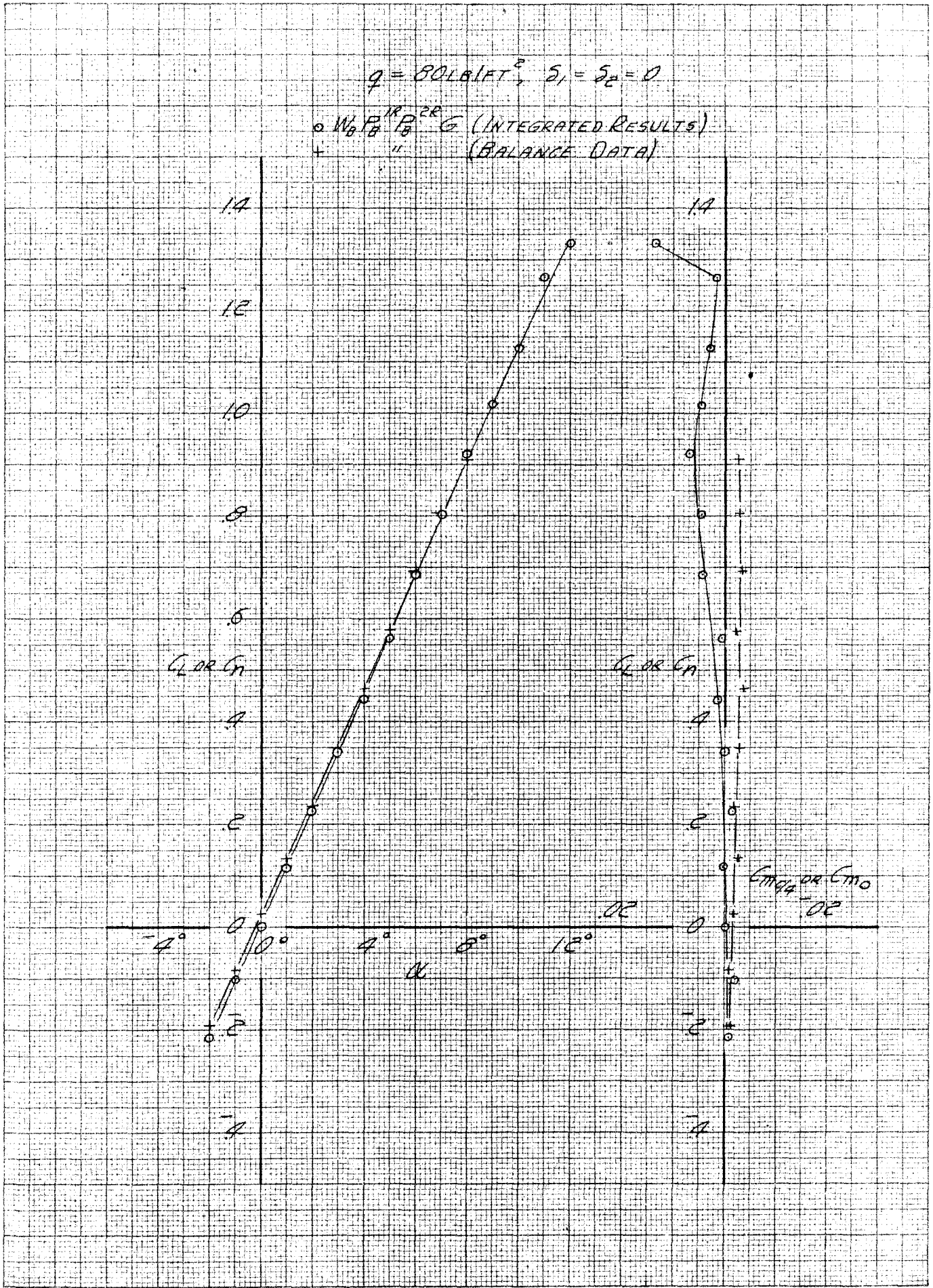

Fig. 12. Comparison of lift and pitching moment results obtained from balance data and from integrated pressure data, q = 80 lb/ft^2

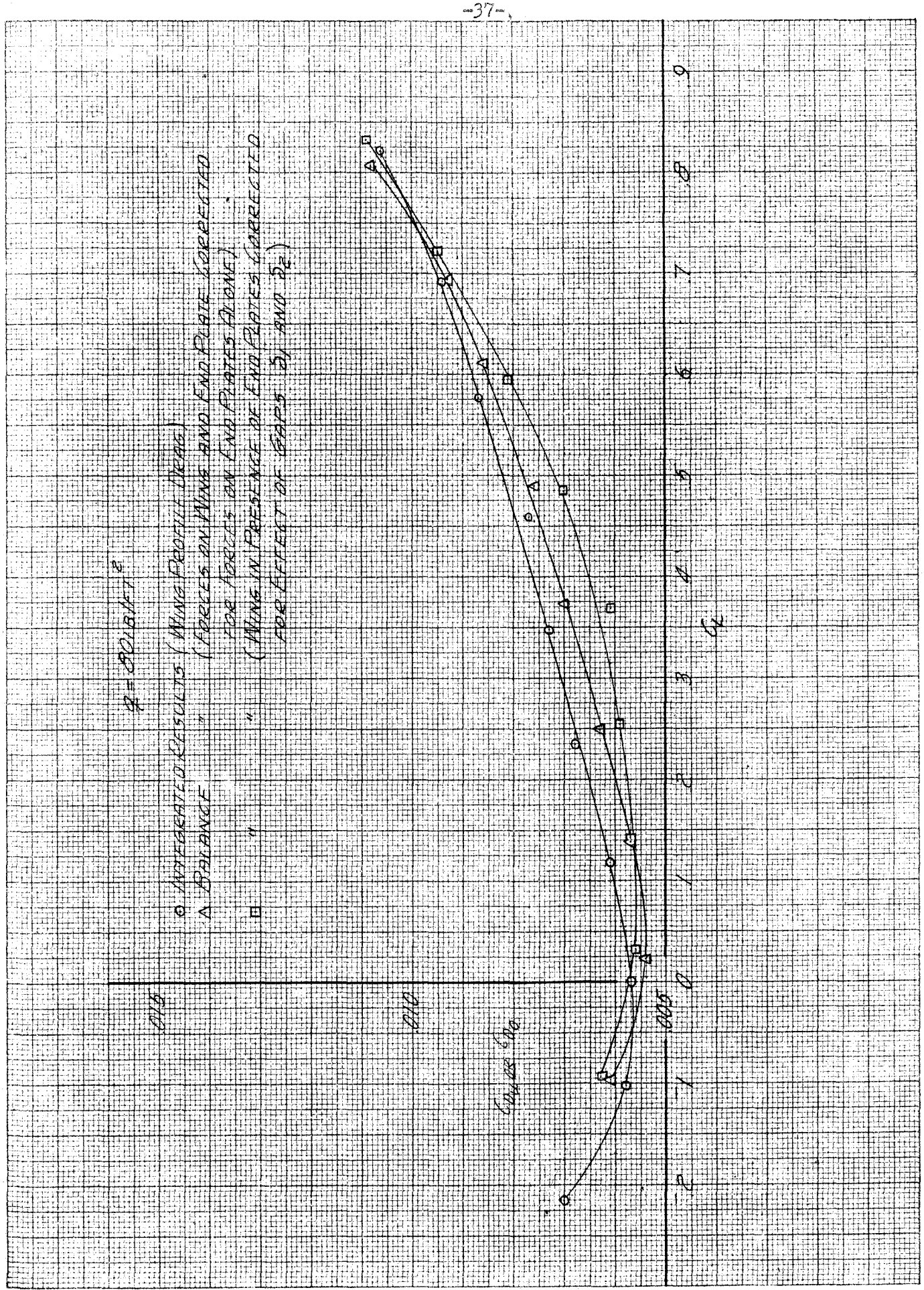

Fig. 13. Comparison of drag results obtained from balance data and from integrated pressure data, q = 80 lb/ft^2

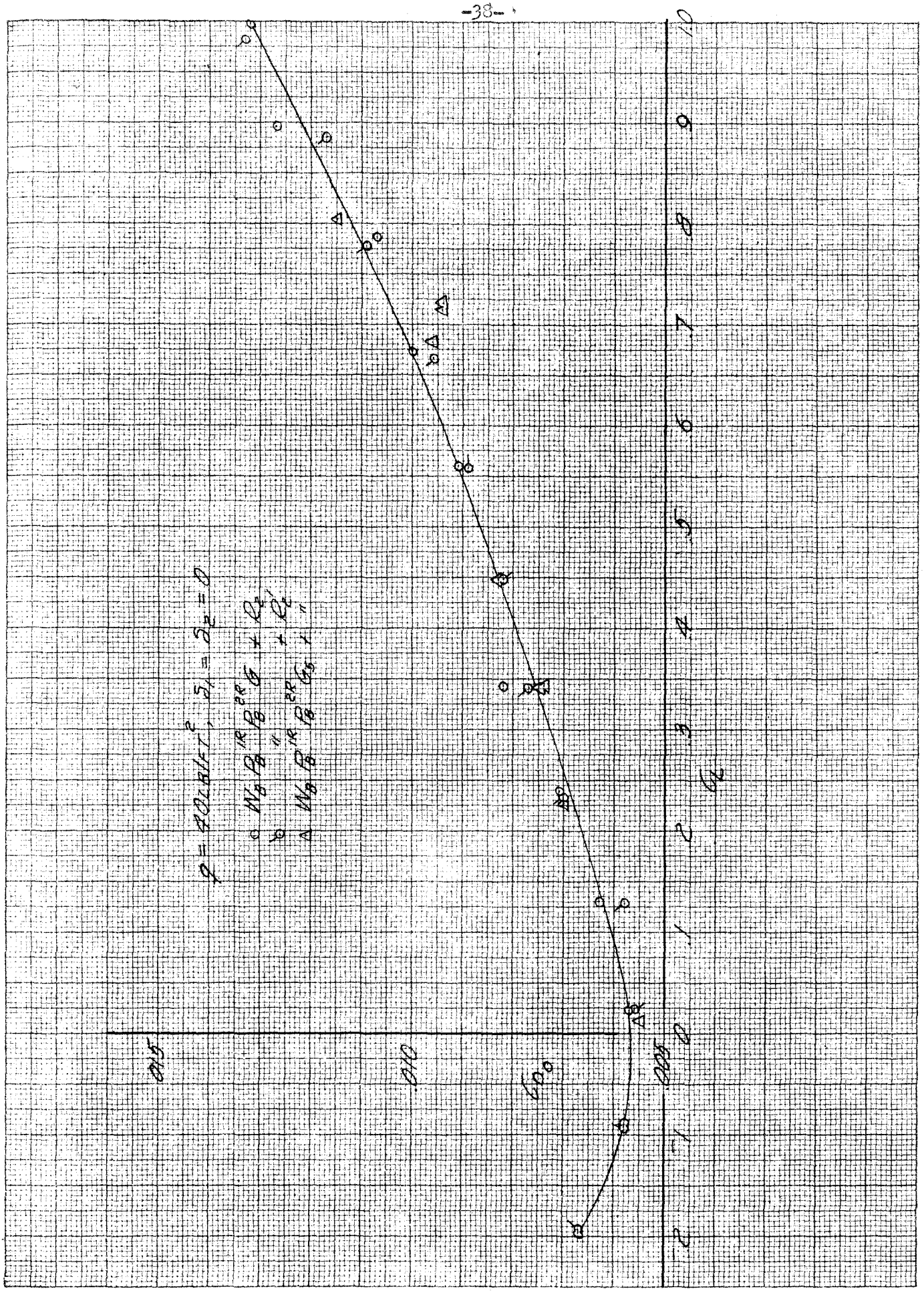

Fig. 14. Effects of spanwise rake position and end plate gap seal on integrated wake drag results, q = 40 lb/ft^2

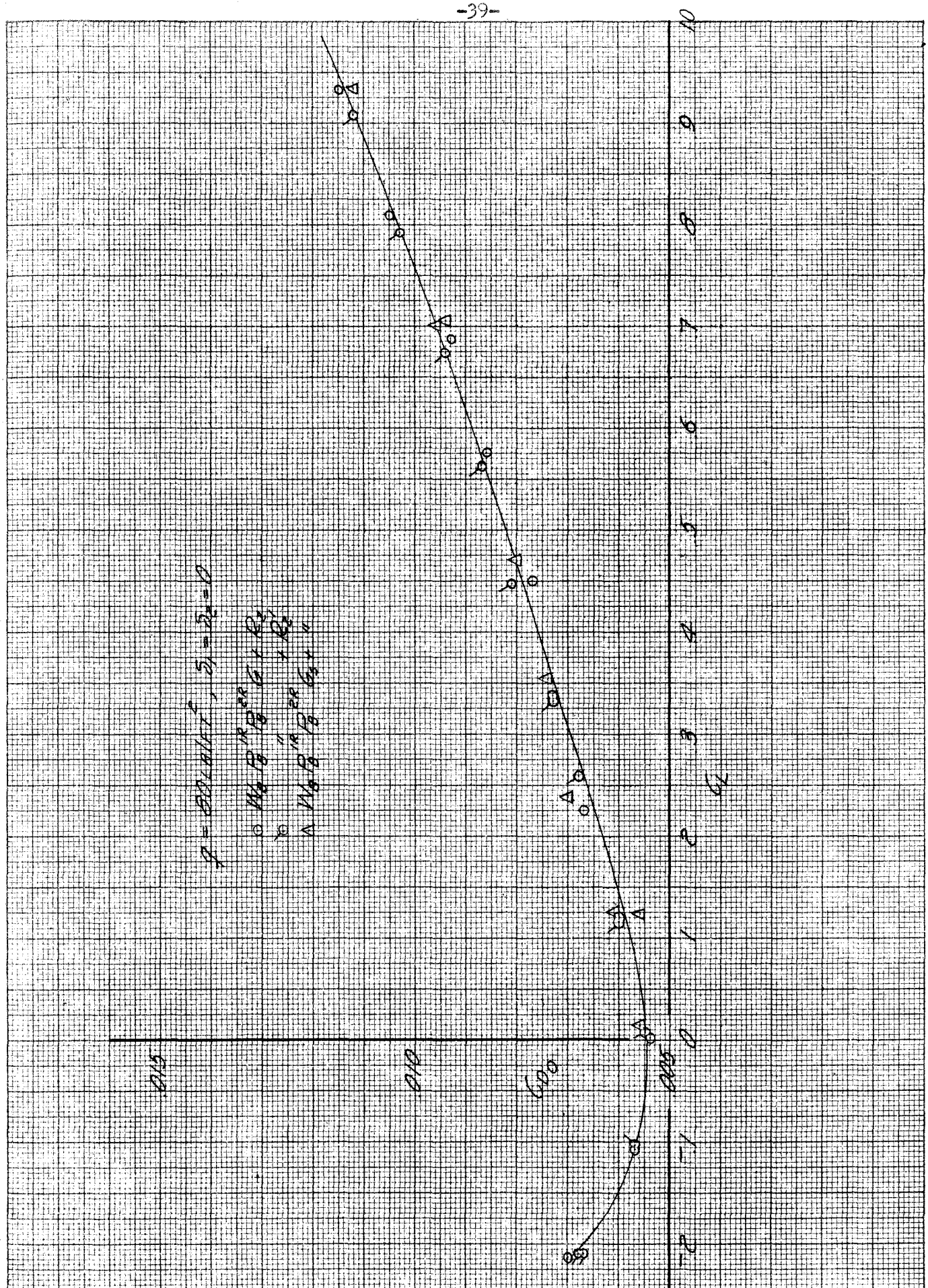

Fig. 15. Effects of spanwise rake position and end plate gap seal on integrated wake drag results, q = 80 lb/ft^2

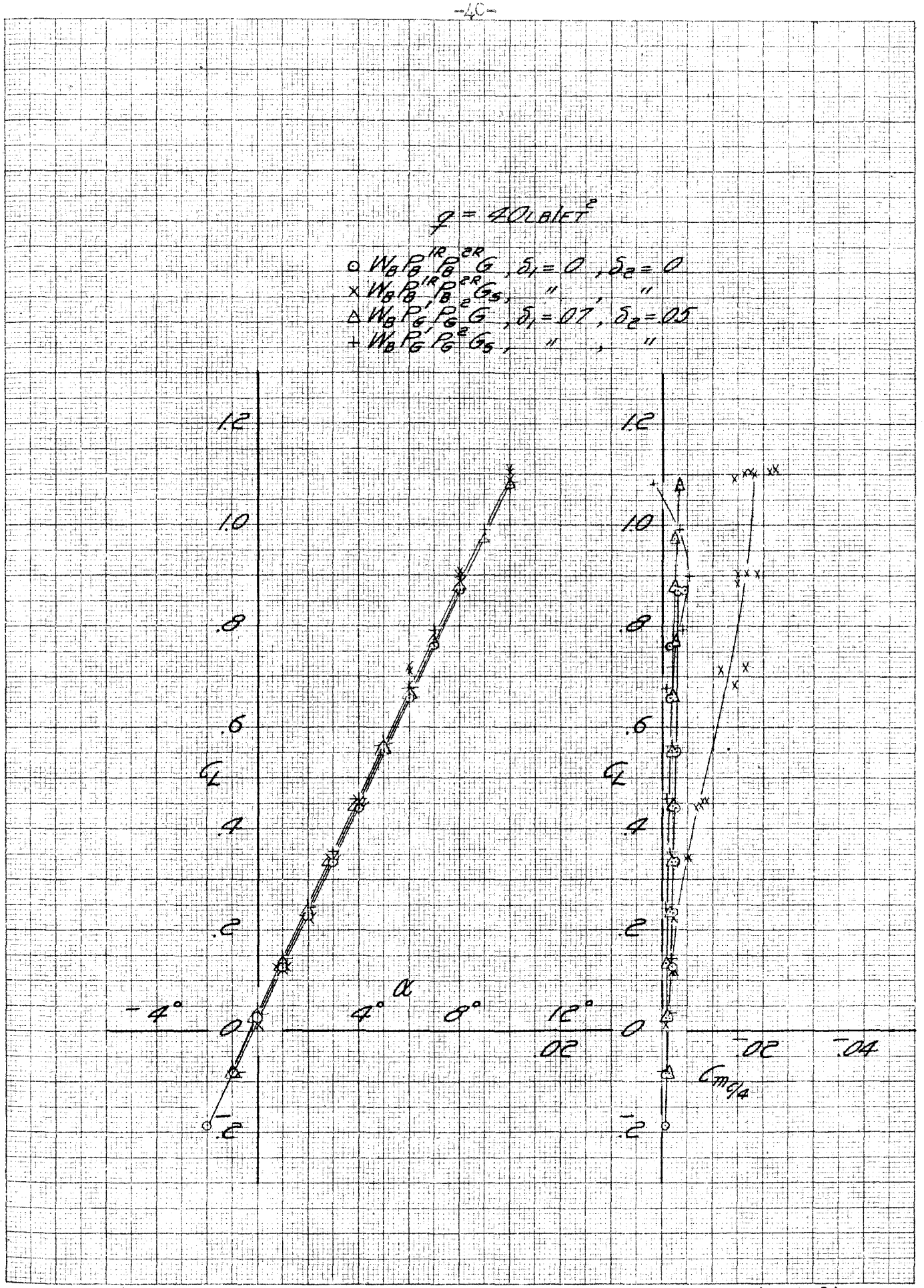

Fig. 16. Effects of end plate gap seal on lift and pitching moment results obtained for wing and for wing and end plate, q = 40 lb/ft^2

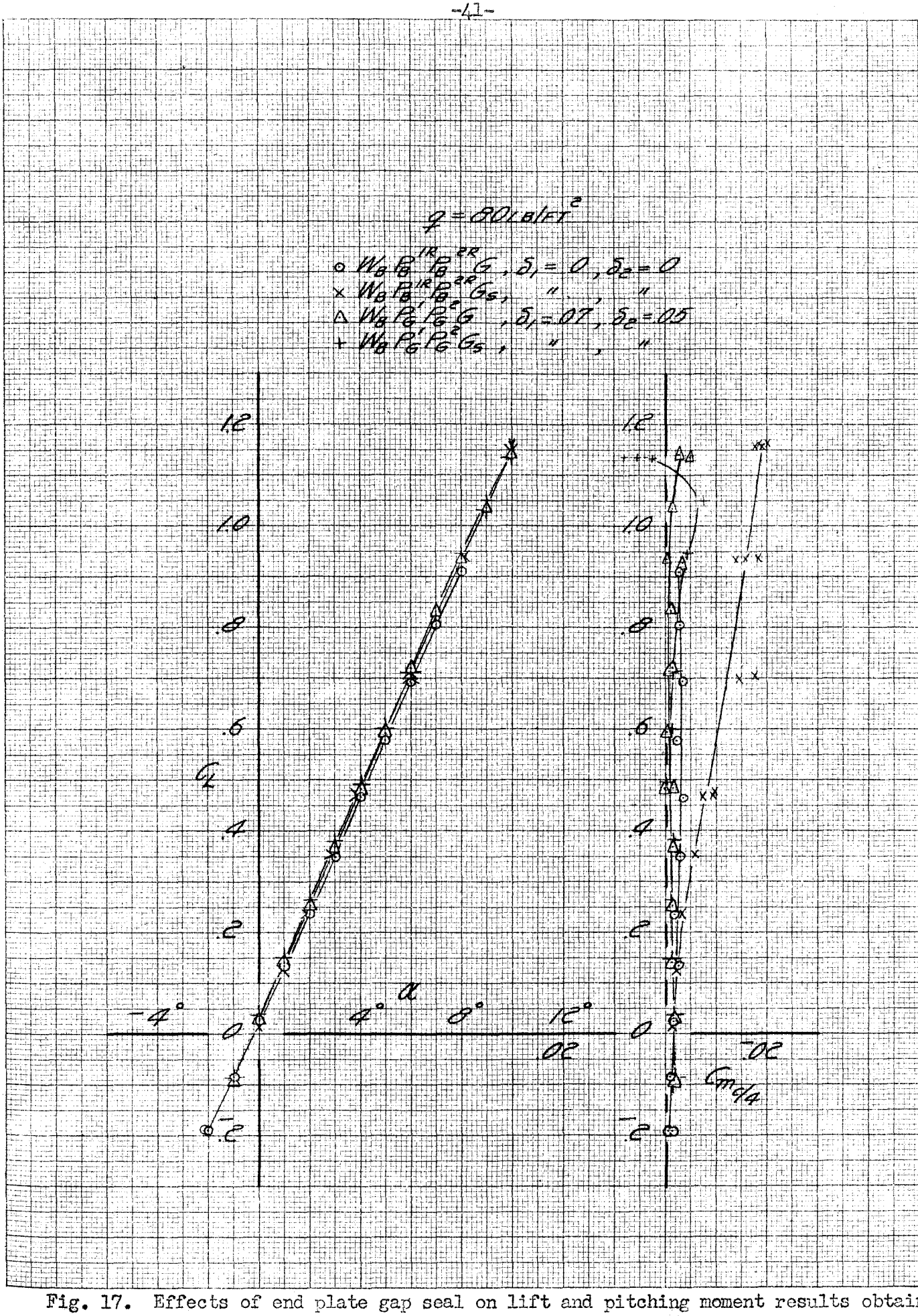

Fig. 17. Effects of end plate gap seal on lift and pitching moment results obtained for wing and for wing and end plate. q = 80 lb/ft^2

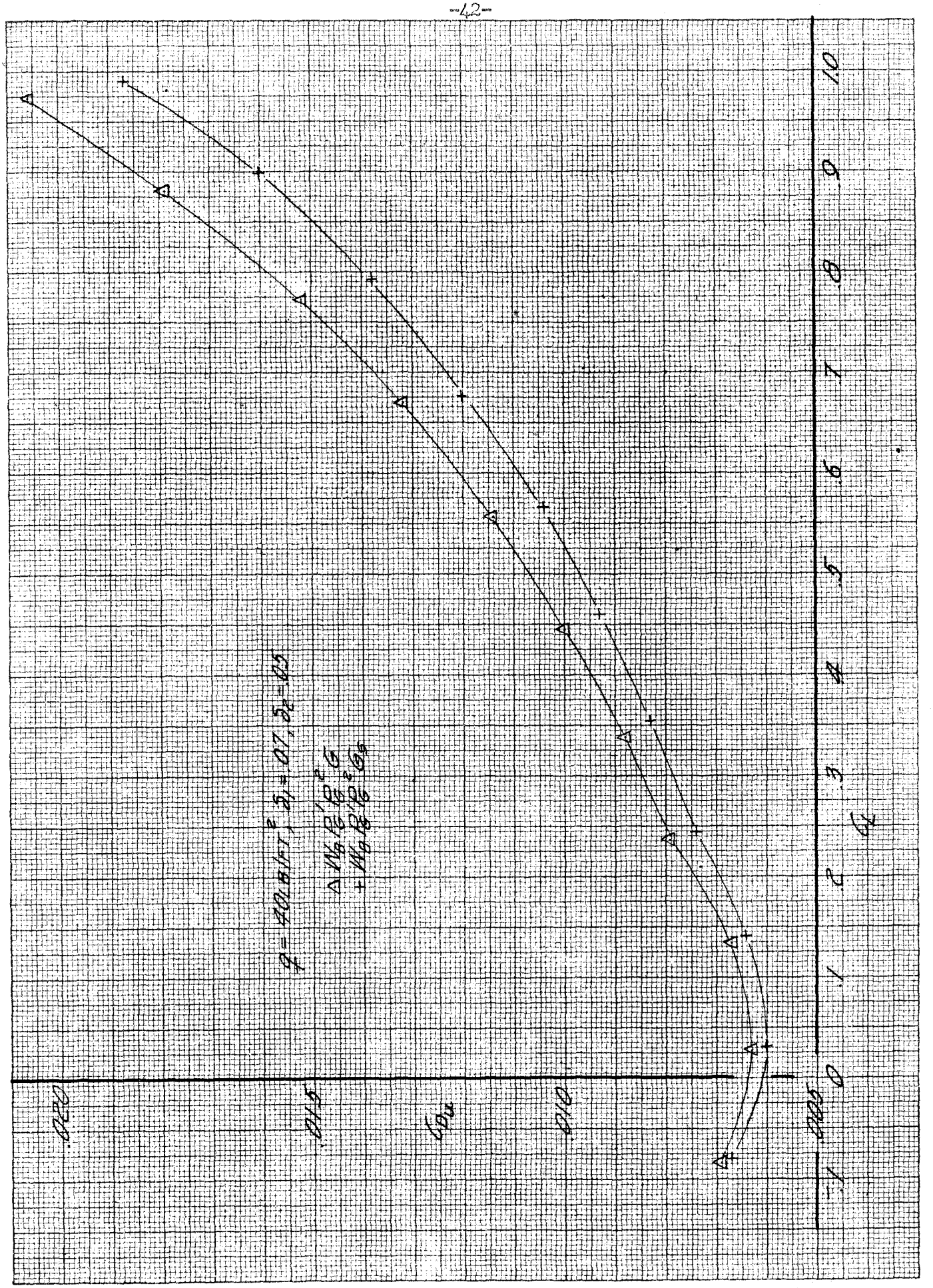

Fig. 18. Effect of end plate gap seal on drag results obtained for wing, $q = 40$ lb/ft^2

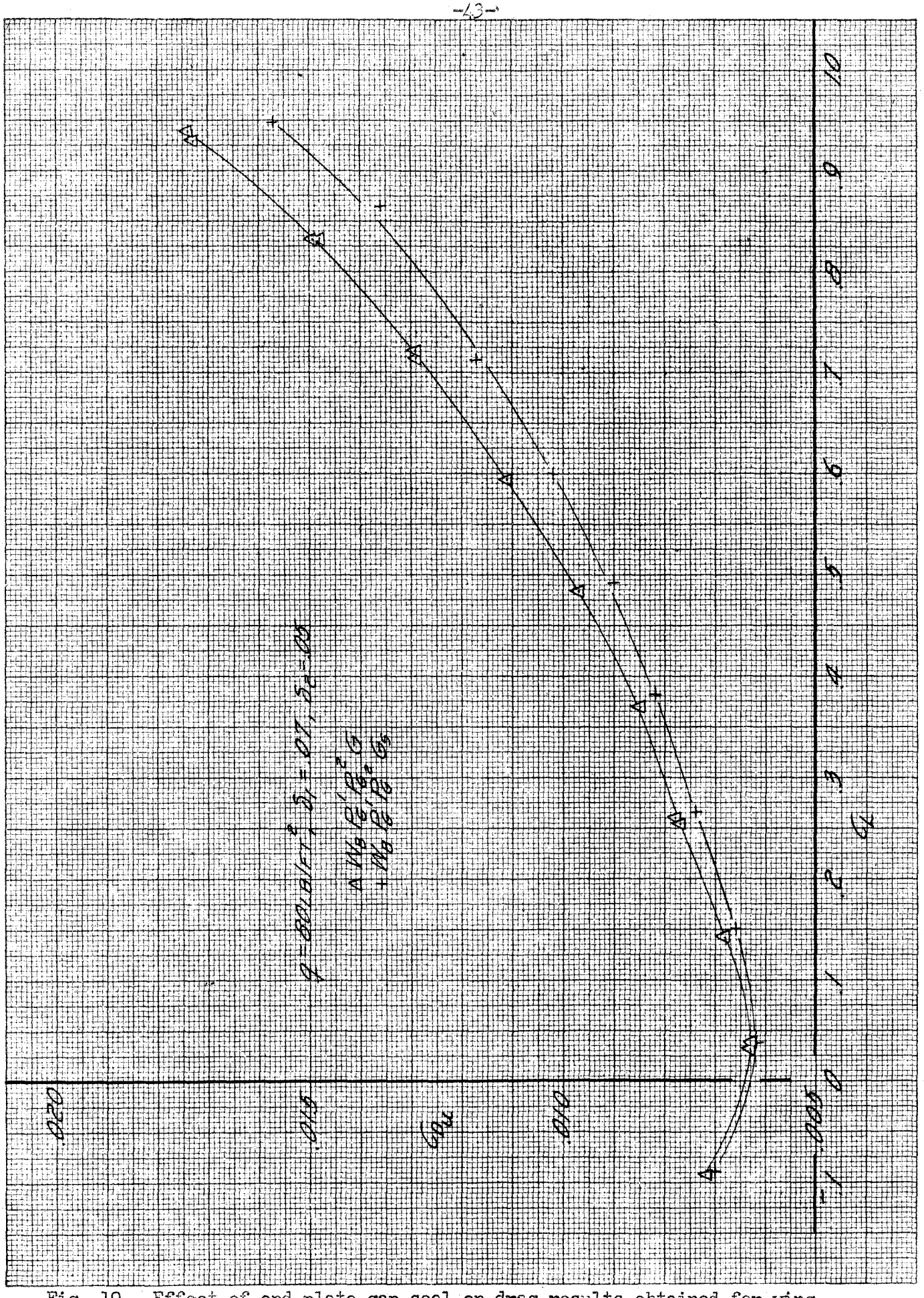

Fig. 19. Effect of end plate gap seal on drag results obtained for wing, q = 80 lb/ft^2

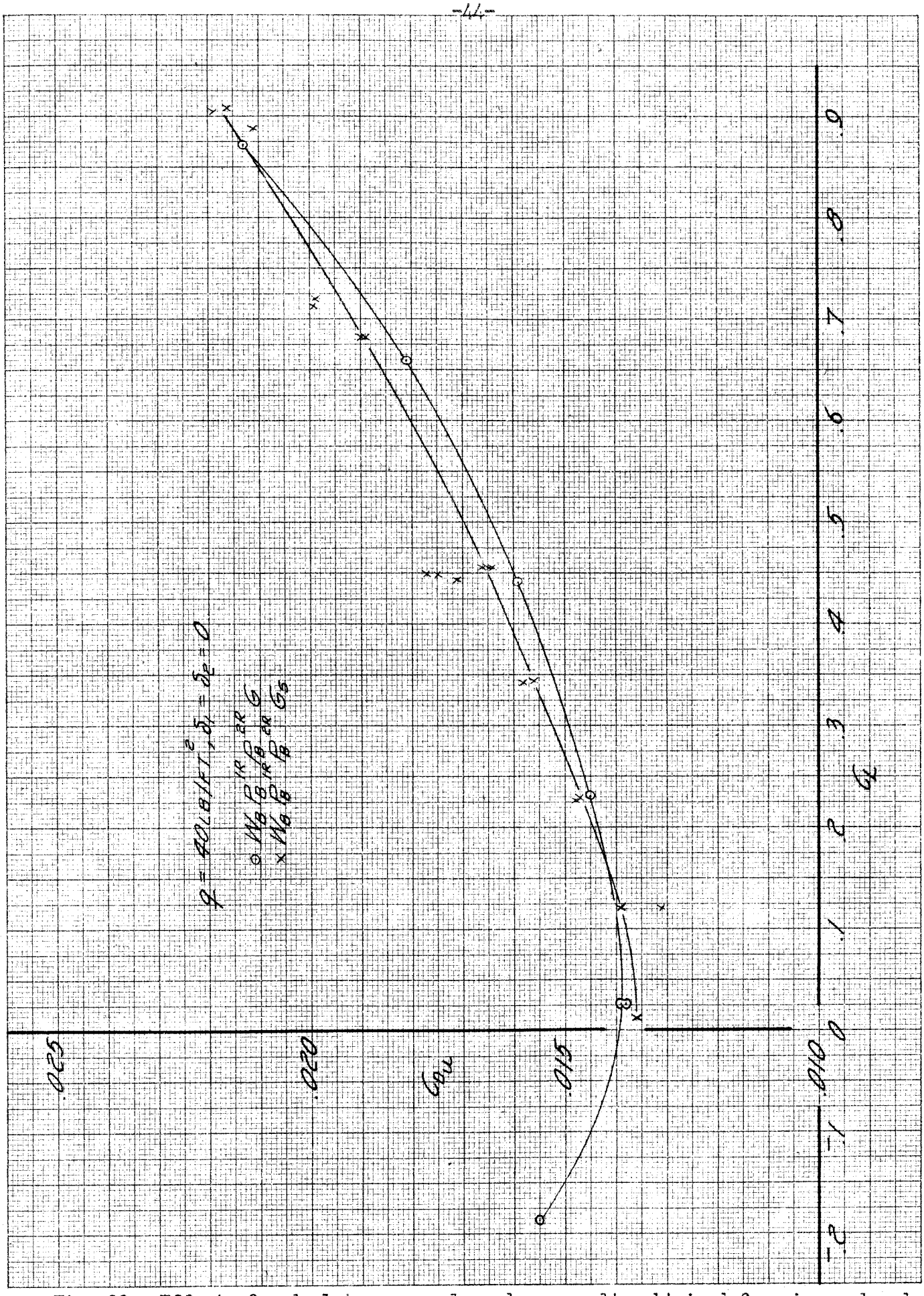

Fig. 20. Effect of end plate gap seal on drag results obtained for wing and end plate, q = 40 lb/ft^2

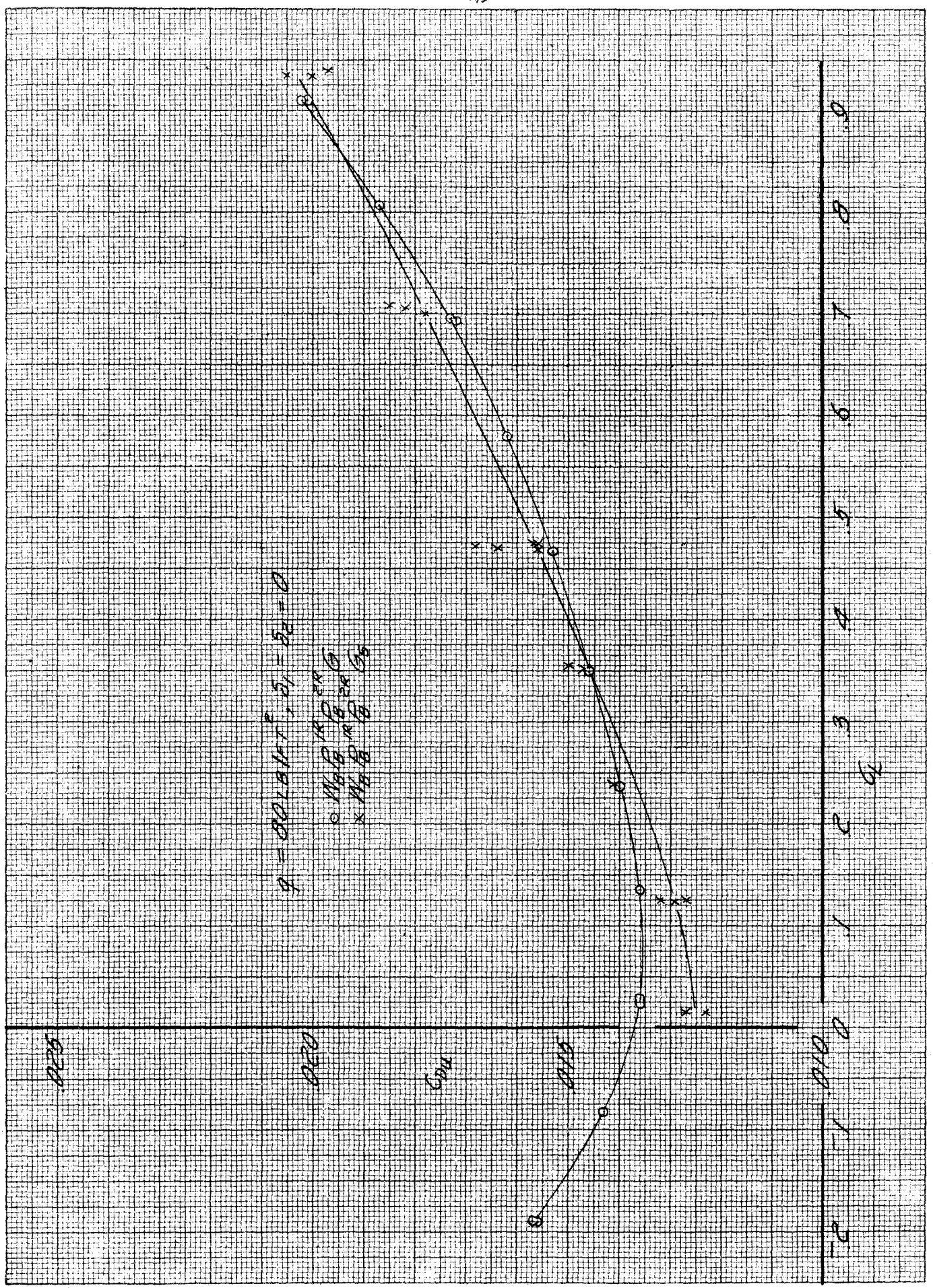

Fig. 21. Effect of end plate gap seal on drag results obtained for wing and end plate, q = 80 lb/ft^2

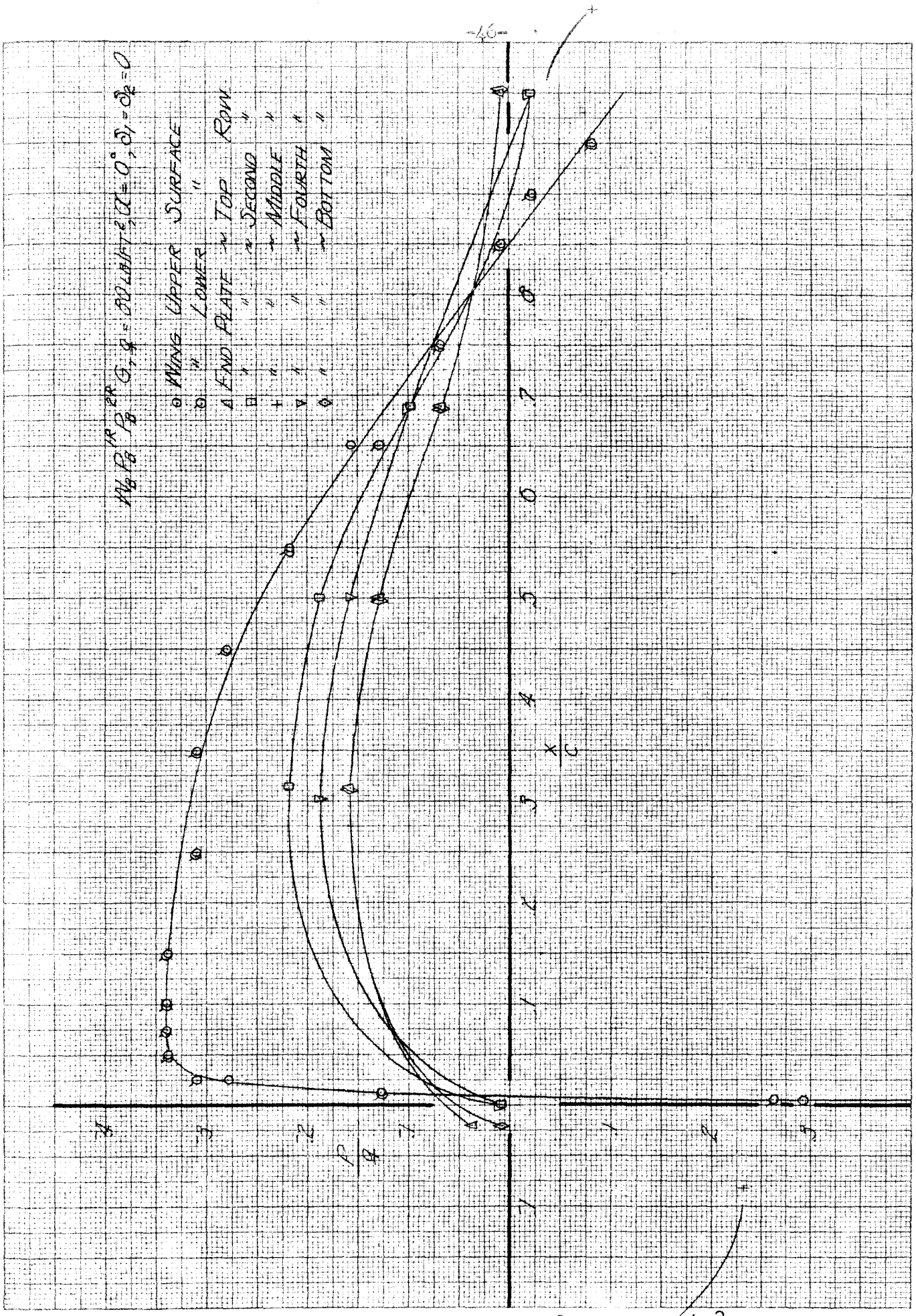

Fig. 22. Pressure field around wing at $\alpha = 0°$, $q = 80$ lb/ft^2

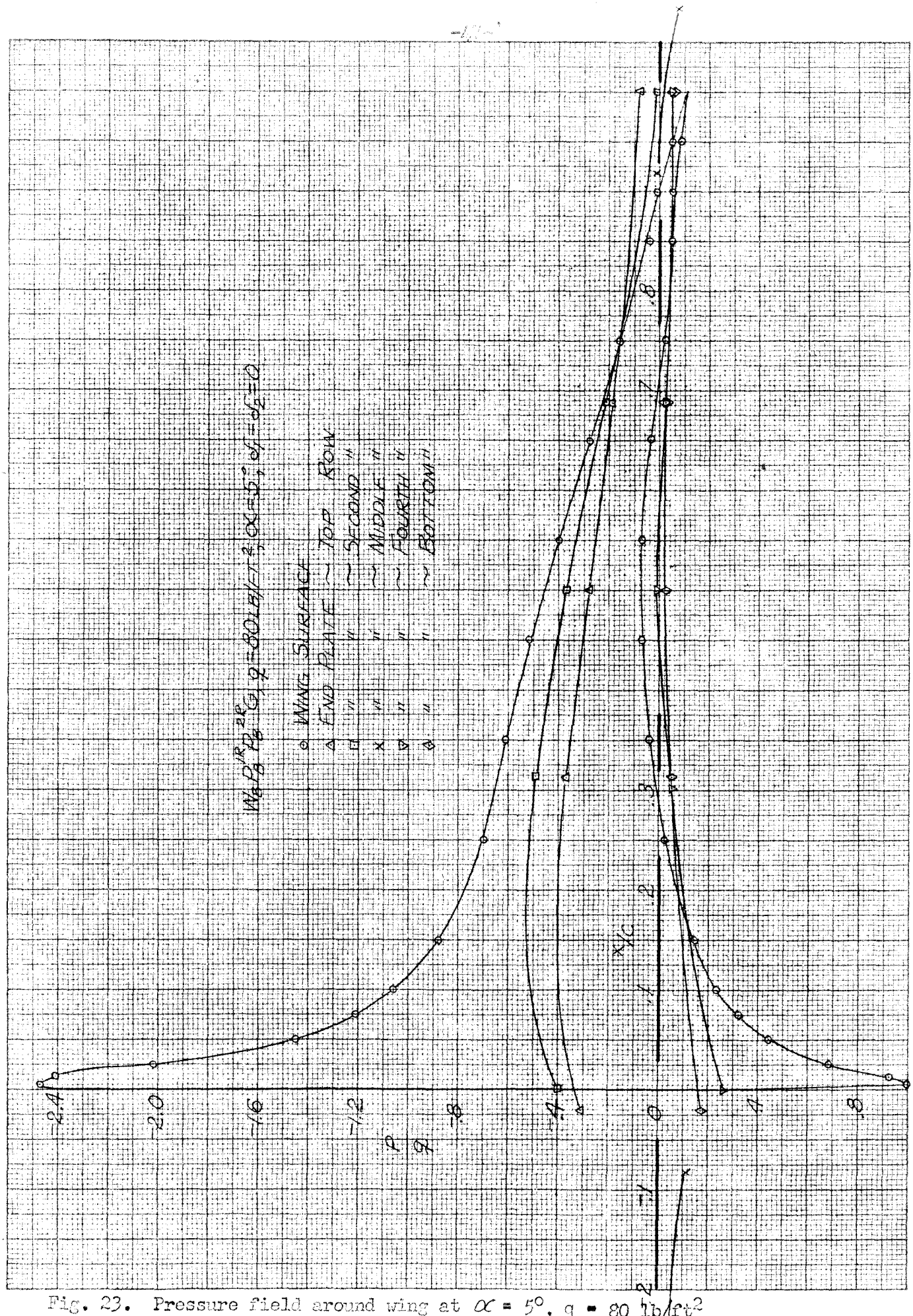

Fig. 23. Pressure field around wing at $\alpha = 5°$, $q = 80$ lb/ft^2

Fig. 24. Pressure field around wing at α = 10°, q = 80 lb/ft^2

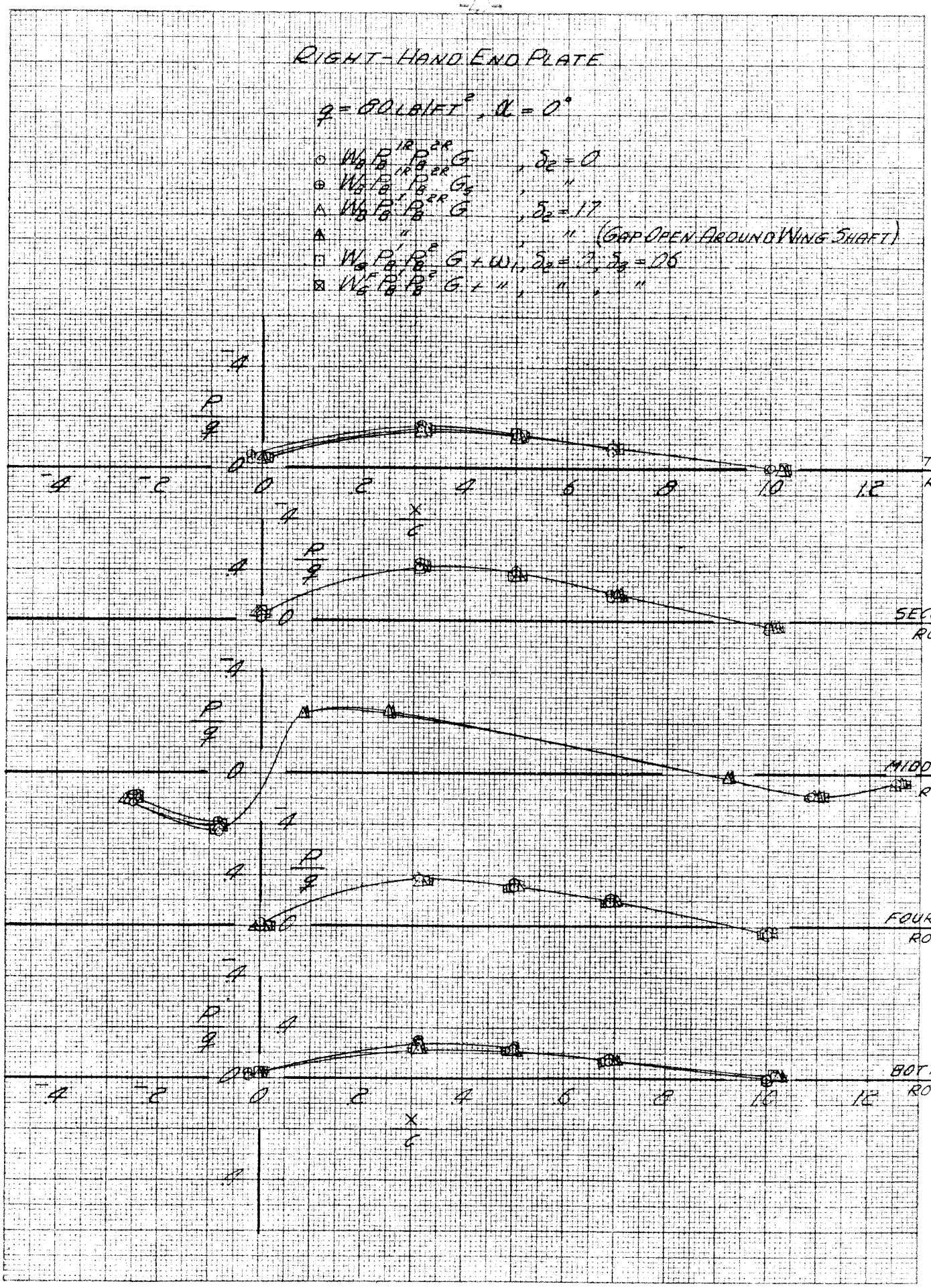

Fig. 25. Effects of end plate shaft seal and other modifications on end plate static pressure distribution; $\alpha = 0^{\circ}$, q = 30 lb/ft^2

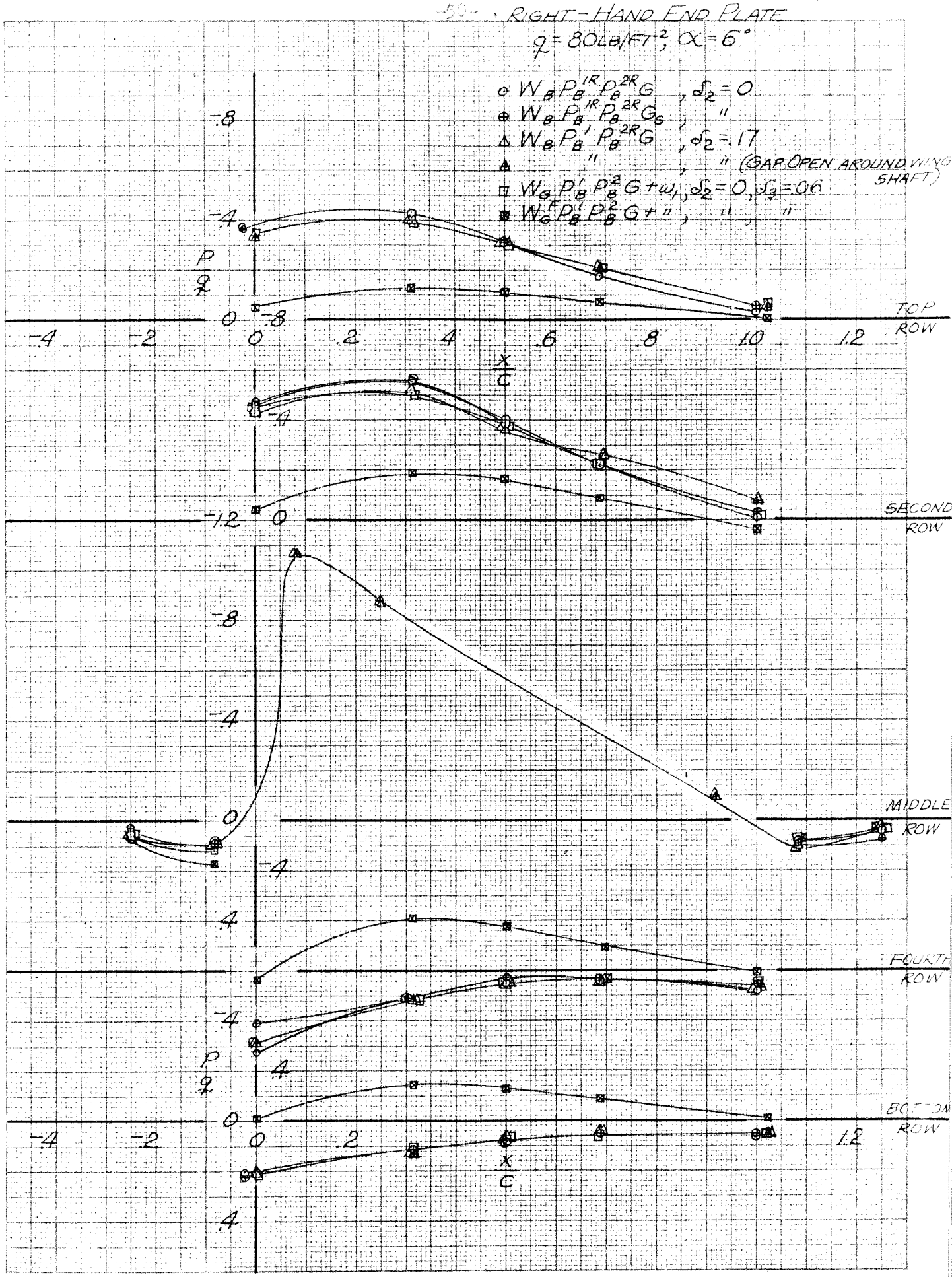

Fig. 26. Effects of end plate shaft seal and other modifications on end plate static pressure distribution; α = 6°, q = 80 lb/ft^2

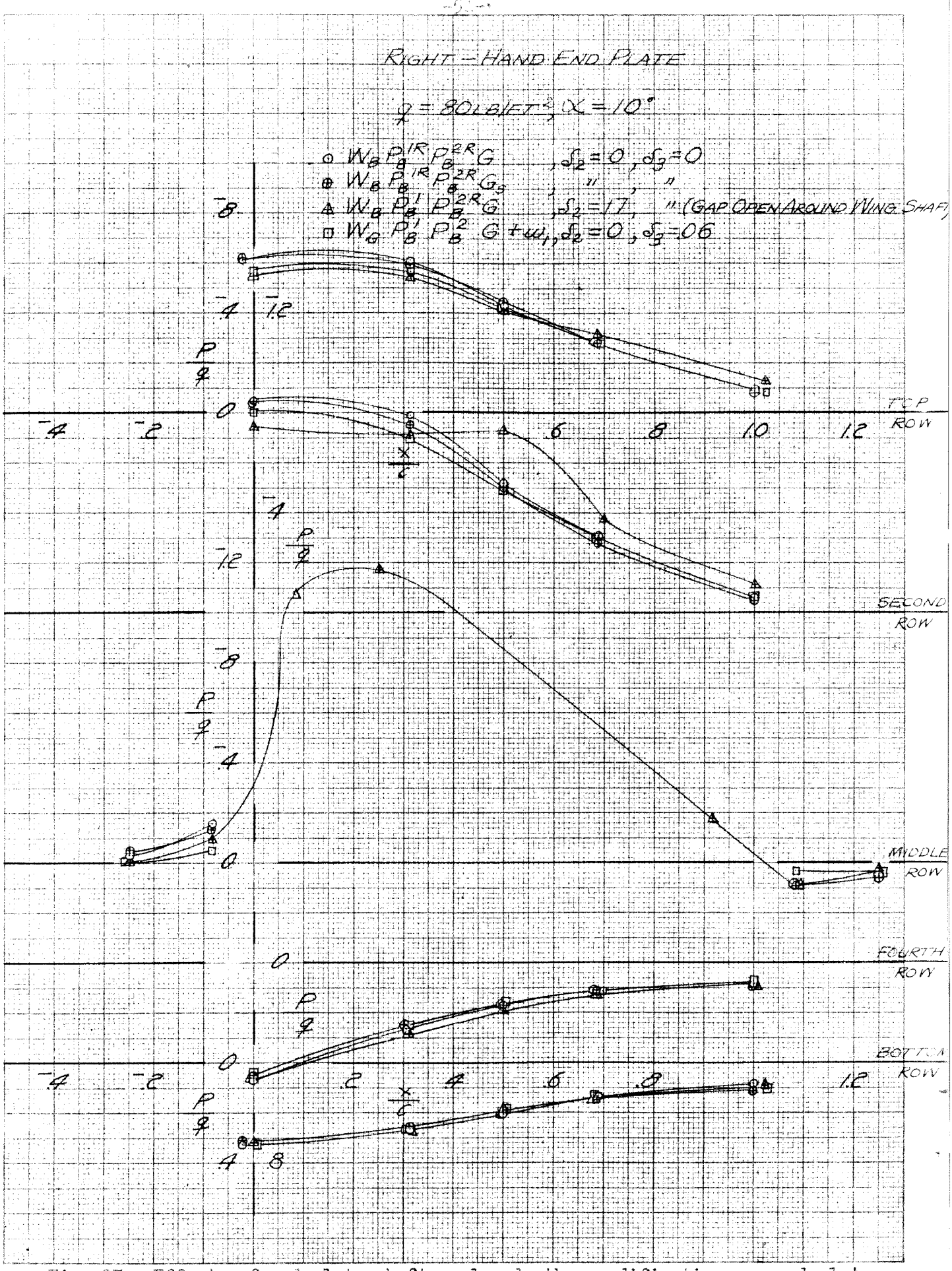

Fig. 27. Effects of end plate shaft seal and other modifications on end plate static pressure distribution; α = 10°, q = 80 lb/ft^2

B. Forces on Portion of Wing in Boundary Layer

Forces on the portion of the wing in the boundary layer were determined by mounting steel templates on the end plate. A clearance gap was left between these templates and the wing. The wing was grounded but followed the motion of the metrical portion of the wing which was mounted on the end plate (i.e. the template). The forces which were measured were those on the end plates and template.

Two different spanwise thicknesses of templates were tested. Both of these templates were completely within the boundary layer on the end plate. Despite the fact that these templates were in the boundary layer and therefore were in a region in which the total head was considerably lower than the free stream total head, they carried a lift load which was in the same ratio to the total lift carried by the wing as the ratio of the template span to wing span (within 3-7%). This was true at both values of dynamic pressure. These results are shown on Figs. 23 to 37 and are tabulated below. Note the expanded scales on some of these plots.

	q=40 lb/ft^2		q=80 lb/ft^2	
	w_1	w_2	w_1	w_2
(1) Template span/wing span	.0122	.0192	.0122	.0192
(2) Incr. in C_L (over results for end plate in presence of wing) due to w_1 or w_2 (per degree)	.0012	.0019	.0013	.0020
(3) $dC_L/d\alpha$ for complete wing (per degree)	.1056	.1058	.1095	.1095
(4) Template lift/wing lift [(2) ÷ (3)]	.0113	.0180	.0119	.0183

This result is in agreement with results which were obtained by pressure measurements made on a two dimensional wing and reported in NACA TN 1244.[5]

It was further determined that the lift which was carried by the portion of the wing in the boundary layer (i.e. the template) was not developed by this portion of the wing but was dependent upon the lift developed by the main portion of the wing. This was determined by setting the wing at zero degree angle of attack and pitching the template through the angle range. Not only did the template no longer develop lift at angles of attack but the induced lift force on the end plate also vanished.

In order to further check the influence of the wing on the template, the gap between the wing and template was varied. Although this gap was increased to as much as 0.31 inch, the lift produced by the main portion of the wing carried across this gap and the template carried the same lift load for all gaps tested (cf. Figs. 34 and 35).

Although the portion of the wing in the boundary layer is carrying its share of lift load, the drag force is almost zero. At the higher dynamic pressure, the templates add only two or three points of drag; at the lower dynamic pressure, the added drag due to the templates is of the same order of magnitude up to an angle of attack of five degrees, beyond which the added drag gets as large as ten points. These results are shown on Figs. 30 and 31.

One thing which is very apparent from the results shown on Figs. 36 and 37 is the critical nature of the wing-template gap with respect to the drag results obtained. Increasing this gap increases the drag of the template by a very considerable amount.

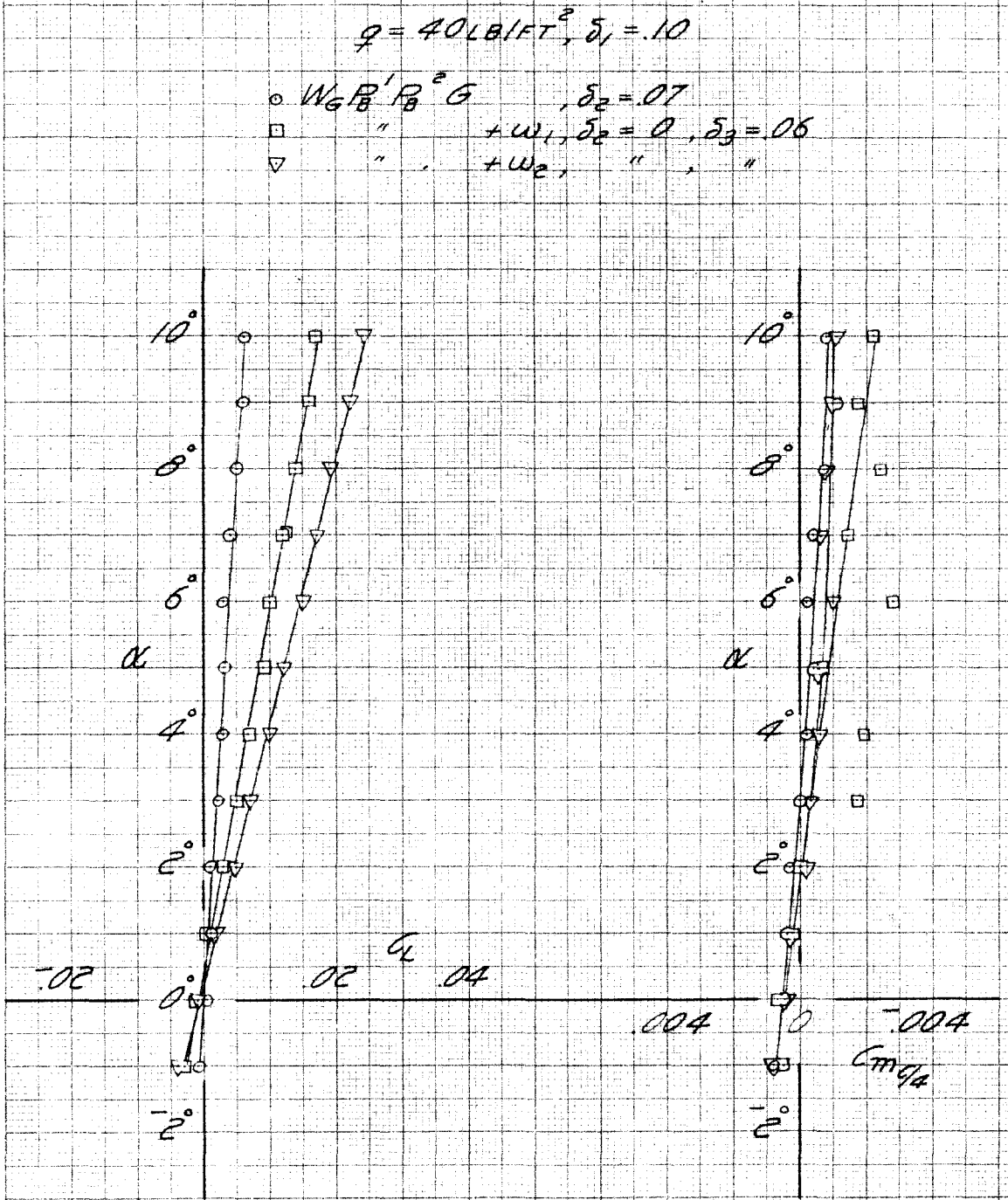

Fig. 28. Lift and pitching moment results obtained with tee plates w_1 and w_2, q = 40 lb/ft^2

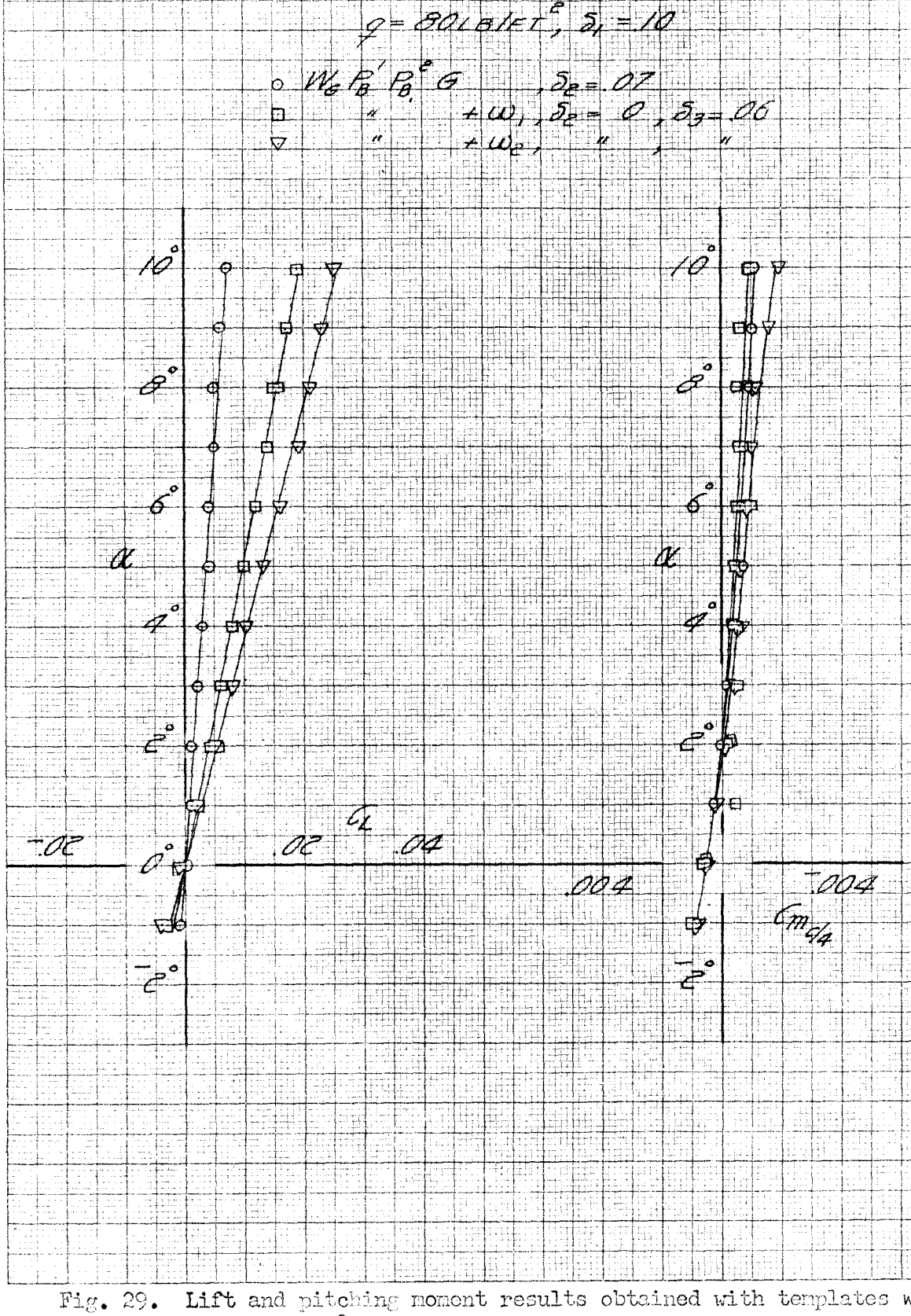

Fig. 29. Lift and pitching moment results obtained with templates w_1 and w_2, q = 80 lb/ft^2

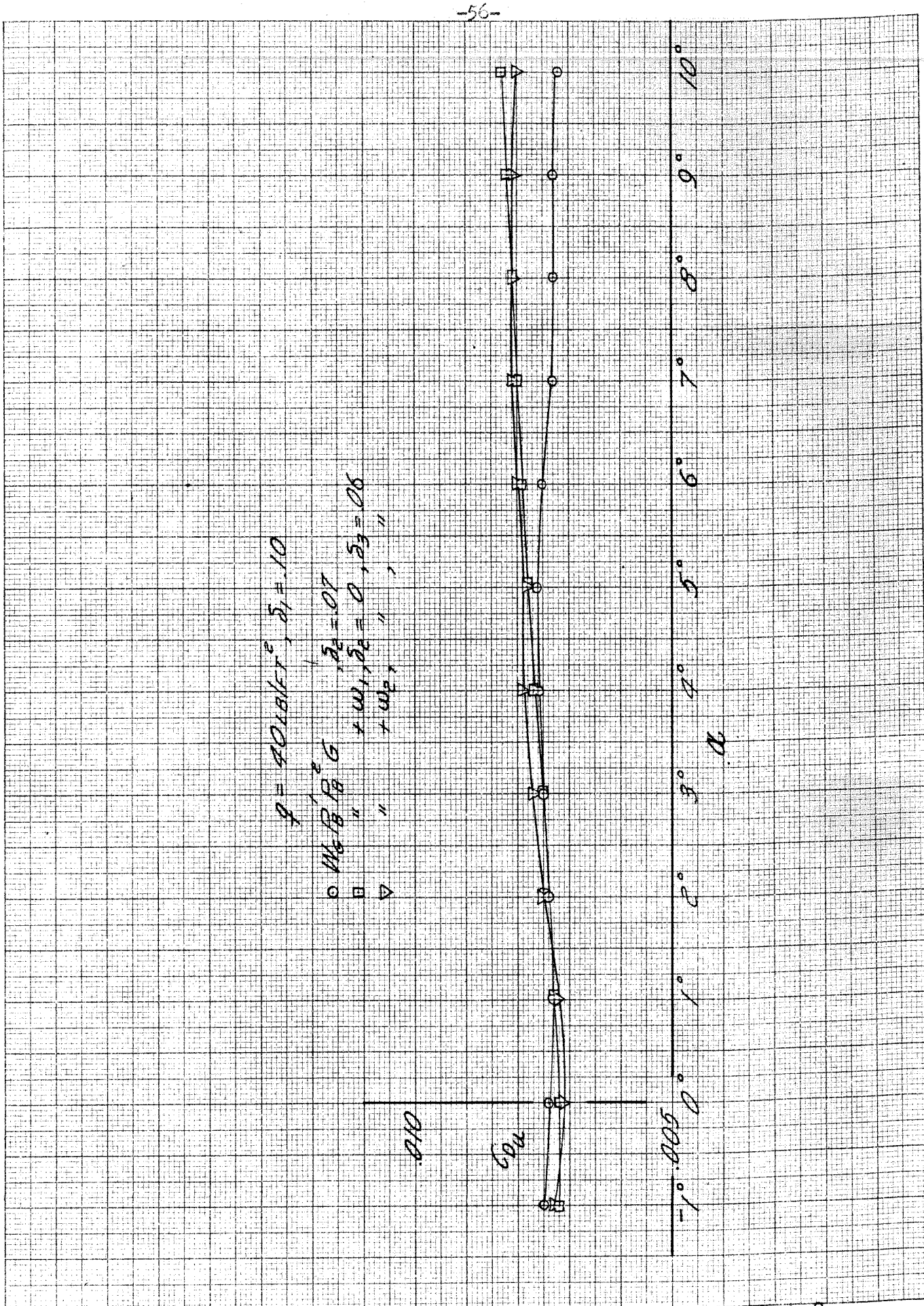

Fig. 30. Drag results obtained with templates, $w_{\perp}$ and w_2, q = 40 lb/ft^2

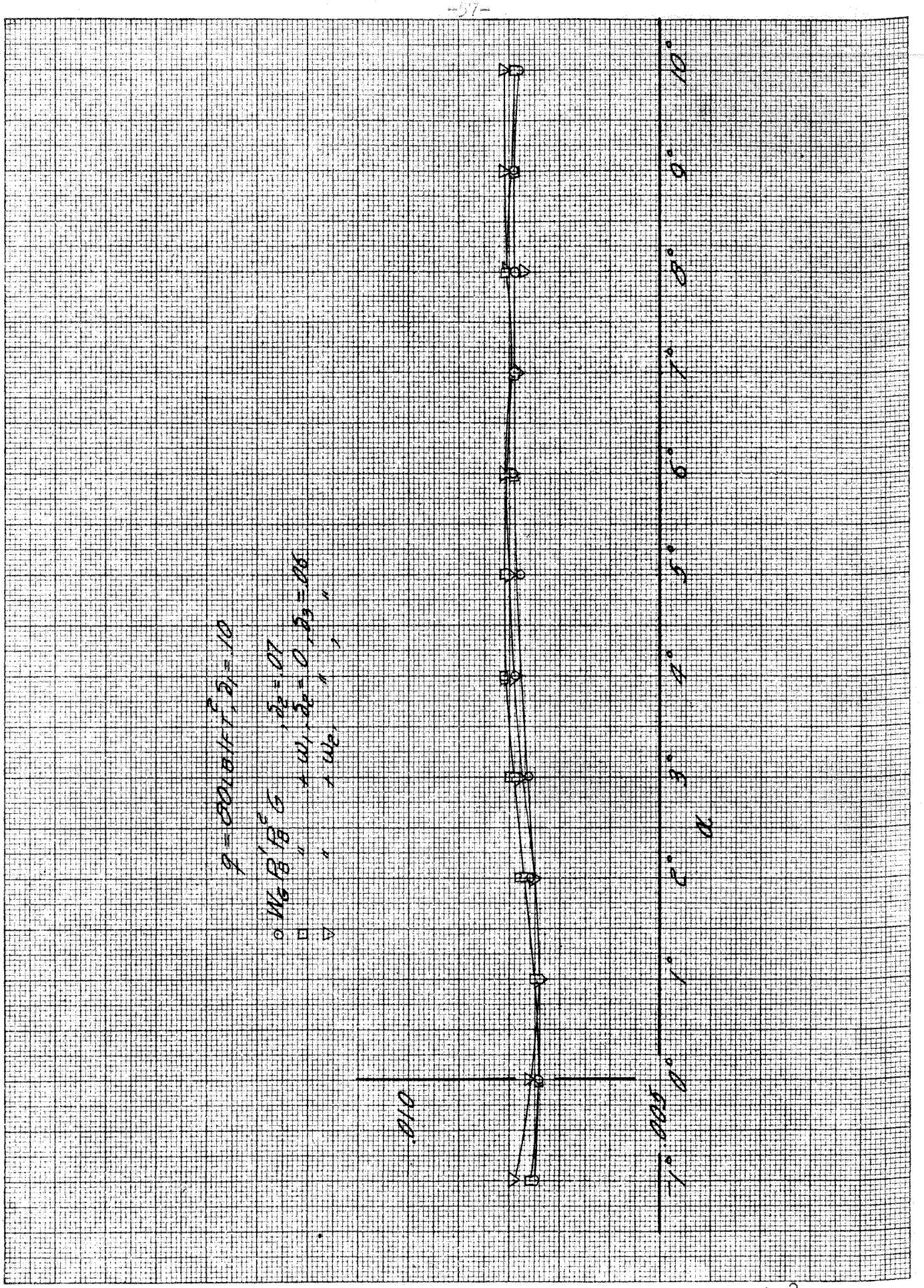

Fig. 31. Drag results obtained with templates w_1 and w_2, q = 80 lb/ft^2

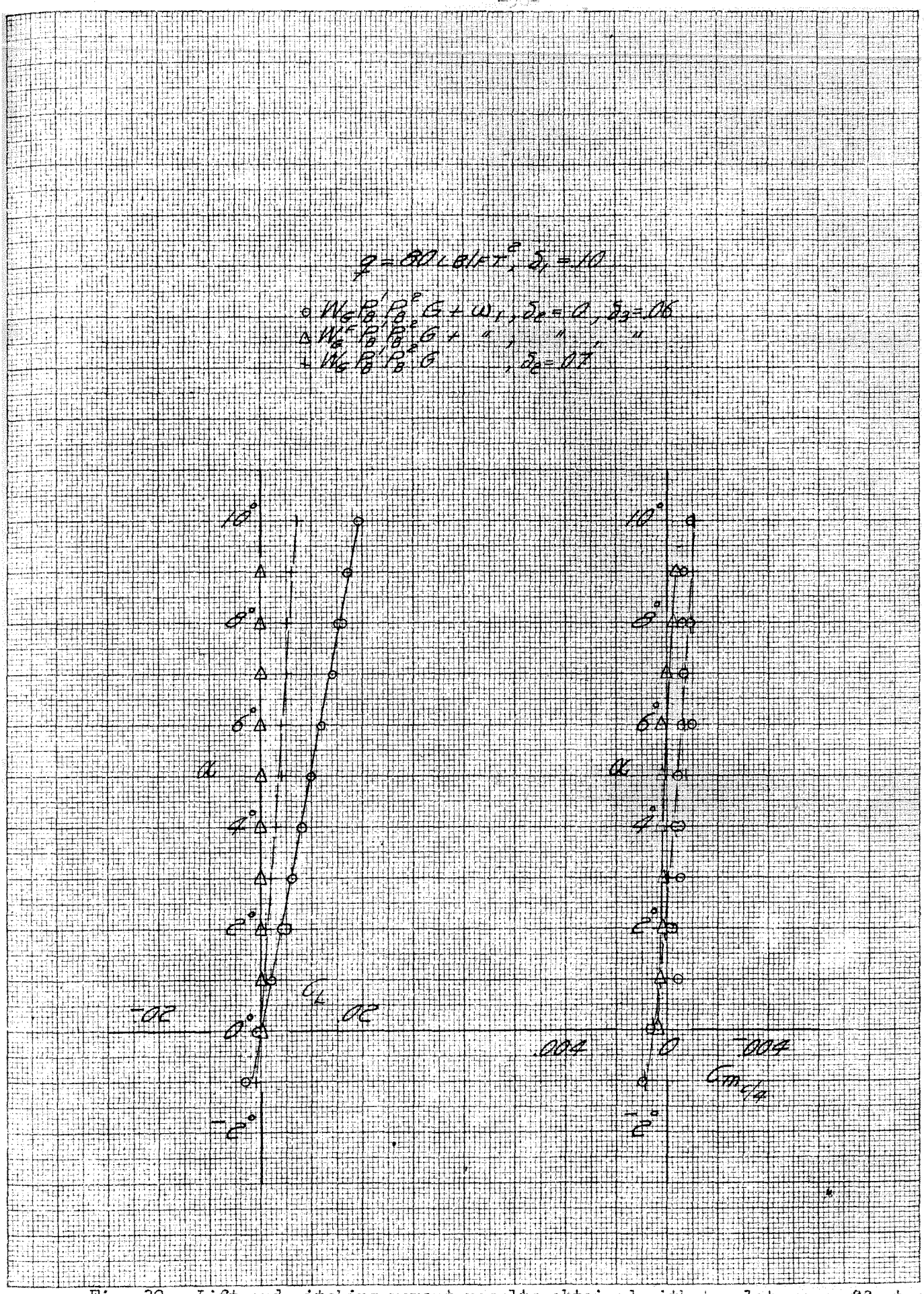

Fig. 32. Lift and pitching moment results obtained with template w_1; effect of holding angle of attack of main portion of wing at 0°; q = 80 lb/ft^2

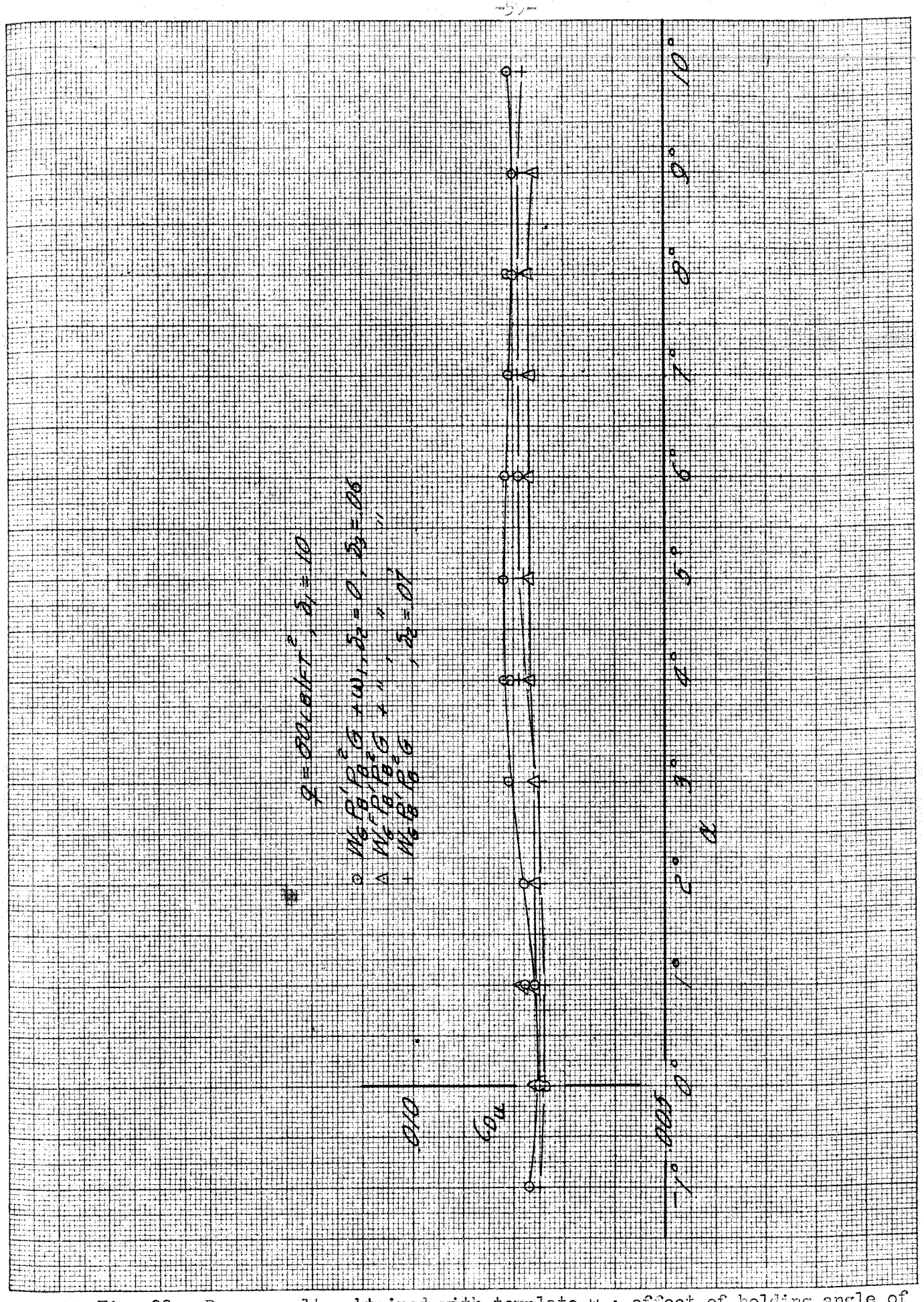

Fig. 33. Drag results obtained with template W_1; effect of holding angle of main portion of wing at 0°, q = 80 lb/ft^2

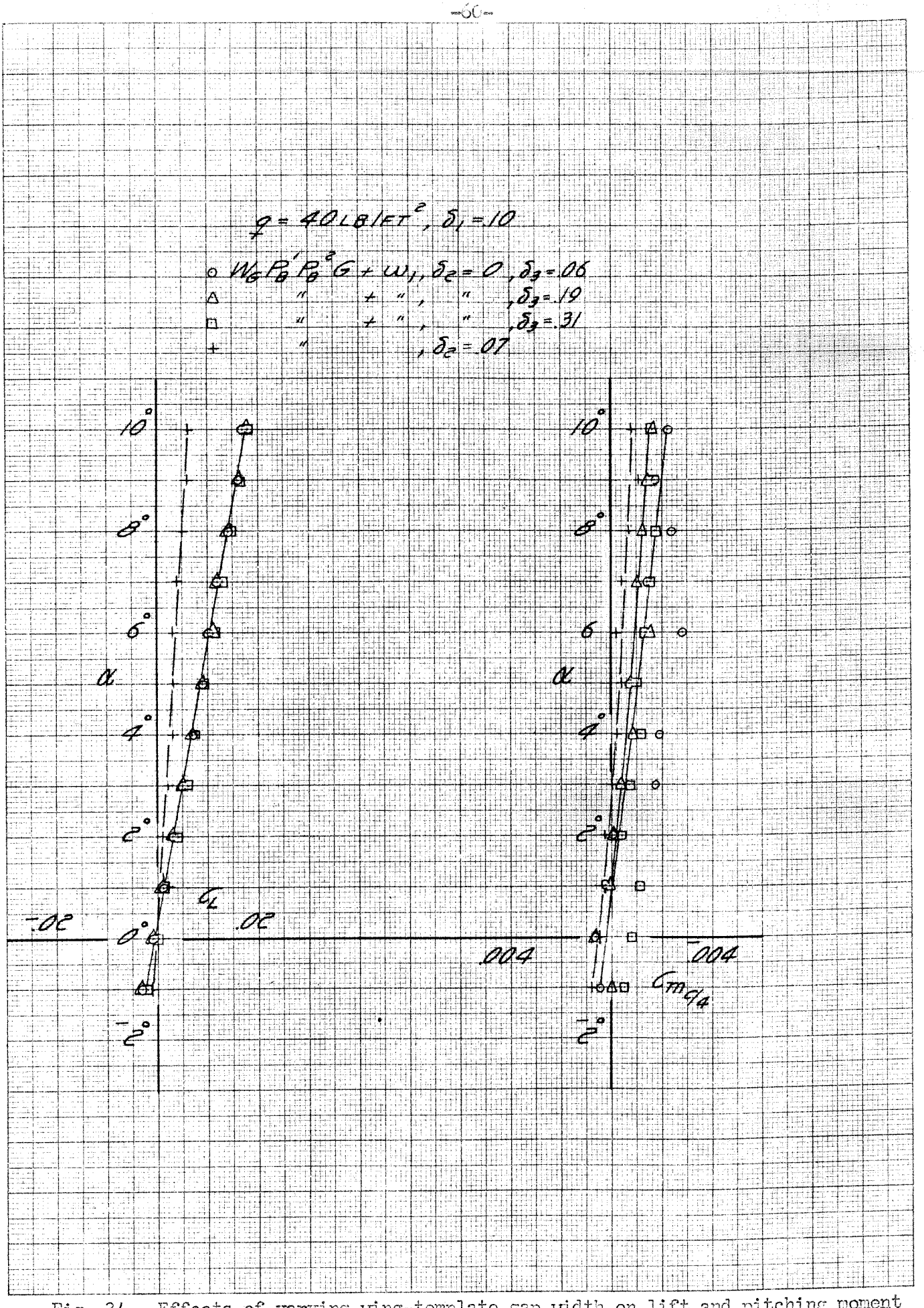

Fig. 34. Effects of varying wing-template gap width on lift and pitching moment results obtained for template W_1, q = 40 lb/ft^2

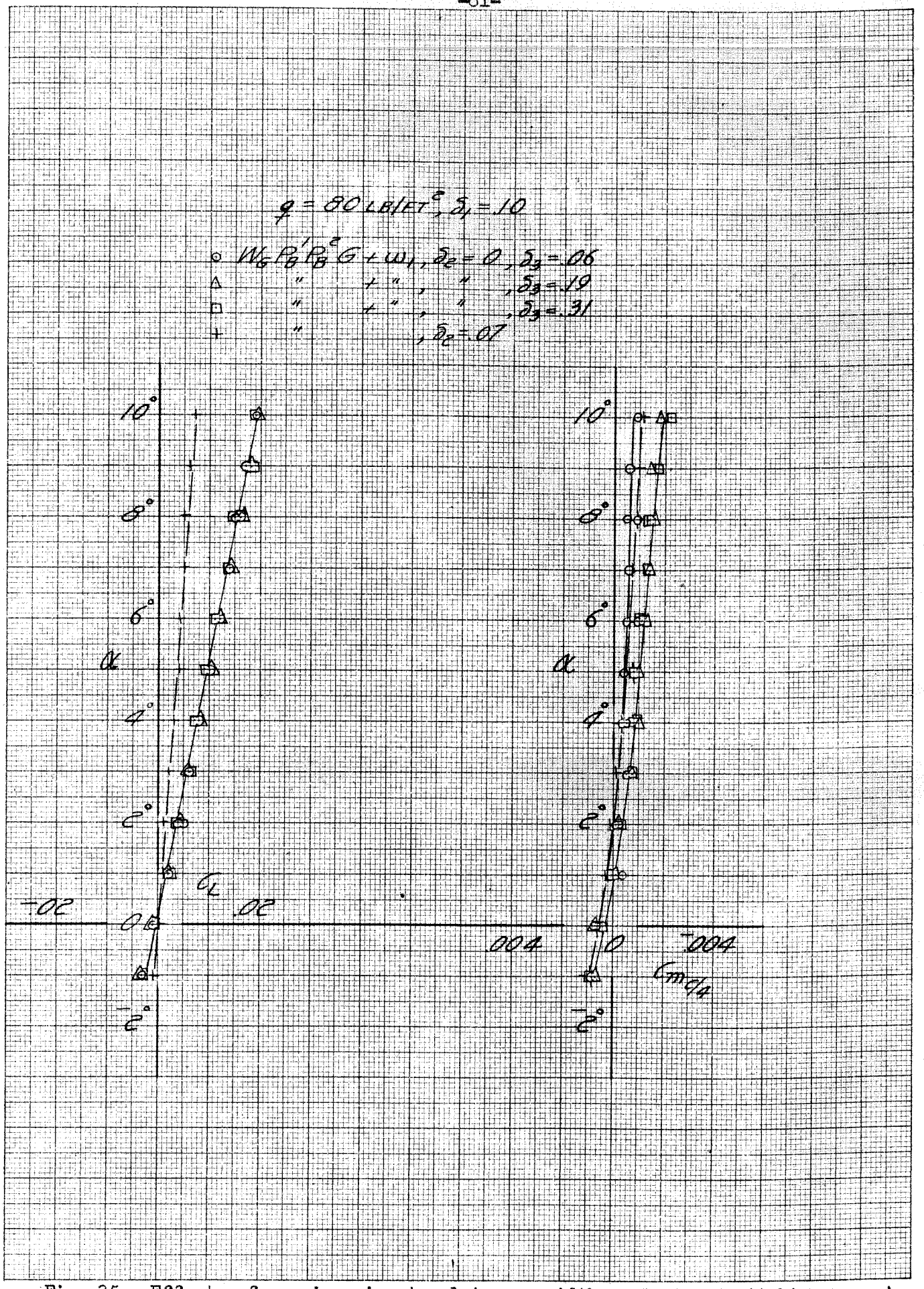

Fig. 35. Effects of varying wing-template gap width on lift and pitching moment results obtained for template W_1, q = 80 lb/ft^2

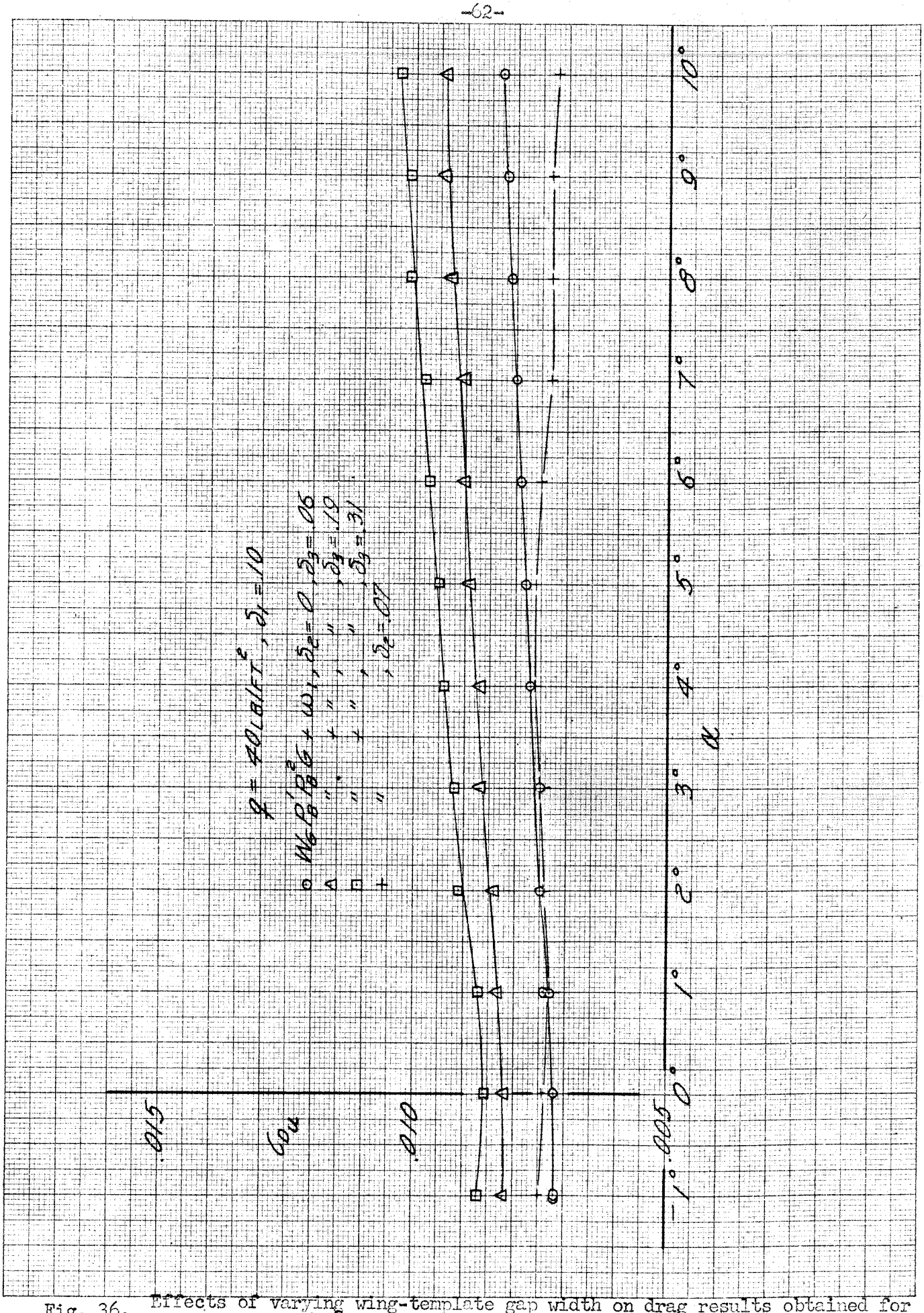

Fig. 36. Effects of varying wing-template gap width on drag results obtained for w_1, q = 40 lb/ft^2

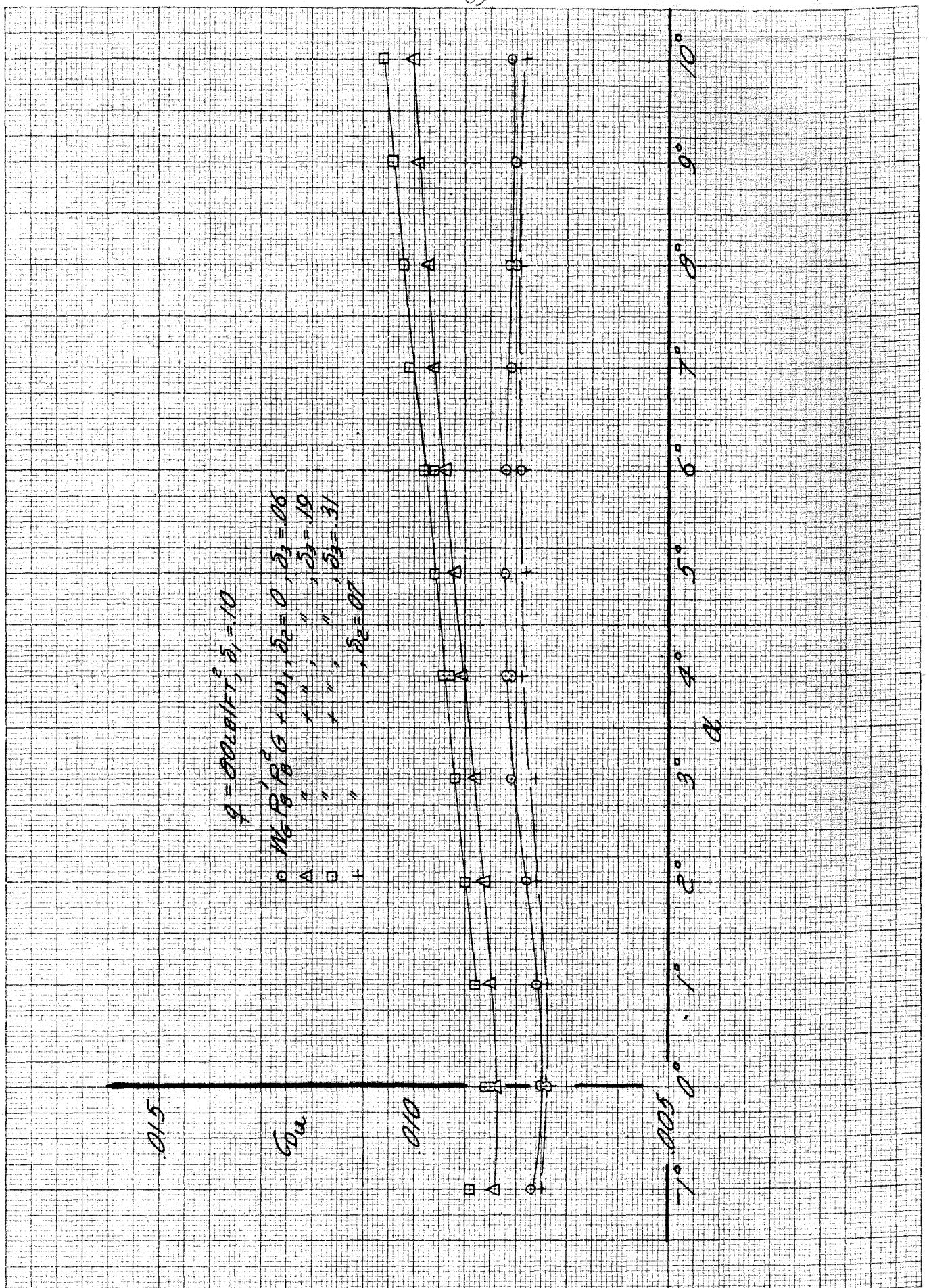

Fig. 37. Effects of varying wing-template gap width on drag results obtained for W_1, q = 80 lb/ft^2

C. Effects of Gaps Between Wing and End Plate

1. Effects of Wind-End Plate Gaps, δ_1 and δ_2 and of Reversing End Plates

The data which are plotted on Figs. 38 to 42 show the effects of wing-end plate gaps δ_1 and δ_2 and the effect of reversing the end plates. No distinguishable change is observed in the pitching moments due to either the gaps or reversing the end plates. The lift curves at the lower dynamic pressure also are unaffected by these changes. At the higher dynamic pressure, the gaps cause a very slight decrease in the slope of the lift curve. The reversal of the end plates causes a slightly larger decrease in lift slope than did the gaps. These end plates were fitted with model mounting plates as shown on Fig. 3. The mounting plates did not present as smooth a surface as the rest of the end plate. The loss in lift associated with the reversal of the end plates was probably due to the insertion of the less smooth portion of the end plate in the windstream ahead of the wing-end plate junction.

Reversing the end plates increased the drag by an amount which remained almost constant over the angle range. This increase in drag was of the order of ten drag points at either dynamic pressure. The wind-end plate gaps also increased the drag. The increase due to the gap was not constant however, but increased almost linearly with increasing lift coefficient. Since the increase varies as the first power of C_L and not as the second power of C_L (as it would if it were an induced effect), the increase in drag is probably the combination of an induced effect and the effect of the airflow through the wing-end plate gaps. The increase in drag due to the reversal of the end plates was due to the previously described roughness of the end plates ahead of the wing when the end plates were reversed.

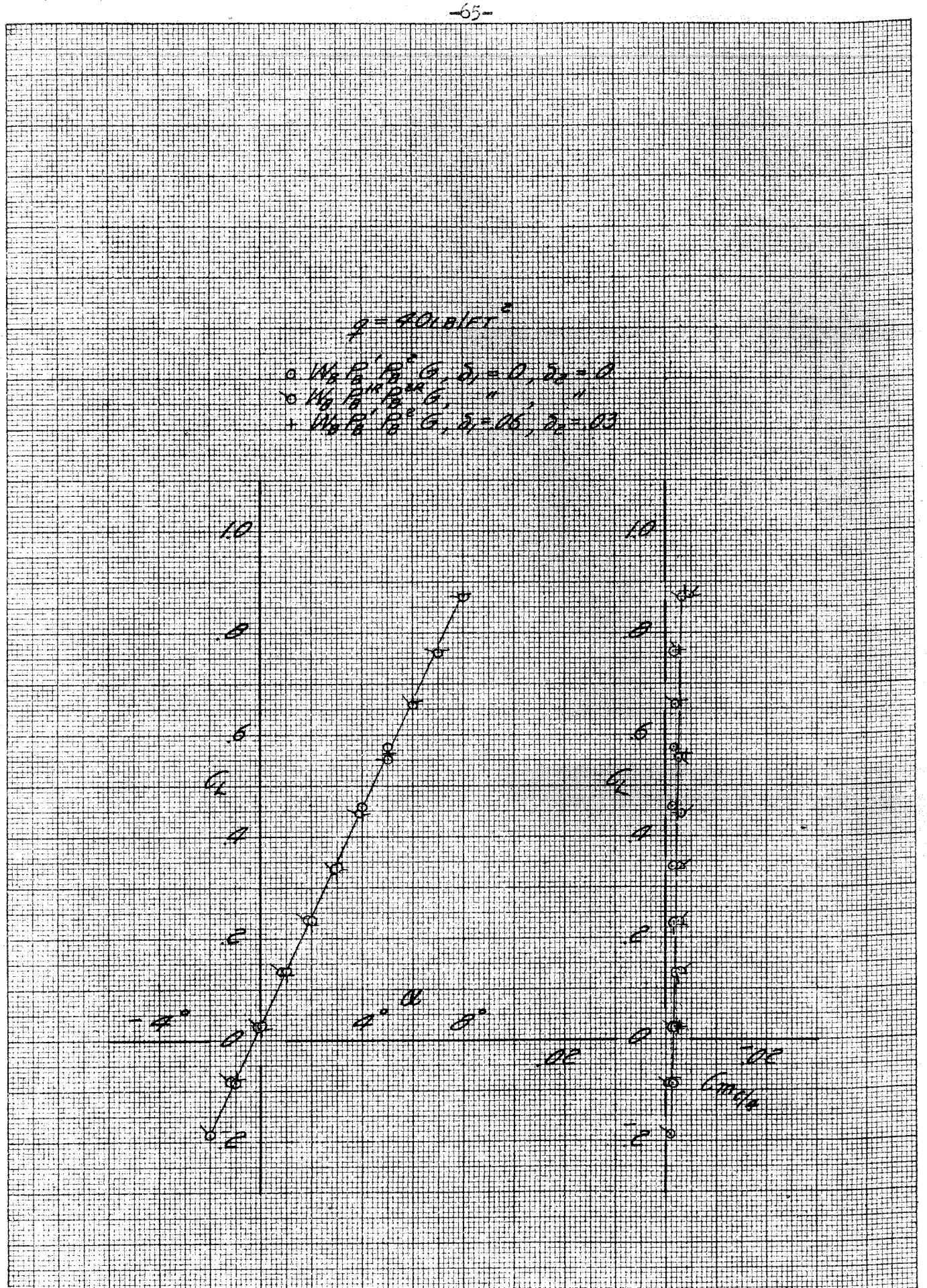

Fig. 38. Effects of wing-end plate gaps δ_1 and δ_2 and of reversing end plates on lift and pitching moment results, q = 40 lb/ft^2

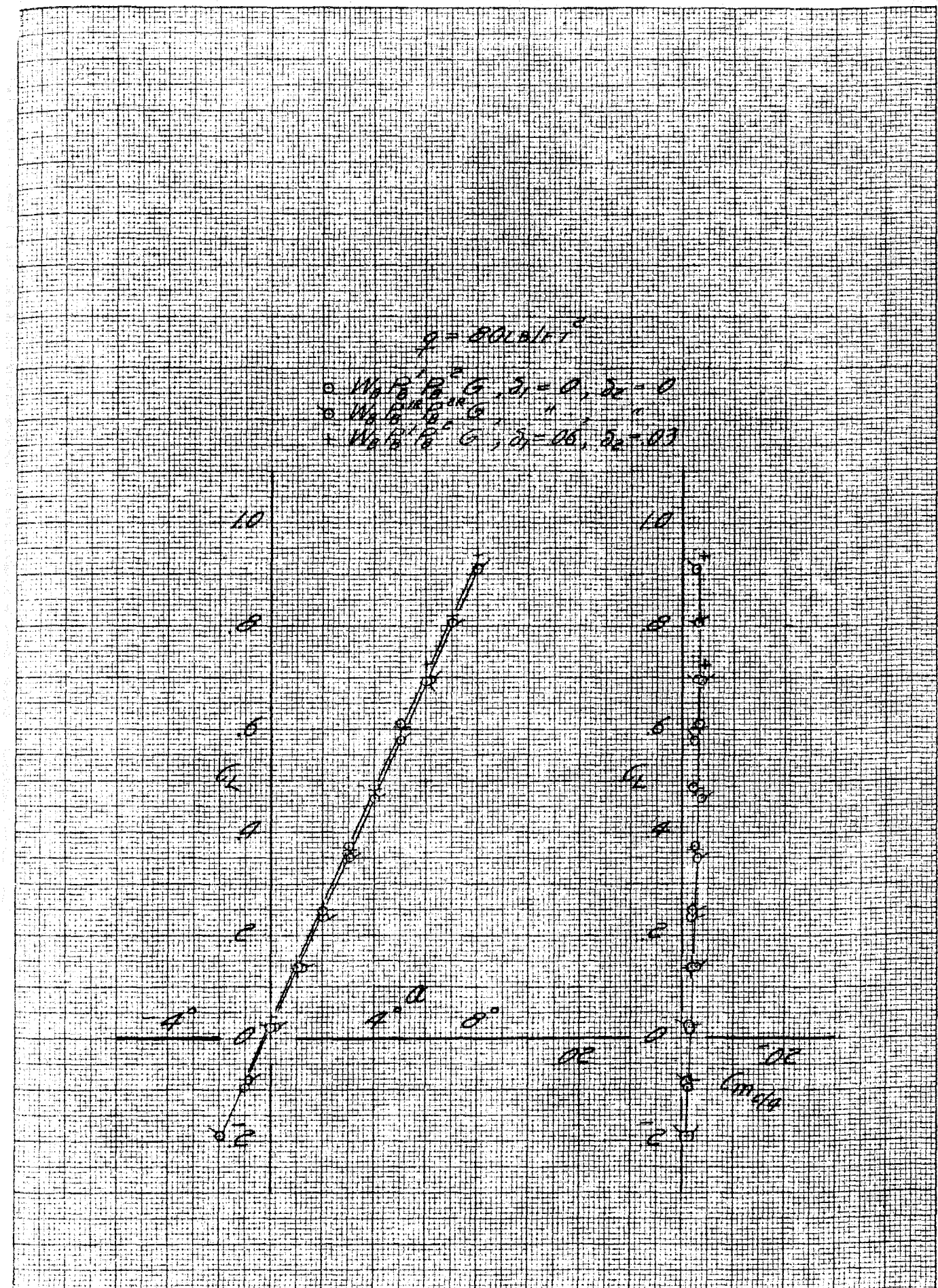

Fig. 39. Effects of wing-end plate gaps δ_1 and δ_2 and of reversing end plates on lift and pitching moment results, q = 80 lb/ft^2

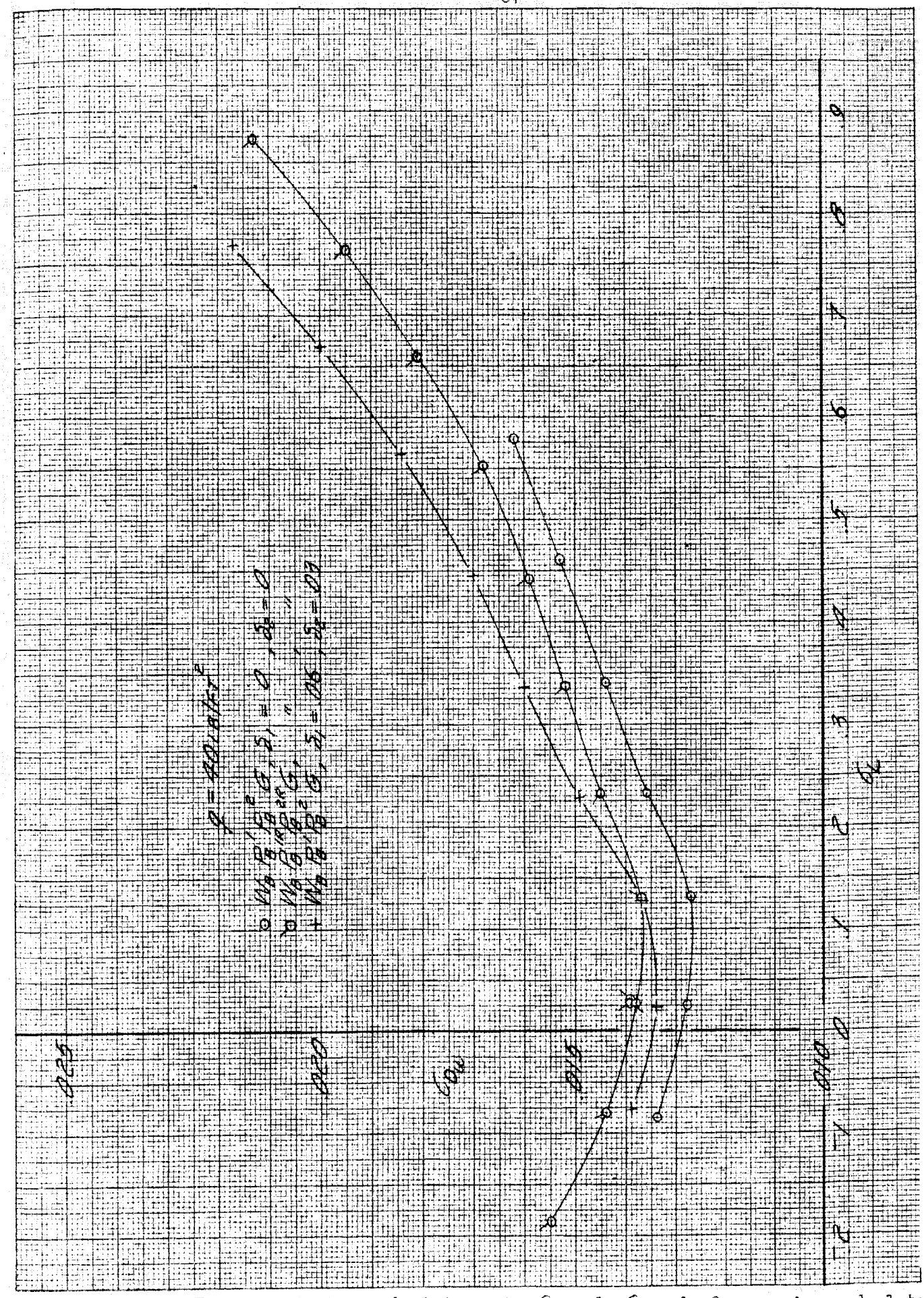

Fig. 40. Effects of wing-end plate gaps δ_1 and δ_2 and of reversing end plates on drag results, q = 40 lb/ft^2

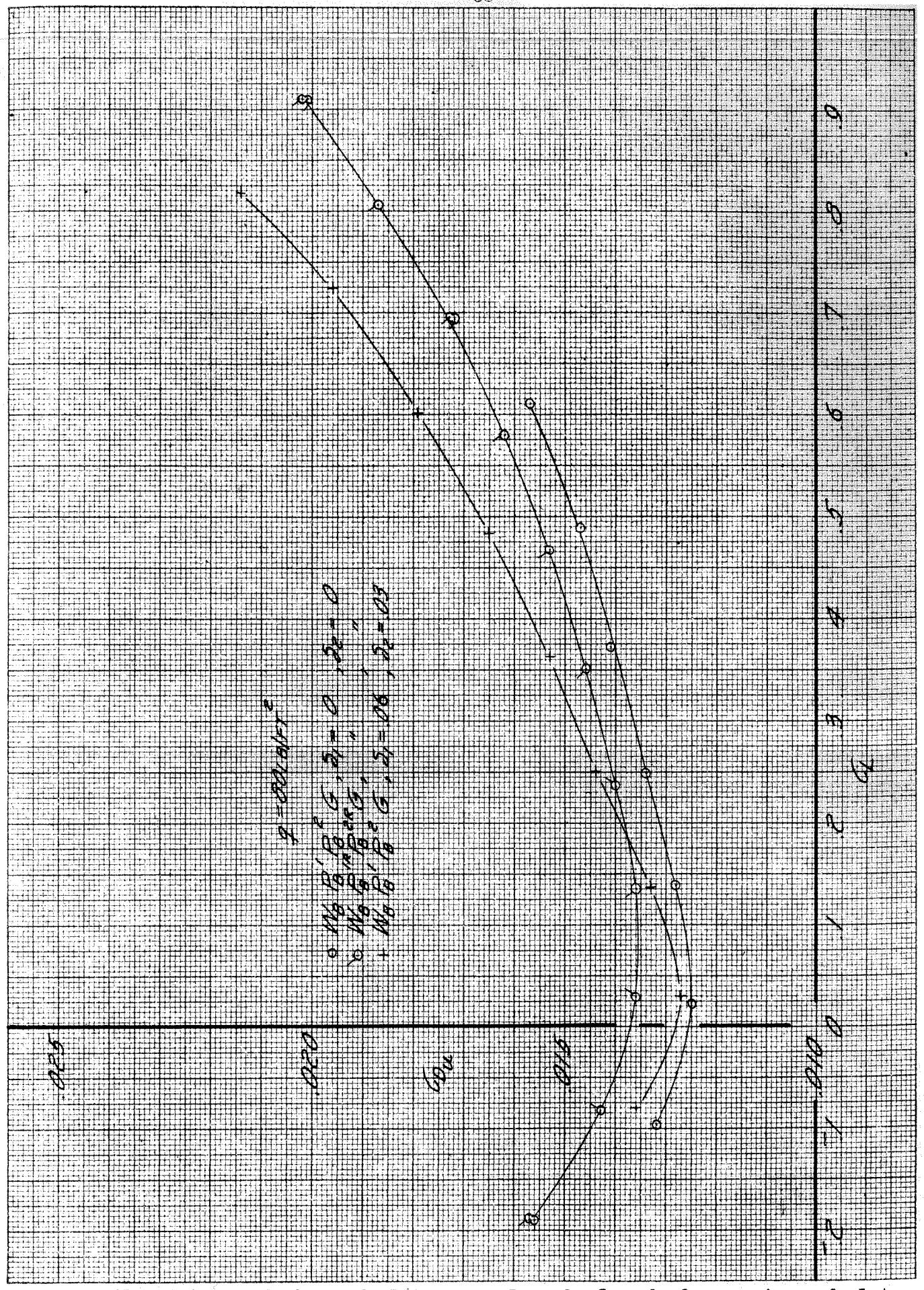

Fig. 41. Effects of ring-end plate gaps δ_1 and δ_2 and of reversing end plates on drag results, q = 80 lb/ft^2

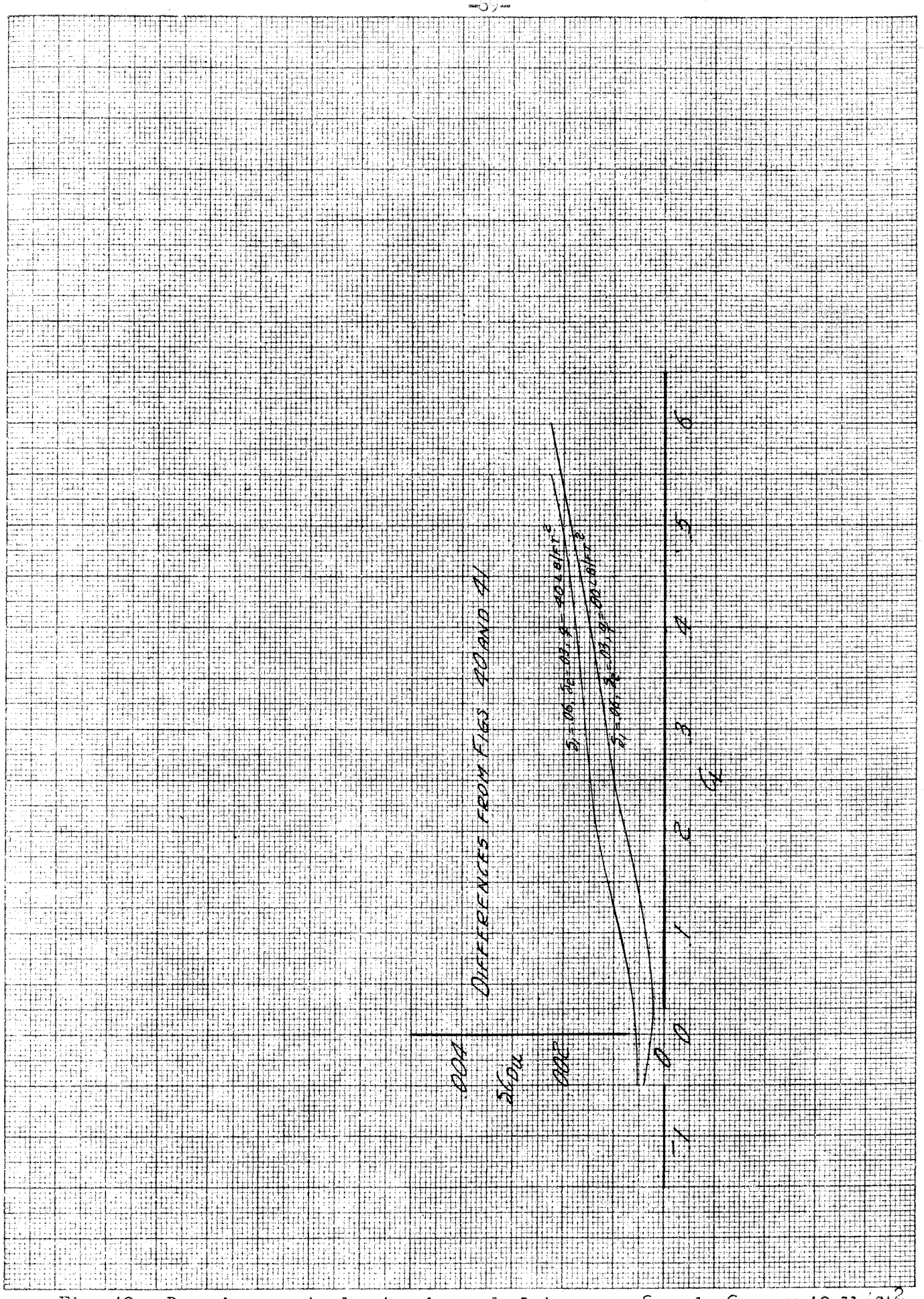

Fig. 42. Drag increments due to wing-end plate gaps δ_1 and δ_2, q = 40 lb/ft^2 and 80 lb/ft^2

2. Effects of Wing-End Plate Gap, δ_2

Figures 43 to 59 contain the results obtained during the investigation to determine the effects of varying the wing-end plate gap width. These results are plotted in a normal manner using normal scales; in addition numerical differences were obtained from the experimental data and these numerical differences (δC_L and δC_m) have been plotted to greatly expanded scales to show the effects of gap width. The results indicate a decrease in lift curve slope with increasing gap width and a slight increase in stability with increasing gap width. The increase in stability is of the order of $\frac{1}{2}\%$ for the largest gap tested. These results are consistent at both dynamic pressures. The decrease in lift curve slope and increase in pitching moment slope are due, of course, to the flow through the gap which acts to equalize the pressure on the top and bottom surfaces of the wing. Removing the seal between the wing shaft and end plate had no effect on the lift or pitching moment results.

The effect of the wing-end plate gap variation on the drag results is summarized on Figs. 49 and 50. These figures indicate a large increase in drag with increase in gap width. The drag increment for the smallest gap flattens out at a constant value at the higher C_L's. As the gap width increases the curves diverge from a linear curve and tend toward the shape of a curve of power two. This indicates that for the smaller gaps, the increase in drag is due partly to an induced effect and partly to the flow through the gap and over the wing shaft. As the gap is increased, the induced portion becomes larger and larger and the drag increment curve approaches the curve which would be obtained if the drag were completely induced. Note that the increase in drag at zero lift is very small for all gaps tested.

Static pressure distribution measurements were taken at the same time the wing-end plate gap was being varied. The pressure orifices were located at the mid-span position of the wing (i.e. about 18 inches from the gap). The results obtained at q = 80 lb/ft^2 and α = 5° are presented on Fig. 51. No consistent variation of pressure distribution was obtained with change of gap width. It is felt that the differences on this curve, since they are small, are due to the experimental errors involved in recording and reducing the data.

End plate static pressure data are presented on Figs. 52 to 59. The wing-end plate gap, δ_2 was located at the right-hand end plate and this end plate should show the effect of varying the width of this gap. Static pressure data for the left-hand end plate are also presented for comparison purposes. The middle row of orifices exhibits a very large change with increasing gap. The static pressure peak on this row reaches a higher negative pressure peak as the gap is increased and the influence of the negative pressure peak on the wing becomes more effective on this row. Note that the increase in gap width allows a greater flow through the gap and this flow acts to equalize the pressure on the top and bottom surfaces of the wing, especially in the regions of the peak pressure. This was previously mentioned in explaining the change in lift and pitching moment due to the wing-end plate gap.

The pressure peak which occurs on the second row of orifices at x/c=0.5 at both dynamic pressure with gap δ_2 = 0.29 and α = 10° is due to the flow around the wing shaft. The wing shaft is located at the 50% chord position of the wing. From potential flow theory, it is determined that the pressure coefficient P/q due to the flow pasta cylinder is given by:

$$\frac{P}{q} = -\frac{2}{\left(\frac{r}{a}\right)^2} - \frac{1}{\left(\frac{r}{a}\right)^4} \qquad \text{(for } C_L \text{ on shaft = 0)}$$

where: r = distance from center of cylinder to point on line perpendicular to flow direction

a = radius of cylinder

For the wing shaft $\frac{r}{a} = 1.9$ at $\frac{x}{c} = 0.5$ on second row

$\frac{P}{q} = -0.197$ (If dynamic pressure past cylinder is taken as free stream value)

Although pressure terms are not additive and it would be necessary to work with the velocity terms and then convert back to pressure, it can be seen that the change in pressure is of the right order of magnitude. This indicates that the flow through the gap at this angle of attack approaches the free stream value for a gap width of 0.29 inches.

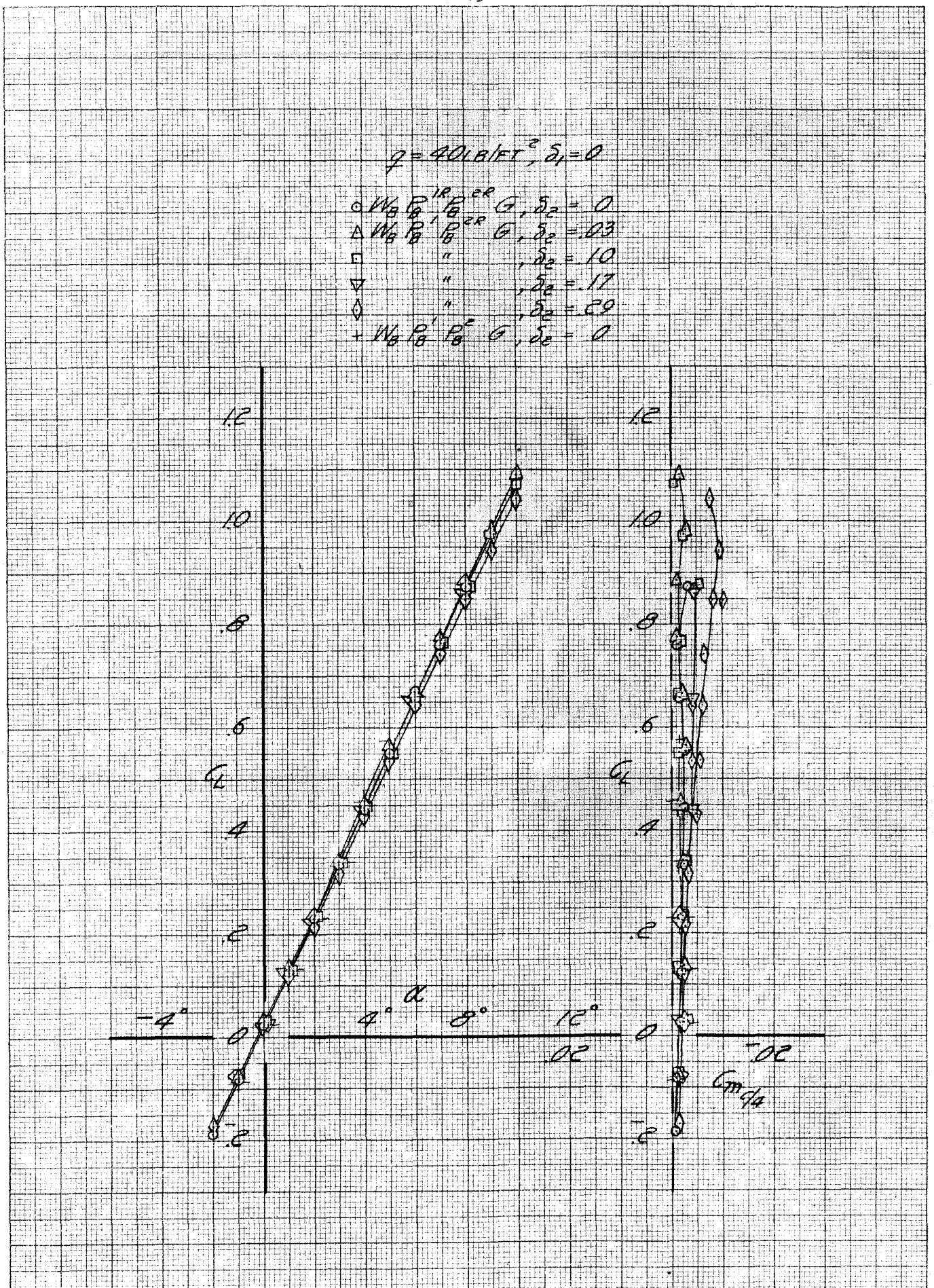

Fig. 43. Effects of wing-end plate gap δ_2 on lift and pitching moment results, q = 40 lb/ft^2

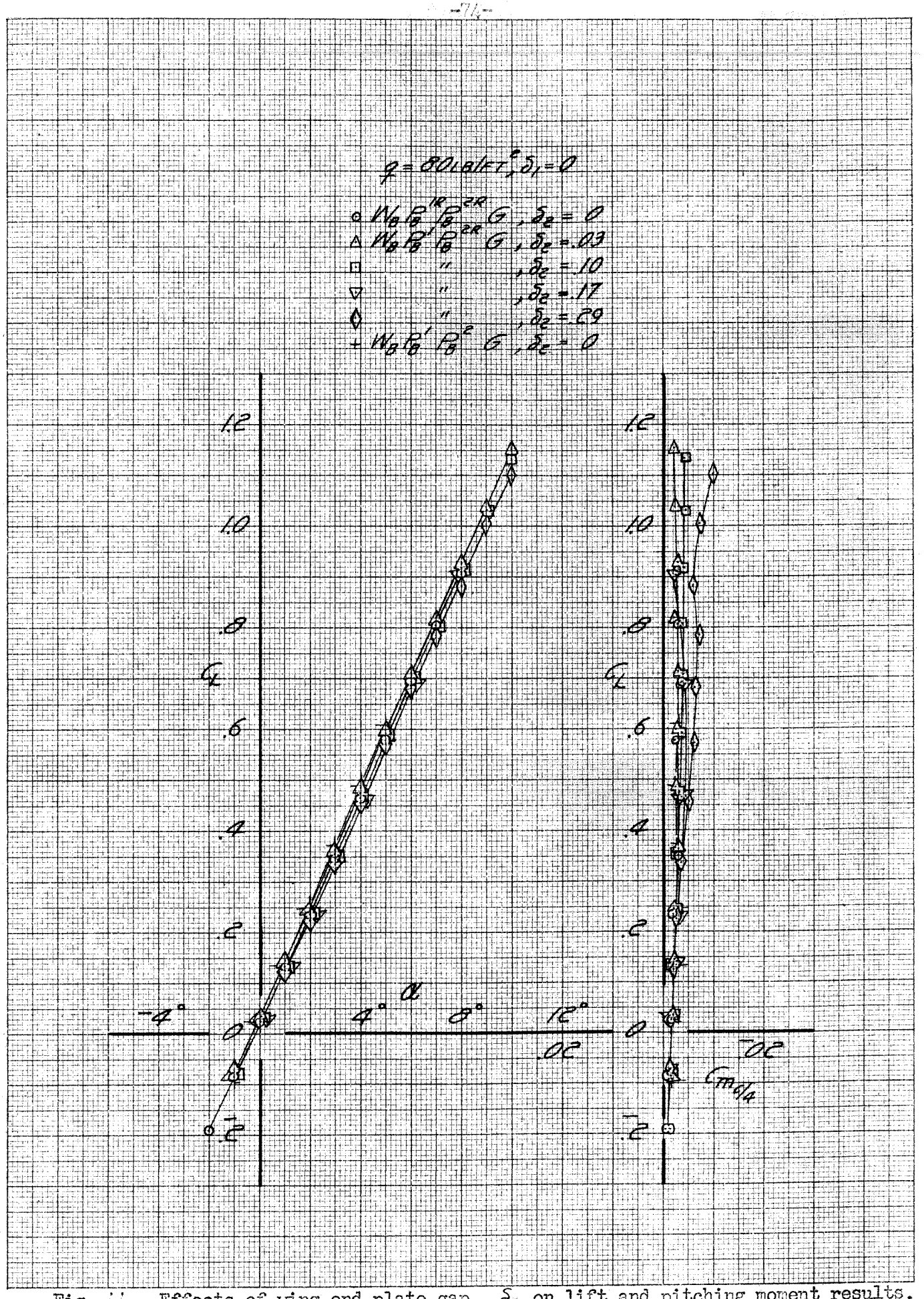

Fig. 44. Effects of wing-end plate gap δ_2 on lift and pitching moment results, q = 80 lb/ft^2

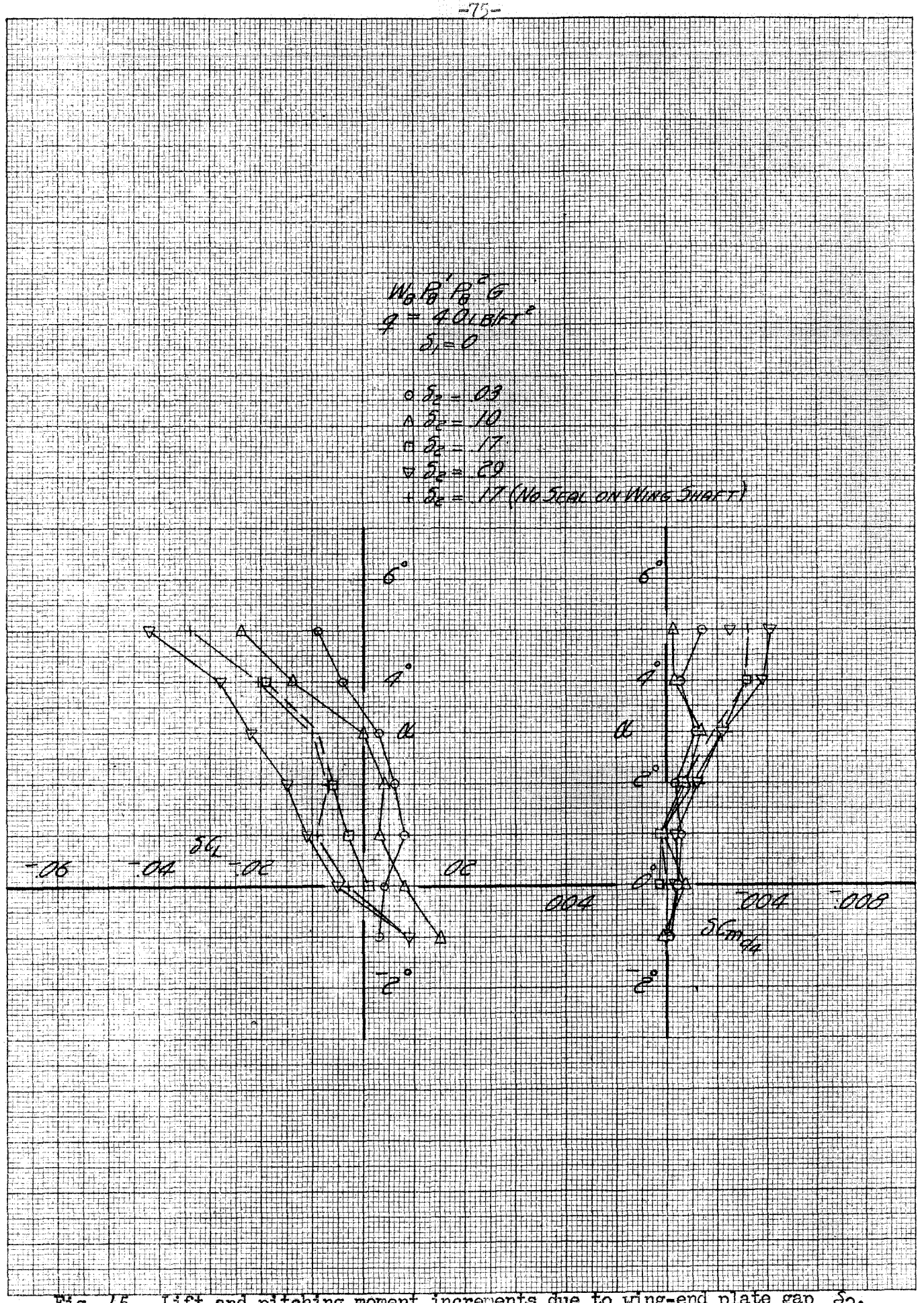

Fig. 45. Lift and pitching moment increments due to wing-end plate gap S_2, q = 40 lb/ft^2

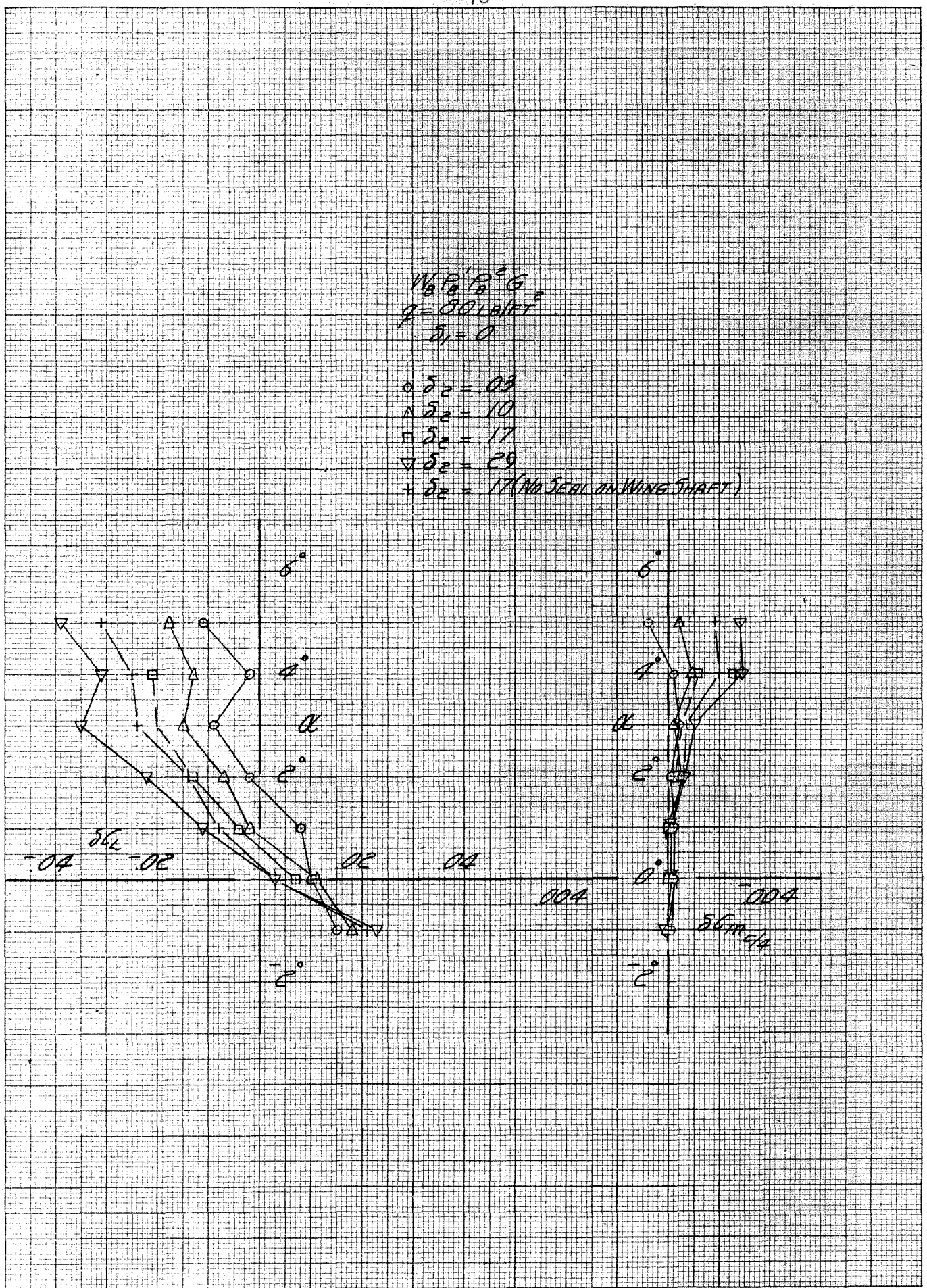

Fig. 46. Lift and pitching moment increments due to wing-end plate gap δ_2, $q = 80$ lb/ft^2

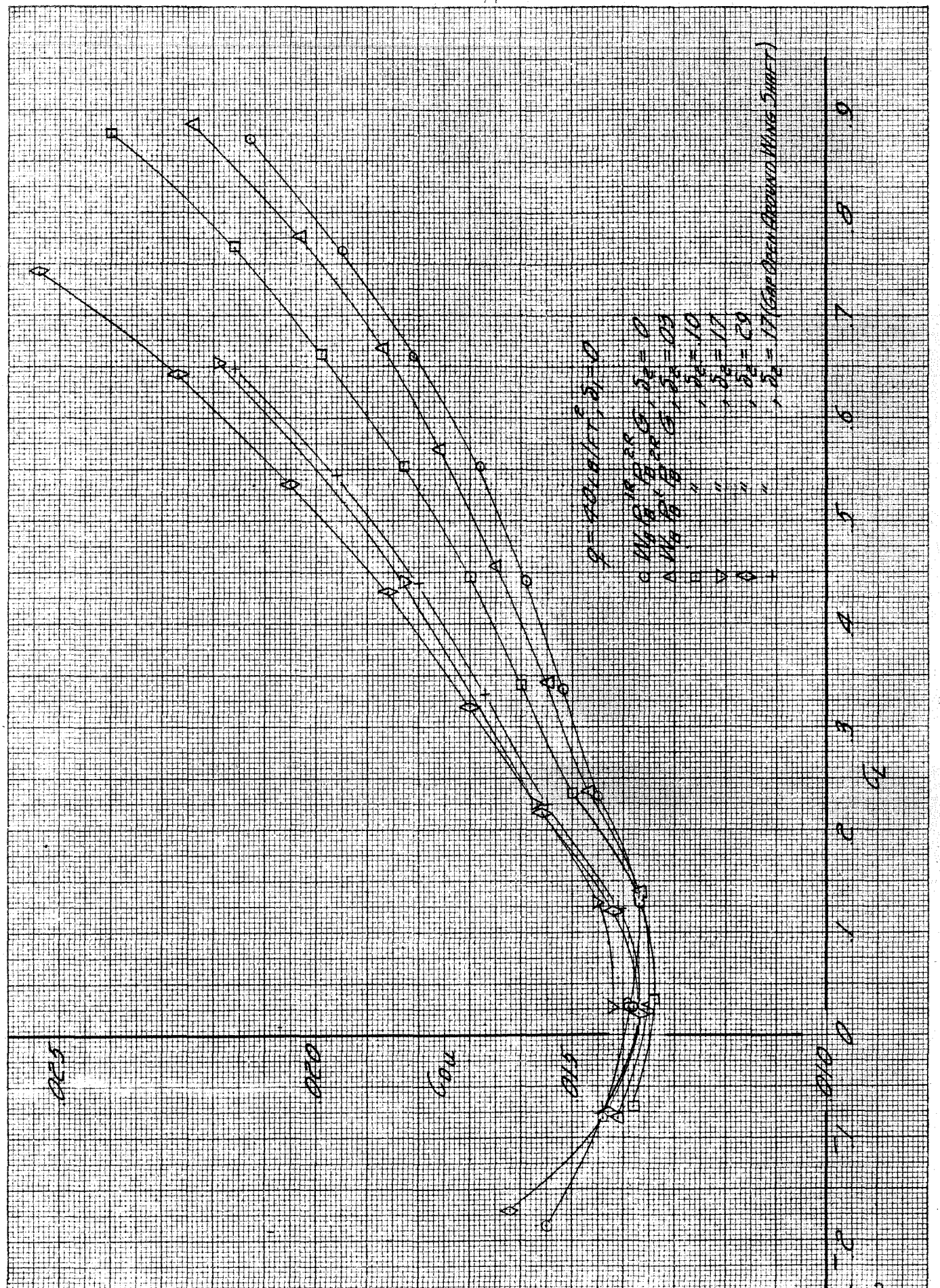

Fig. 47. Effects of wing-end plate gap δ_2 on drag results, q = 40 lb/ft^2

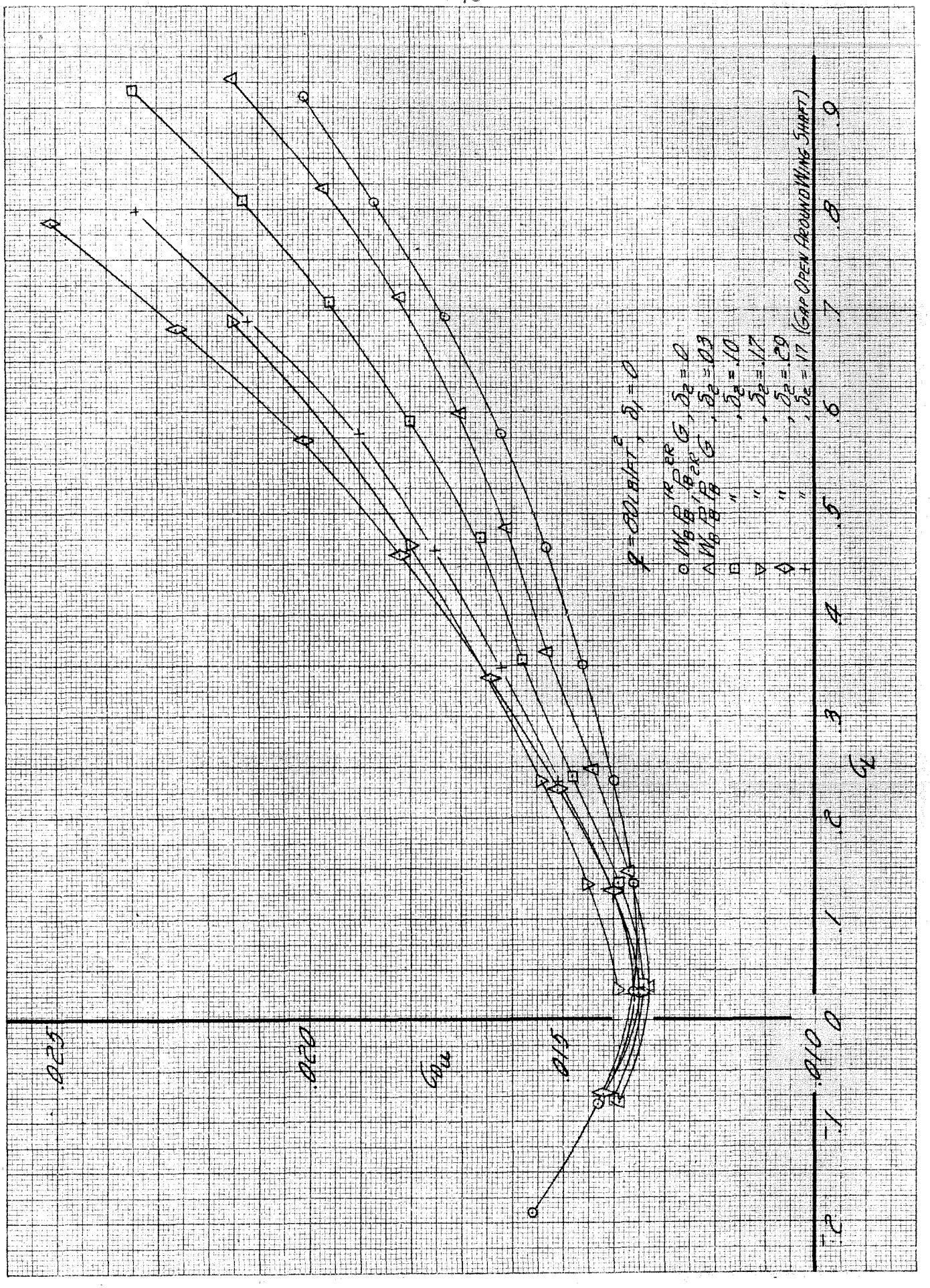

Fig. 48. Effects of wing-end plate gap δ_2 on drag results. $q = 80$ lb/ft^2

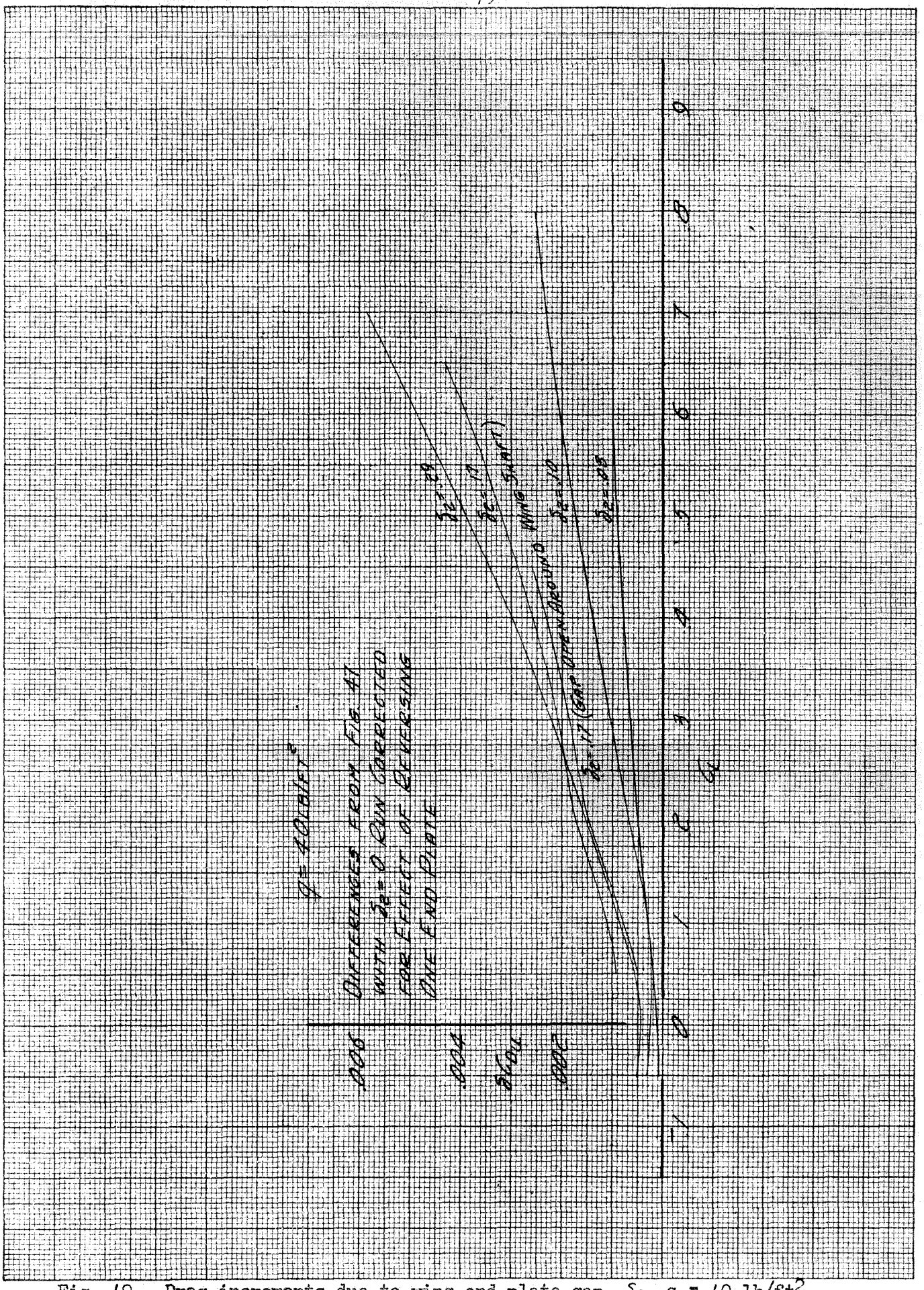

Fig. 49. Drag increments due to wing-end plate gap δ_2, q = 40 lb/ft^2

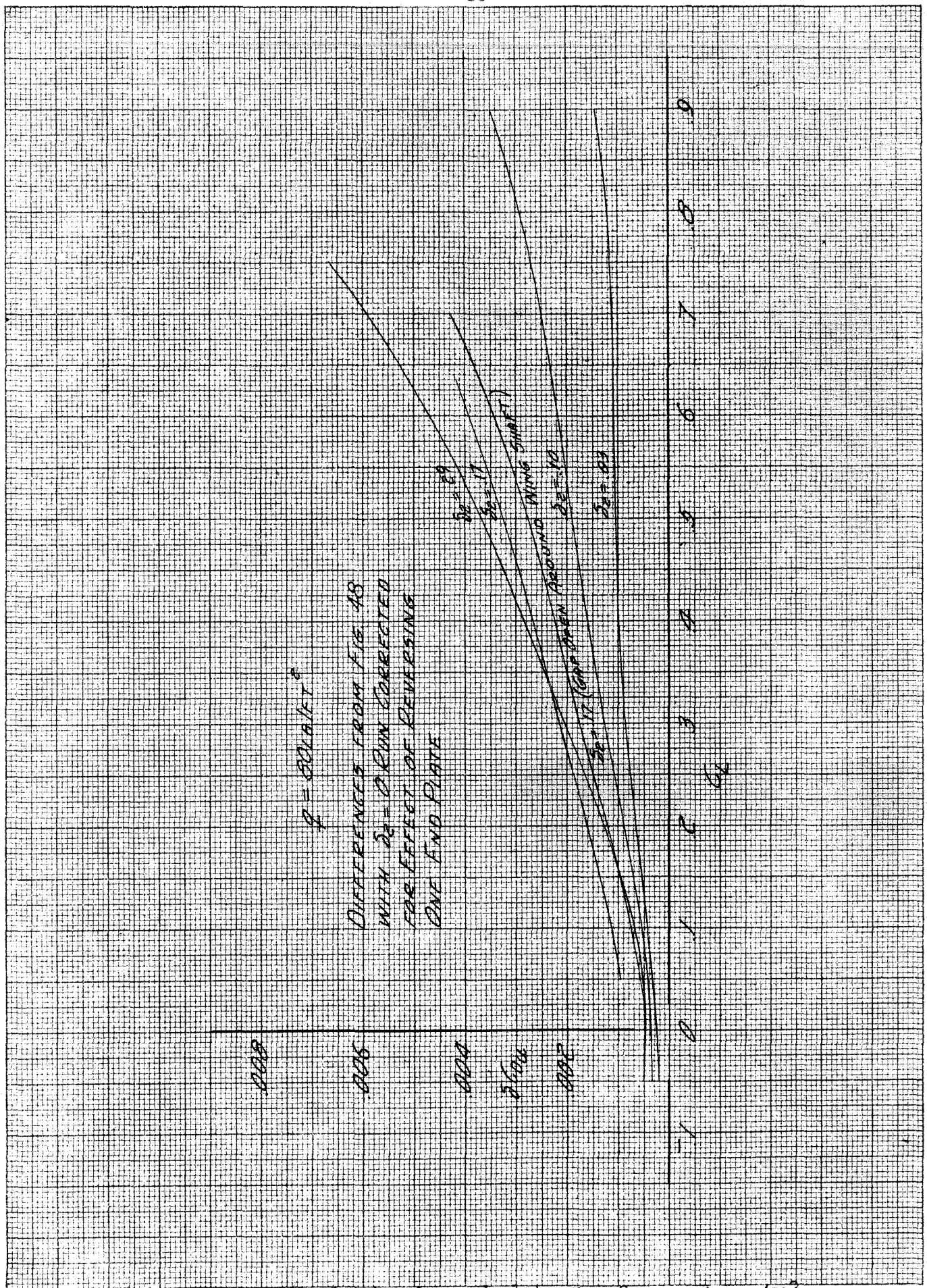

Fig. 50. Drag increments due to wing-end plate gap δ_2, q = 20 lb/ft^2

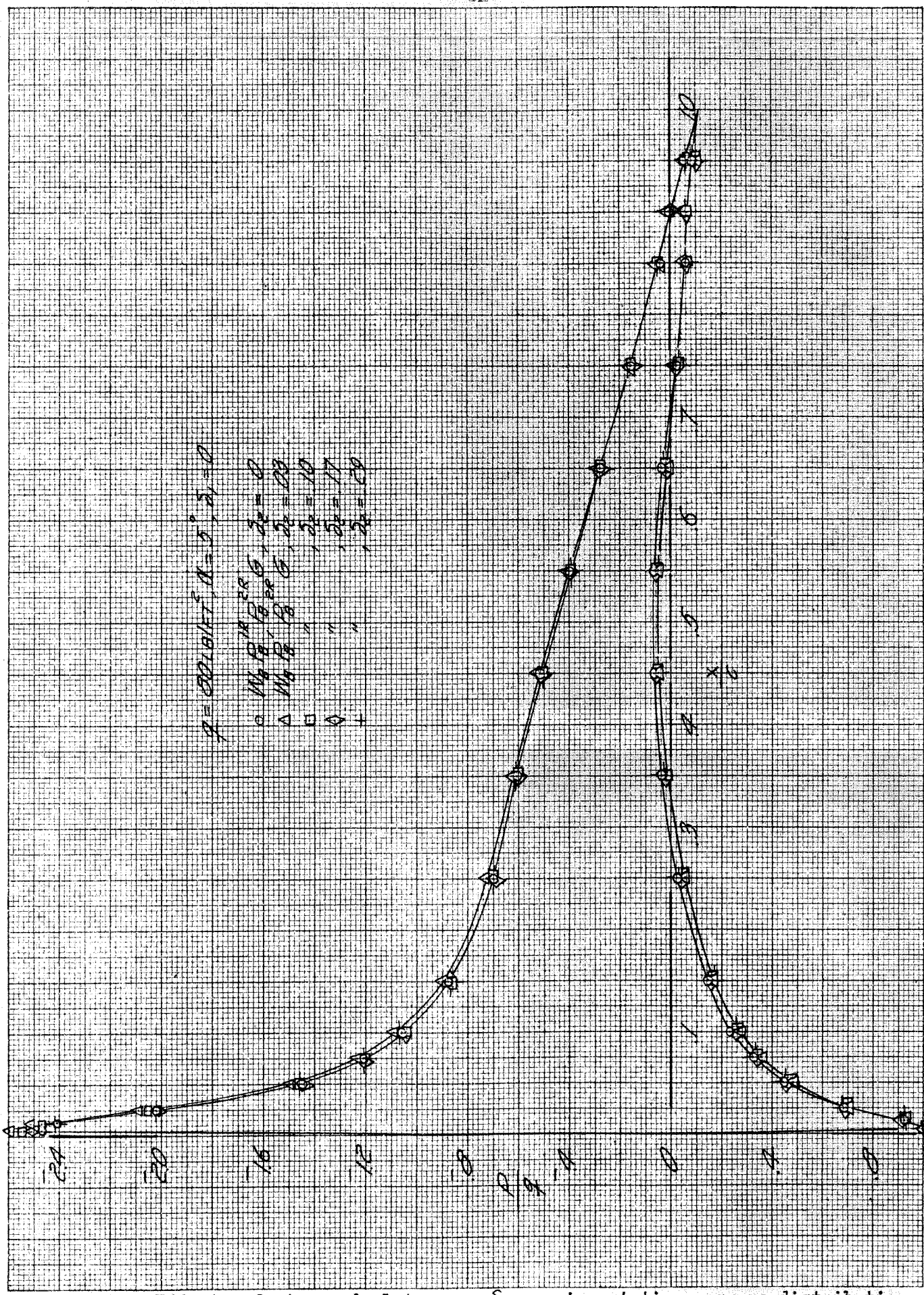

Fig. 51. Effects of wing-end plate gap δ_2 on wing static pressure distribution; $\alpha = 5^{\circ}$, $q = 80$ lb/ft^2

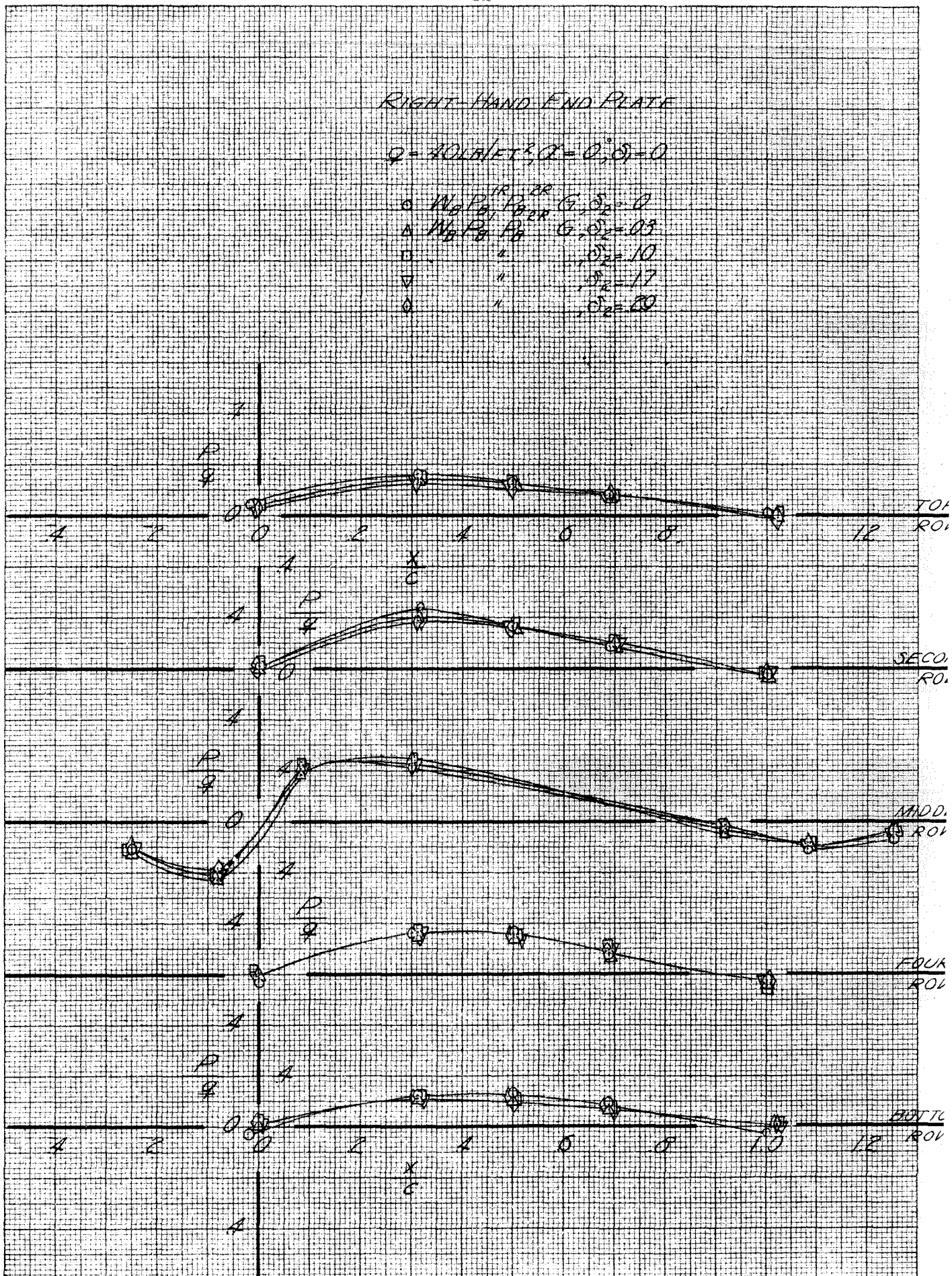

Fig. 52. Effects of wing-end plate gap δ_2 on right-hand end plate static pressures; $\alpha = 0^\circ$, q = 40 lb/ft^2

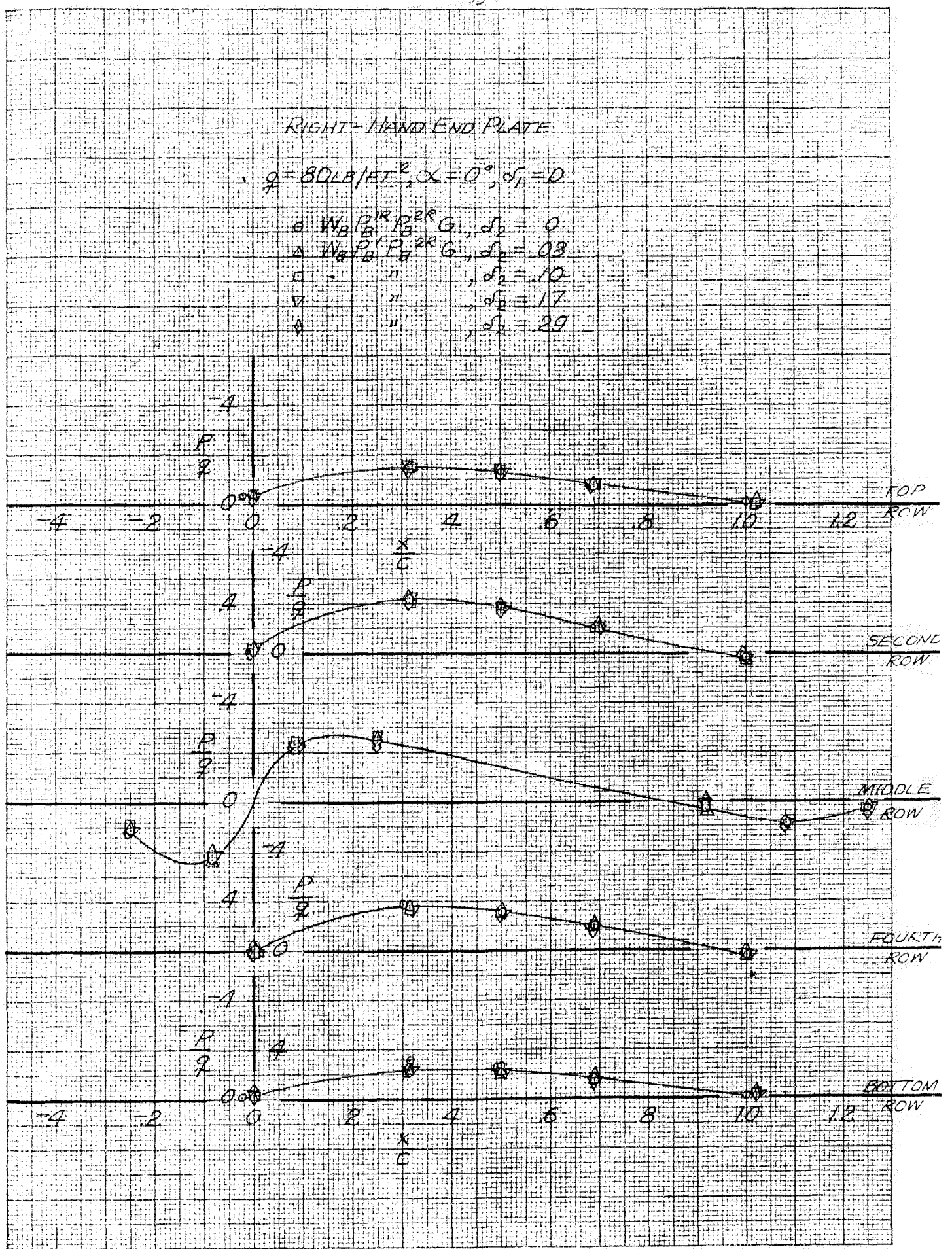

Fig. 53. Effects of wing-end plate gap δ_2 on right-hand end plate static pressures; $\alpha = 0^\circ$, q = 80 lb/ft^2

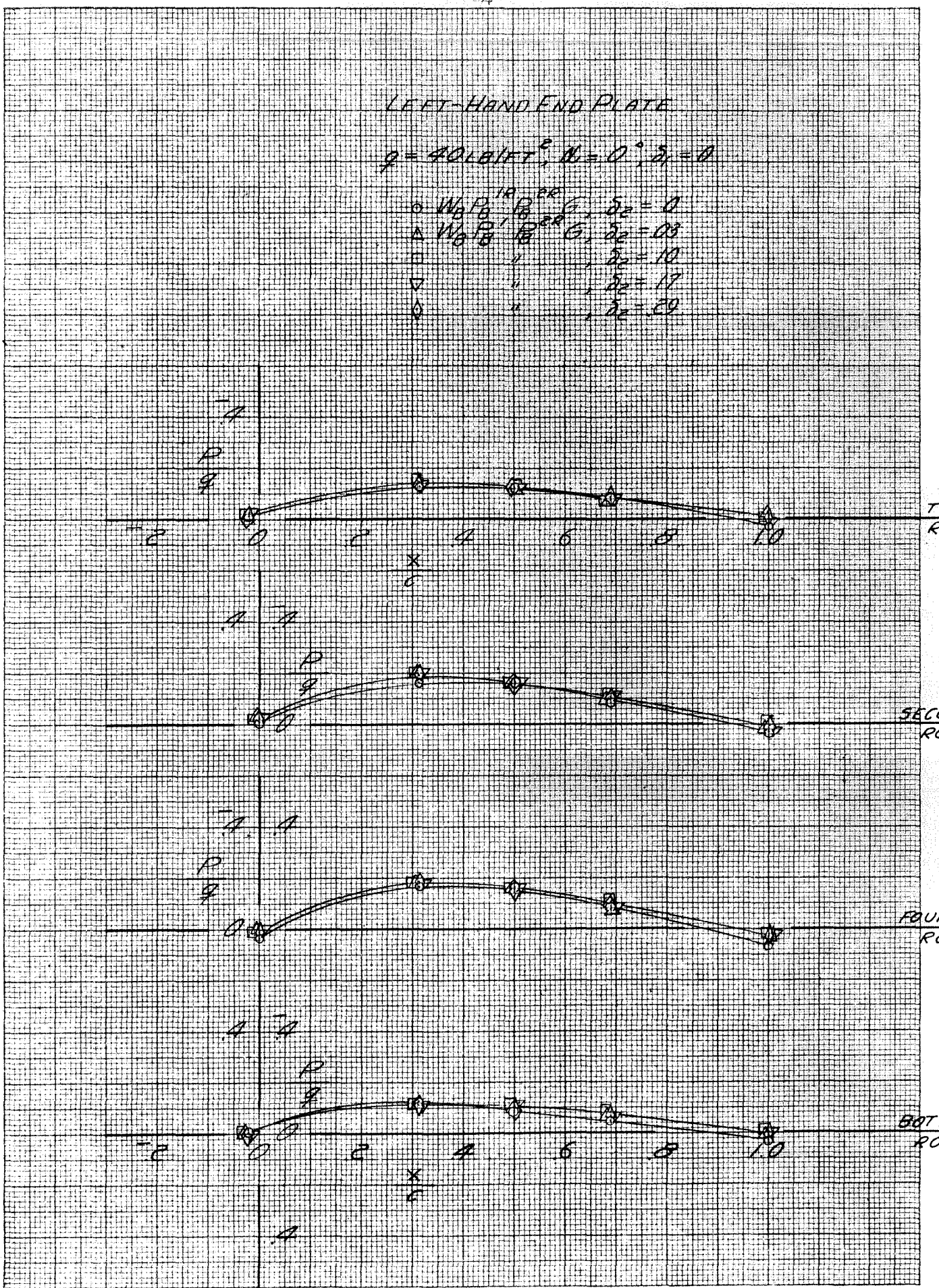

Fig. 54. Effects of wing-end plate gap δ_2 on left-hand end plate static pressures; $\alpha = 0^\circ$, q = 40 lb/ft^2

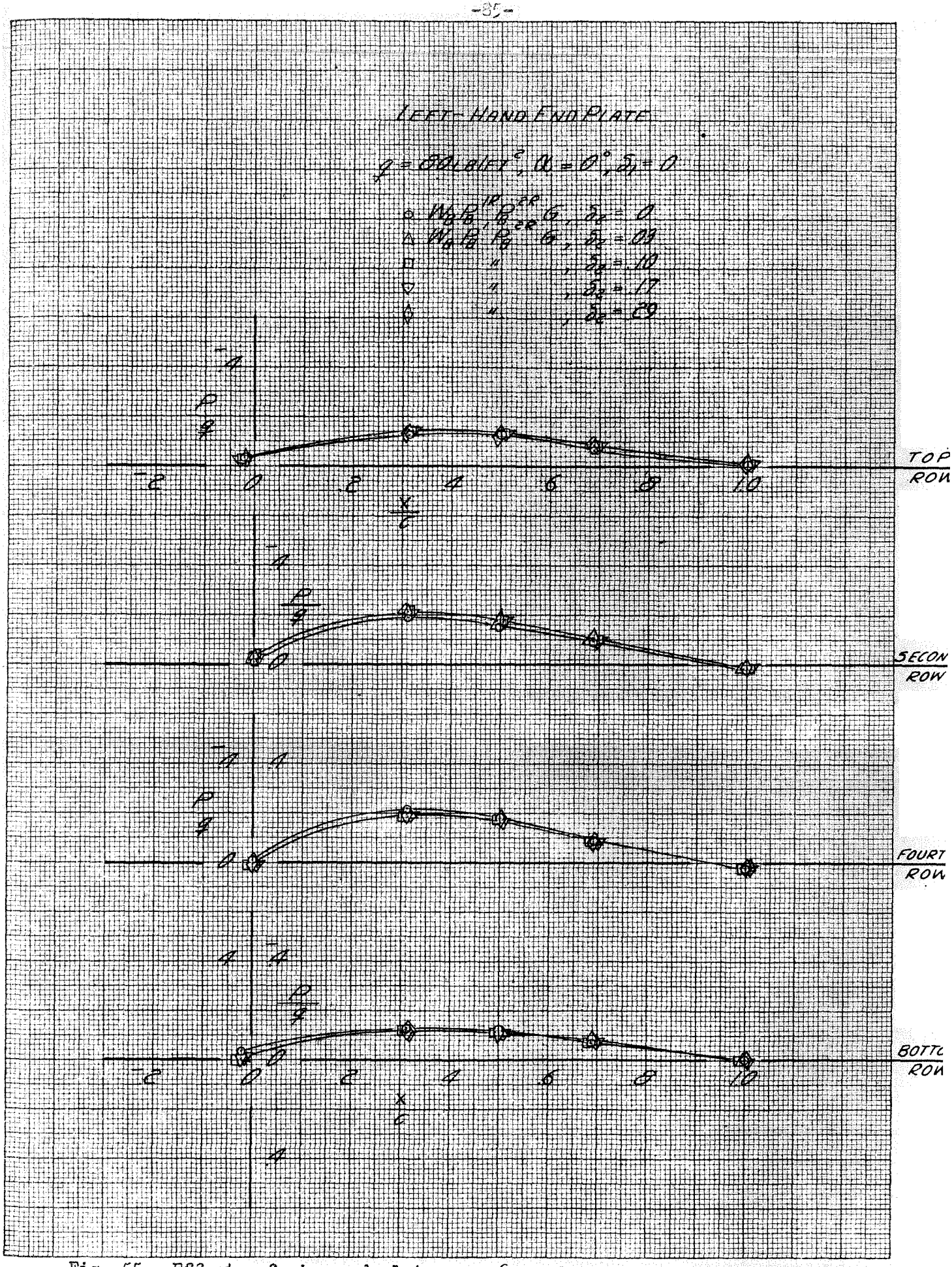

Fig. 55. Effects of wing-end plate gap δ_2 on left-hand end plate static pressures; $\alpha = 0^\circ$, q = 80 lb/ft^2

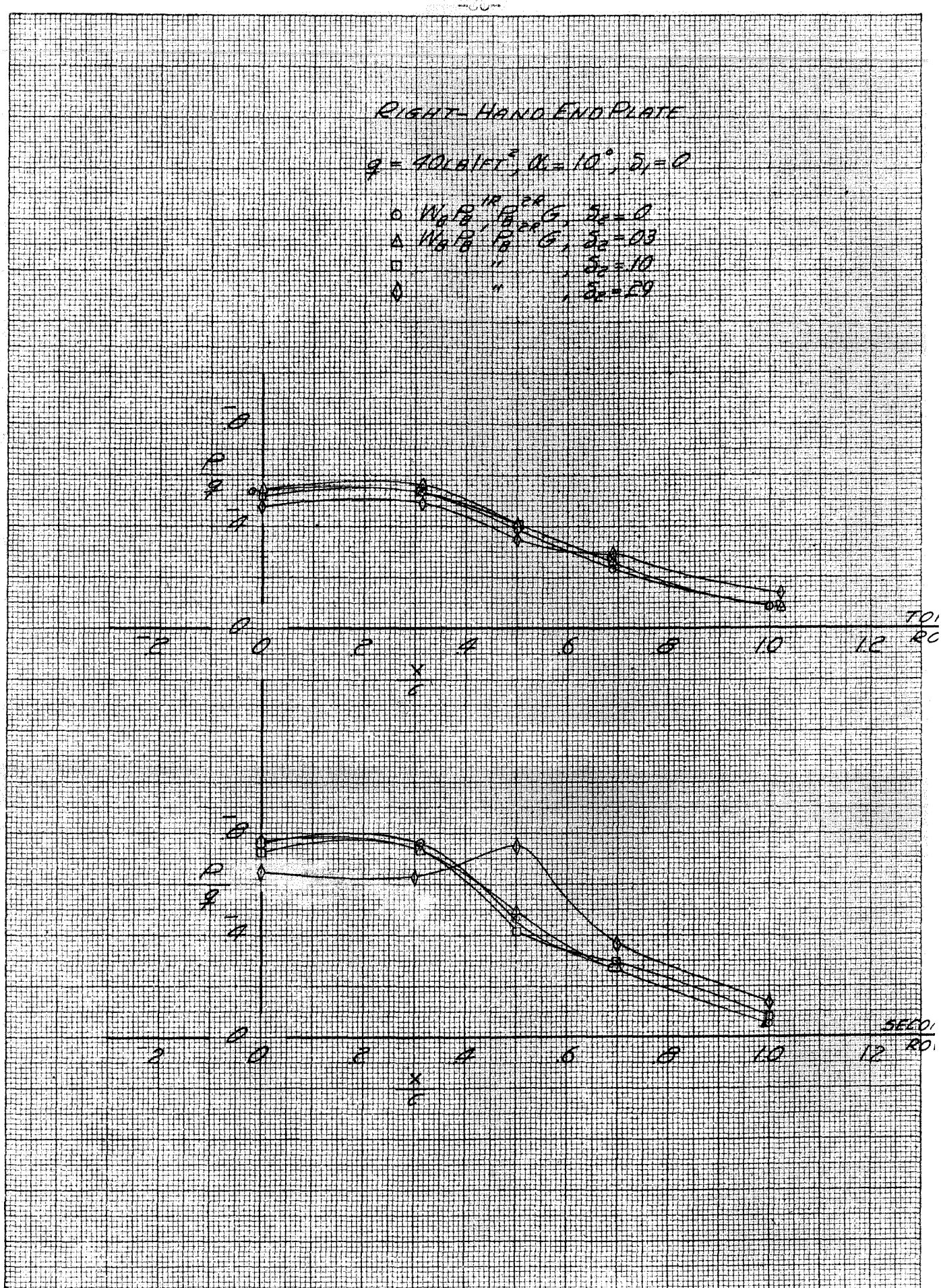

Fig. 56. Effects of wing-end plate gap δ_2 on right-hand end plate static pressures; α = 10°, q = 40 lb/ft^2

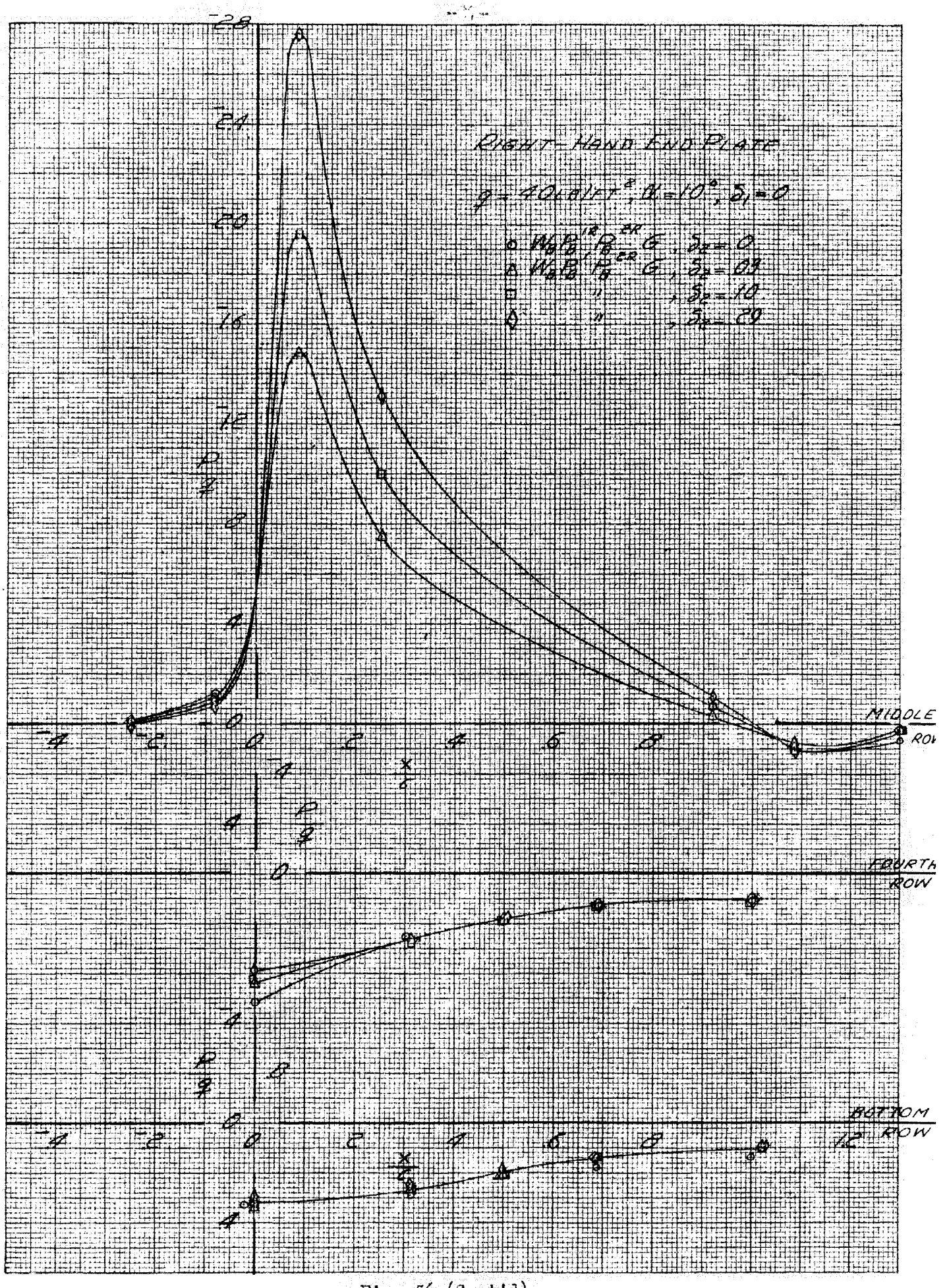

Fig. 56 (Cont'd)

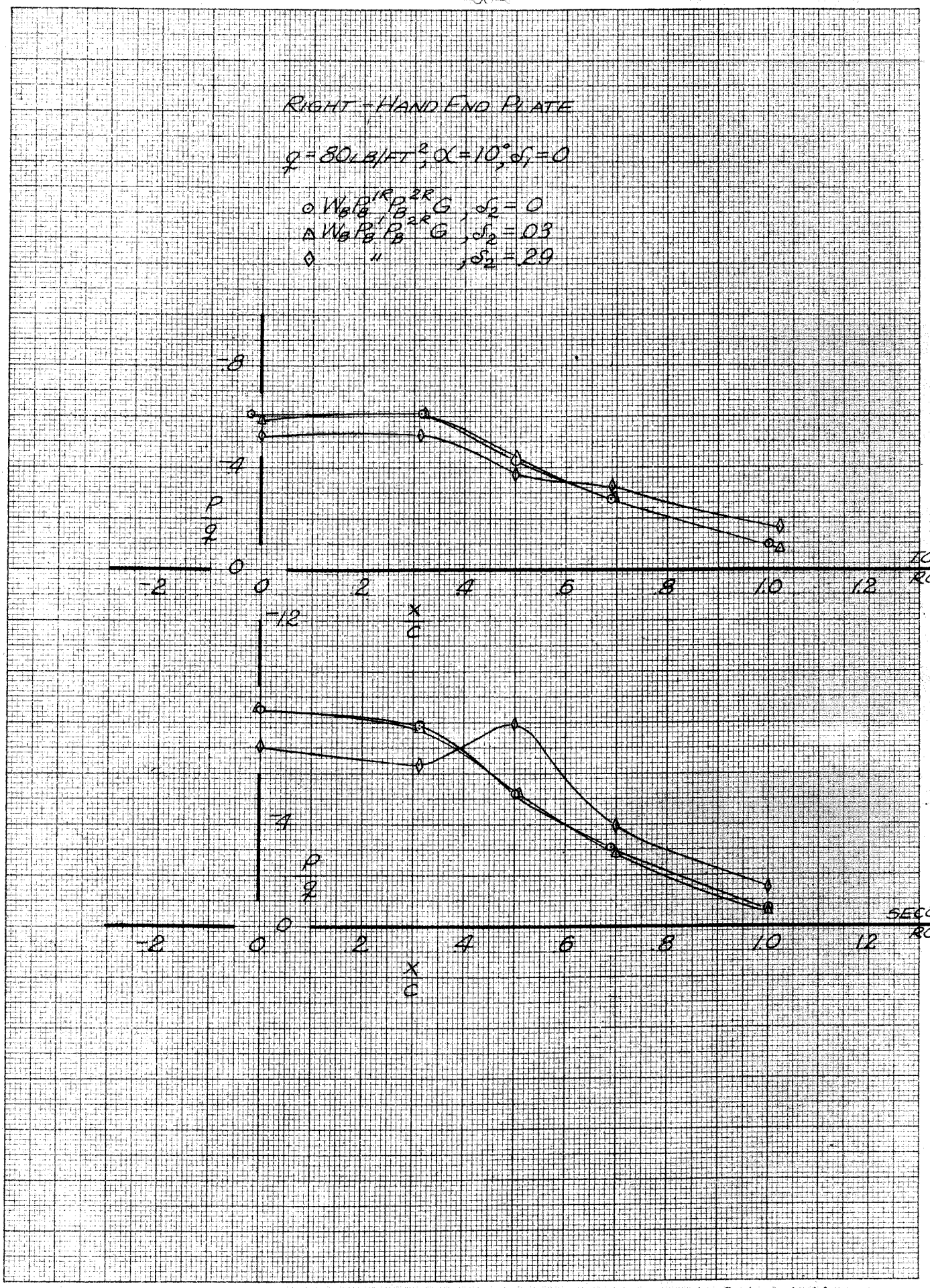

Fig. 57. Effects of wing-end plate gap δ_2 on right-hand end plate static pressures; α = 10°, q = 80 lb/ft^2

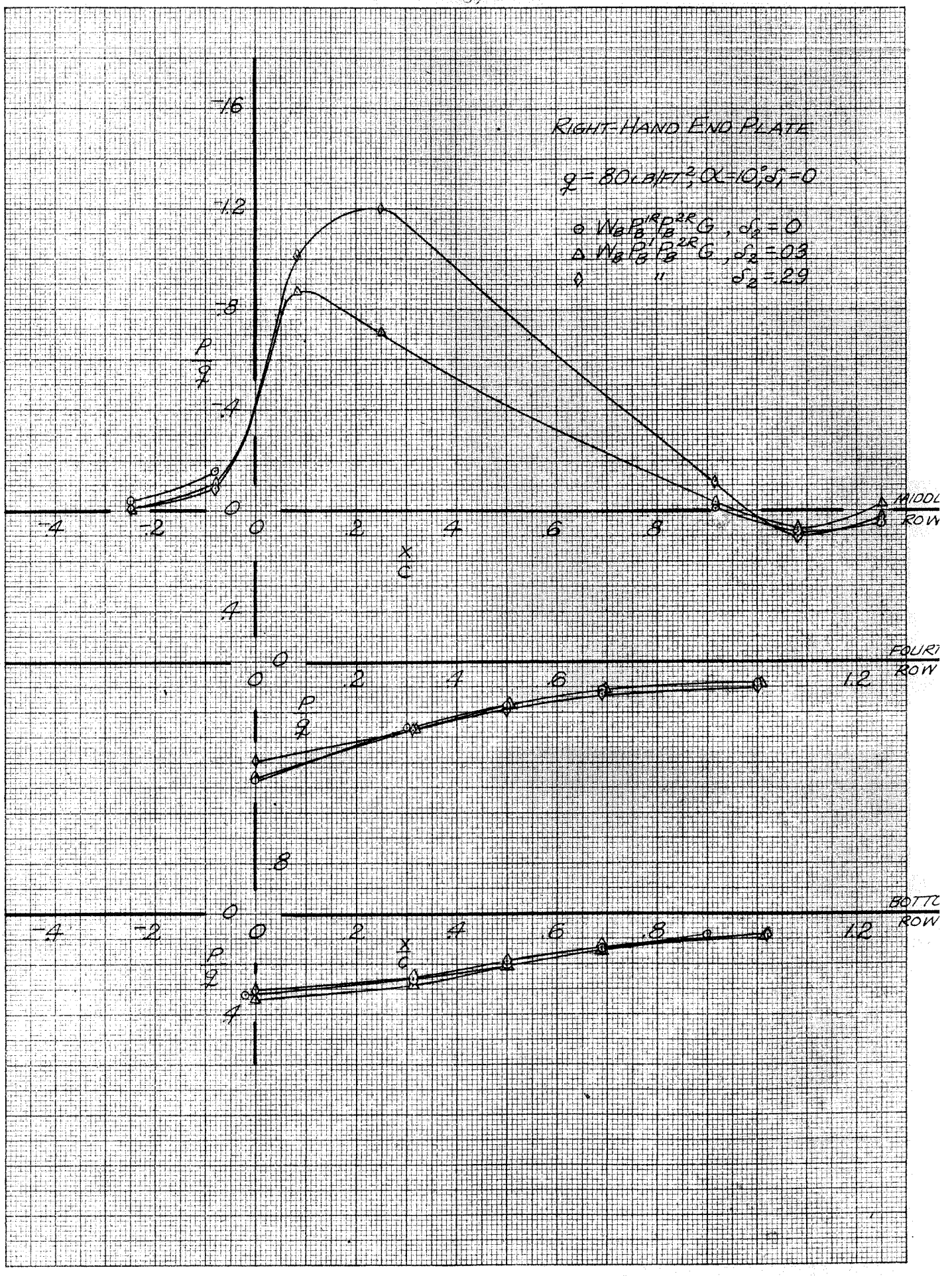
RIGHT-HAND END PLATE
q = 80 LB/FT², α = 10°, δ₁ = 0
○ W_B P_B^1R P_B^2R G , δ₂ = 0
△ W_B P_B^1 P_B^2R G , δ₂ = .03
◇ " δ₂ = .29
-1.6
-1.2
-.8
-.4
0
.4
P/q
x/c
-.4
-.2
0
.2
.4
.6
.8
1.2
MIDDL
ROW
FOURT
ROW
BOTTO
ROW

Fig. 57 (Cont'd)

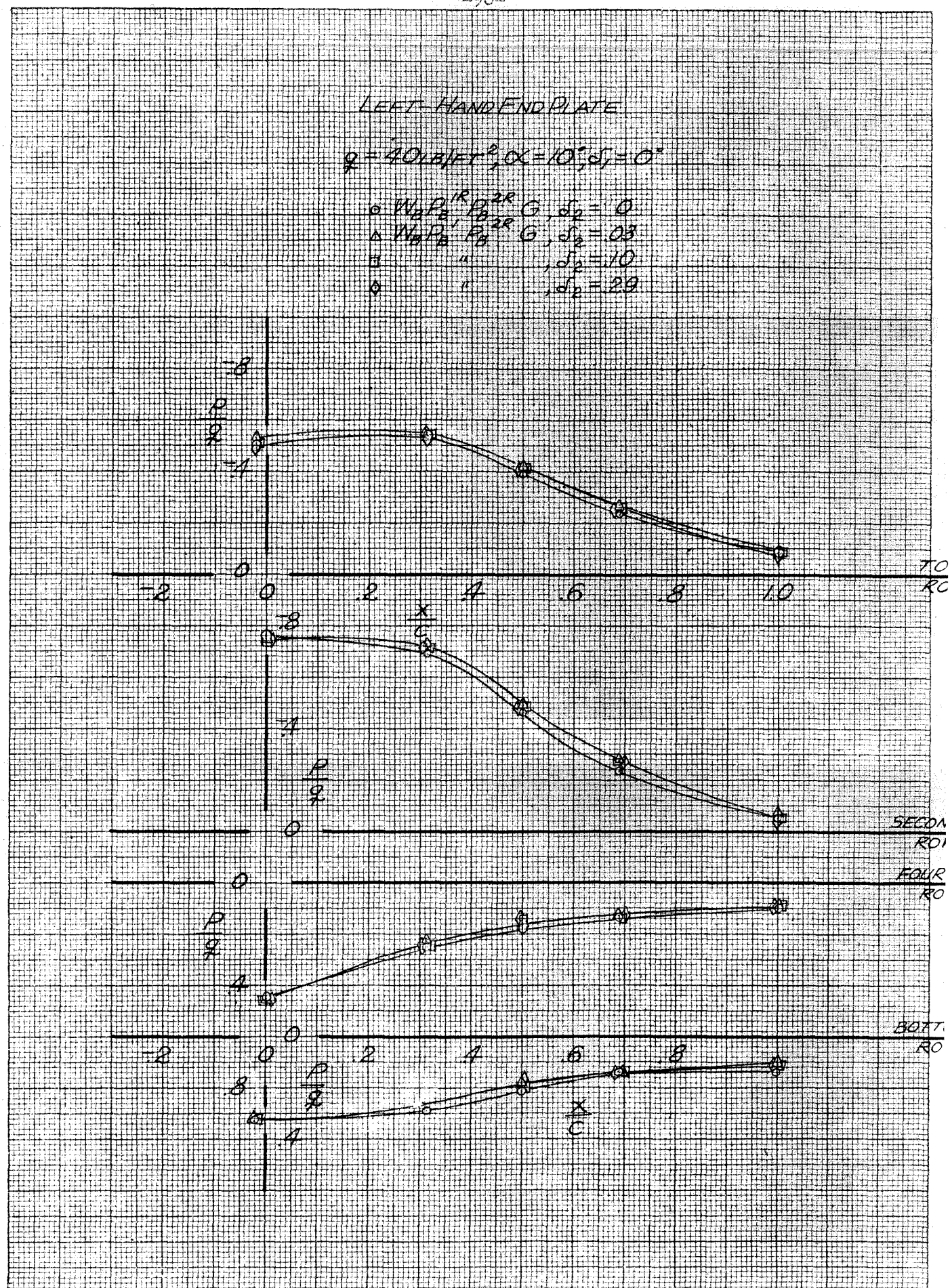

Fig. 58. Effects of wing-end plate gap δ_2 on left-hand end plate static pressures; α = 10°, q = 40 lb/ft^2

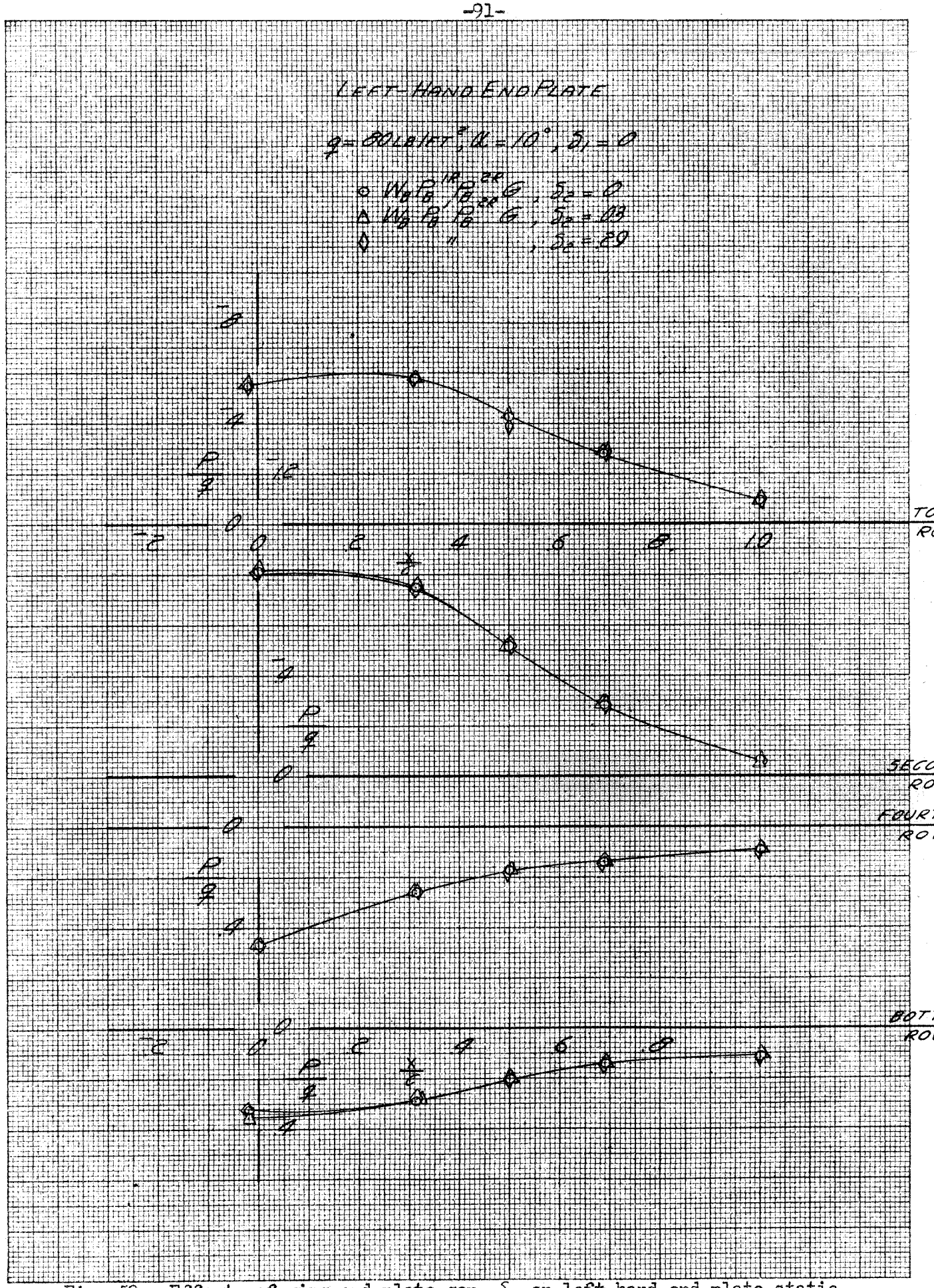

Fig. 59. Effects of wing-end plate gap δ_2 on left-hand end plate static pressures; $\alpha = 10^{\circ}$, q = 80 lb/ft^2

3. Effects of Wing-Template Gap, δ_3

When the tests were made to determine the forces on the portion of the wing in the boundary layer, a template was mounted on one end plate and this template was separated from the main portion of the wing by a gap (δ_3). The tests which were made to determine the effects of this gap are presented in this section. In the tests to check the effects of this gap the measured forces included the forces on the wing as well as those on the end plates and templates. The results are presented on Figs. 60 to 73 in a similar manner to that used for gap δ_2.

Increasing the wing-template gap width decreases the lift only very slightly; the change is much smaller than that produced by a comparable change in wing-end plate gap width (cf. last section). This may be due to the fact that the lift produced by the main portion of the wing carries across the gap to the template (cf. Sec. V-B).

The drag increments due to the wing-template gap, δ_3, are very similar to those obtained for the wing-end plate gap, δ_2, the chief difference between the two being the difference in the drag increments at zero lift. Whereas gap δ_2 showed very little effect on the drag at zero lift, an increase in gap δ_3 produces an appreciable change in the zero lift drag increment. This is probably due to the fact that gap δ_2 is located in the region next to the end plate where the total head is greatly reduced while gap δ_3 is located about one-half inch further out toward the center of the tunnel and is therefore in a region in which the total head is greater. The inference is that since the wing shaft is exposed in both cases, the drag increase due to exposing this shaft is greater when the total head acting on the

shaft is greater. All these results are shown on Figs. 60 to 67.

Static pressure measurements for the right-hand end plate are presented on Figs. 68 to 73. The effect of increasing the wing-template gap width, δ_3, is the same as that noted for gap, δ_2. That is, increasing the gap allows a greater equalization of the pressures on the top and bottom surfaces. The pressure peak due to the presence of the wing shaft which occured with $\delta_2 = 0.29$ (noted in the last section) does not occur with any δ_3 tested since the wing shaft is now separated from the end plate by the template.

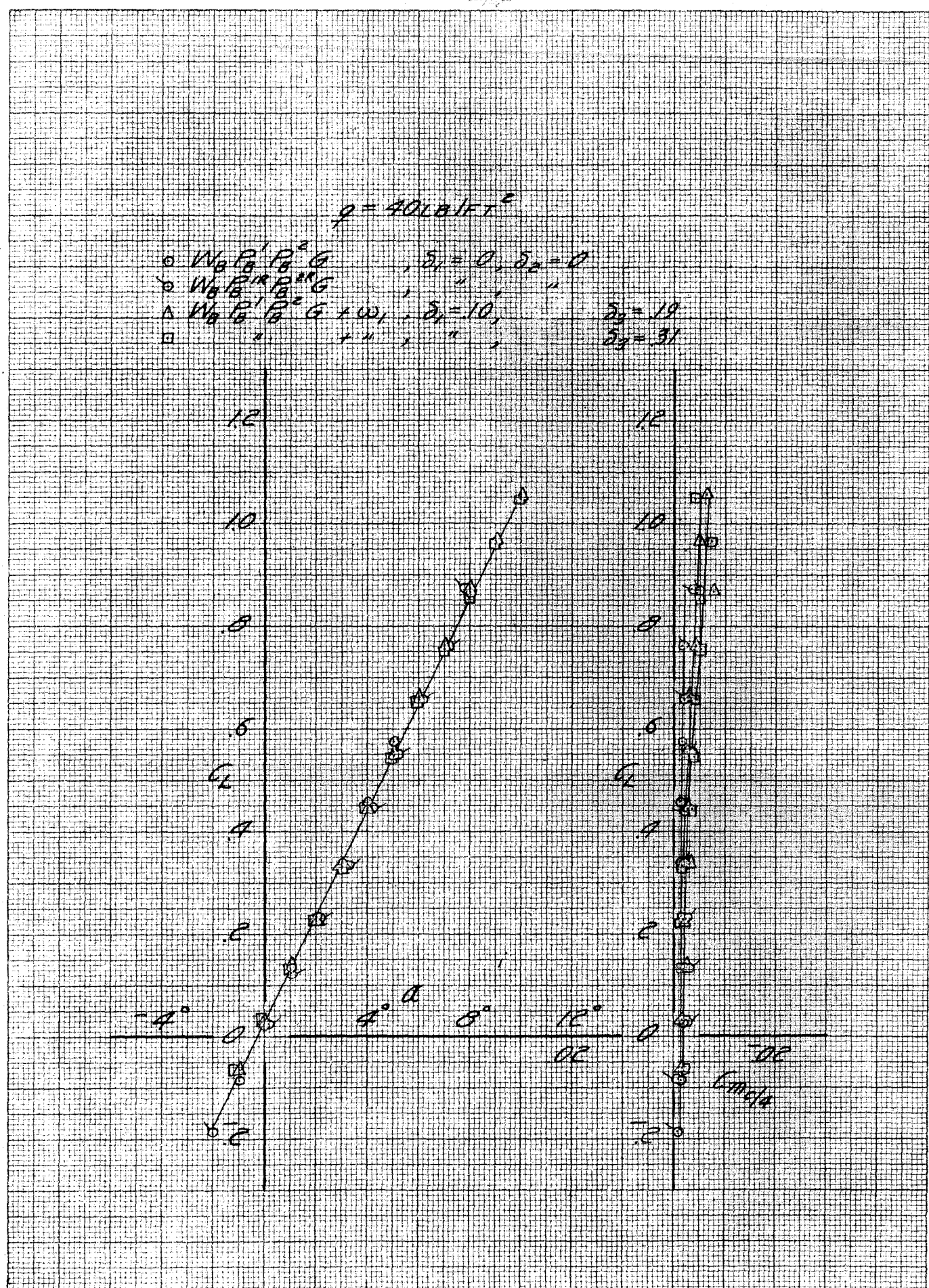

Fig. 60. Effects of wing-template gap δ_3 on lift and pitching moment results, q = 40 lb/ft^2

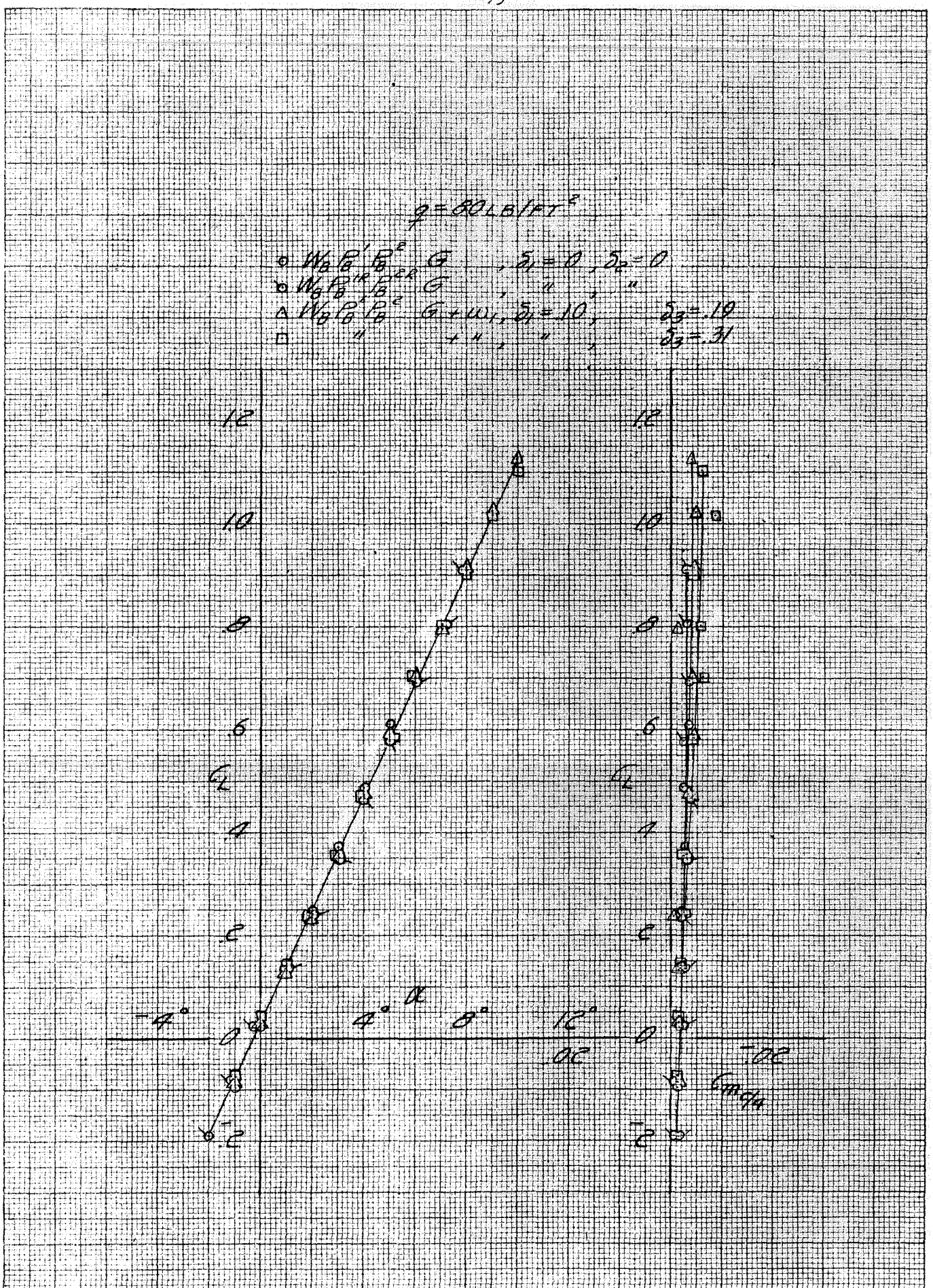

Fig. 61. Effects of wing-template gap δ_3 on lift and pitching moment results, q = 80 lb/ft^2

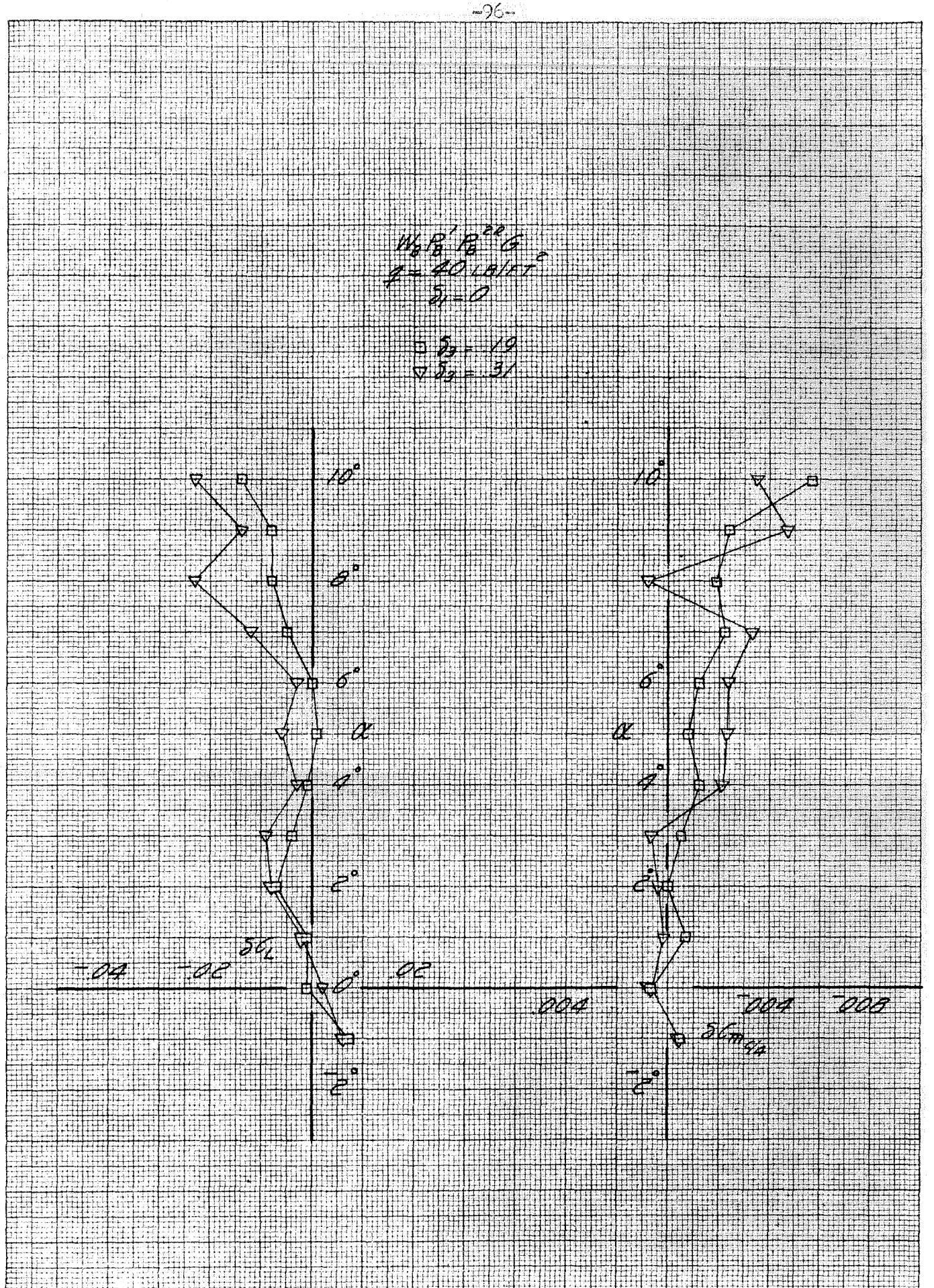

Fig. 62. Lift and pitching moment increments due to wing-template gap δ_3, q = 40 lb/ft^2

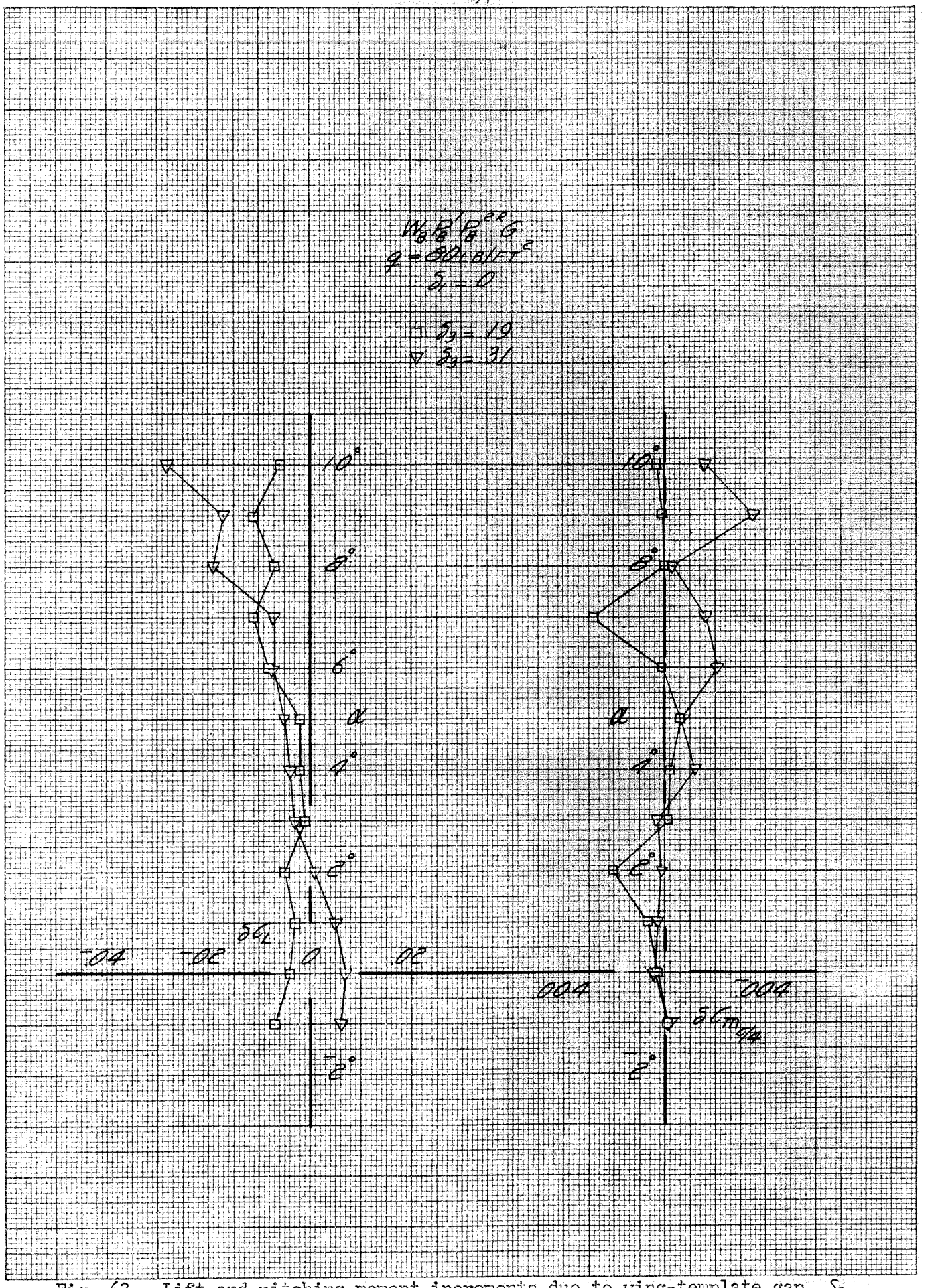

Fig. 63. Lift and pitching moment increments due to wing-template gap δ_3, $q = 80$ lb/ft^2

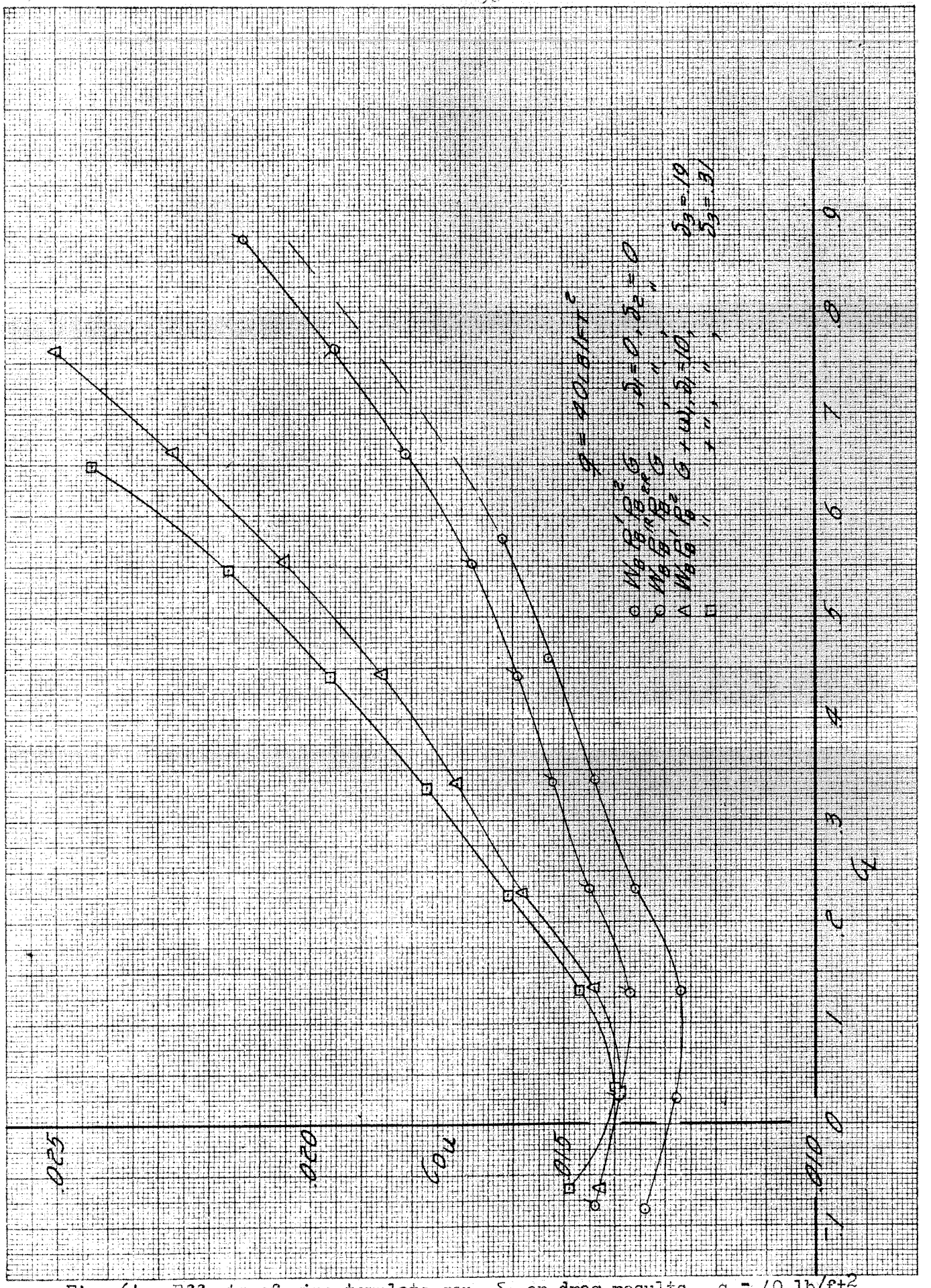

Fig. 64. Effects of wing-template gap δ_3 on drag results, q = 40 lb/ft^2

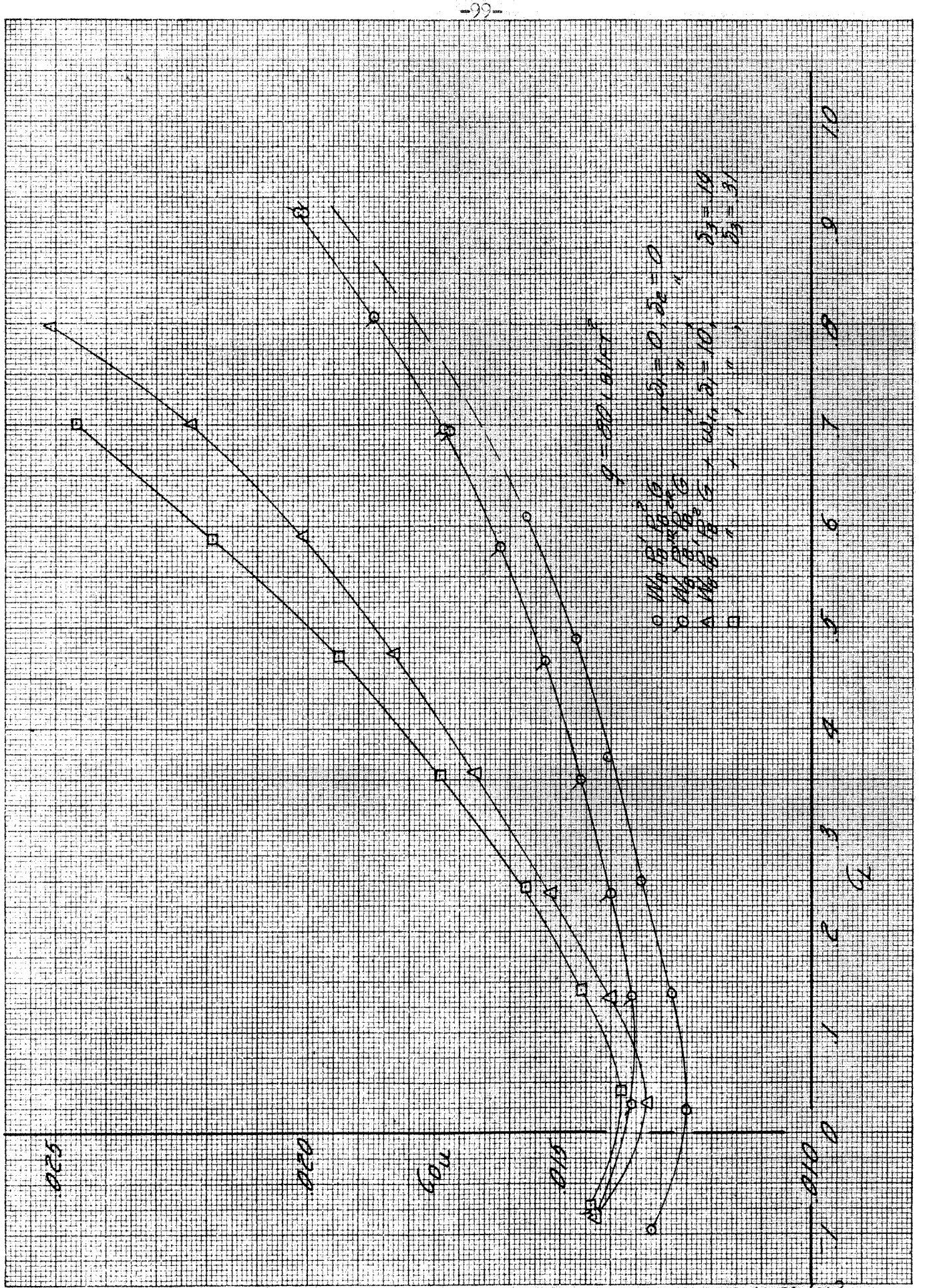

Fig. 65. Effects of wing-template gap δ_3 on drag results, q = 80 lb/ft^2

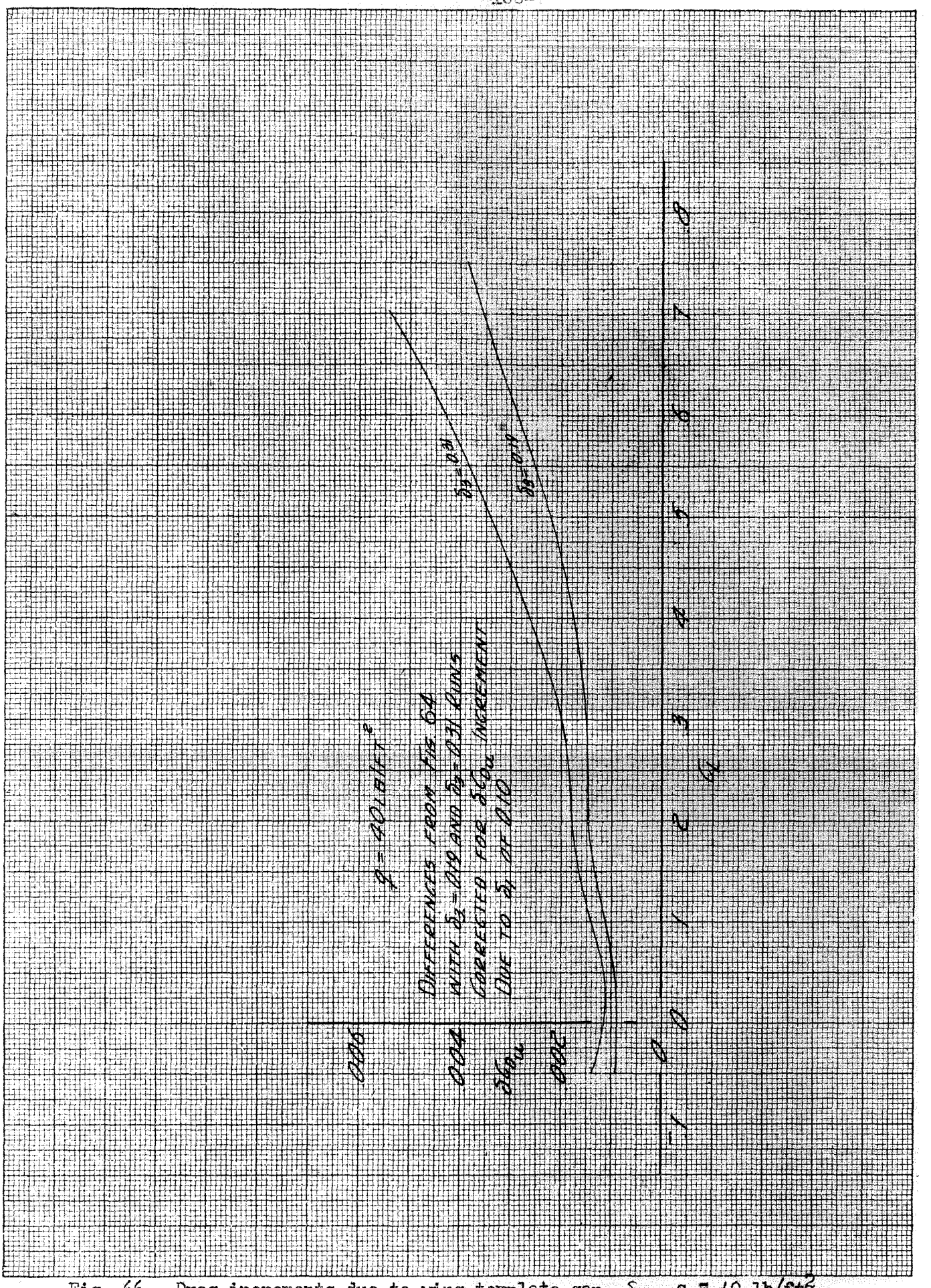

Fig. 66. Drag increments due to wing-template gap δ_3, q = 40 lb/ft^2

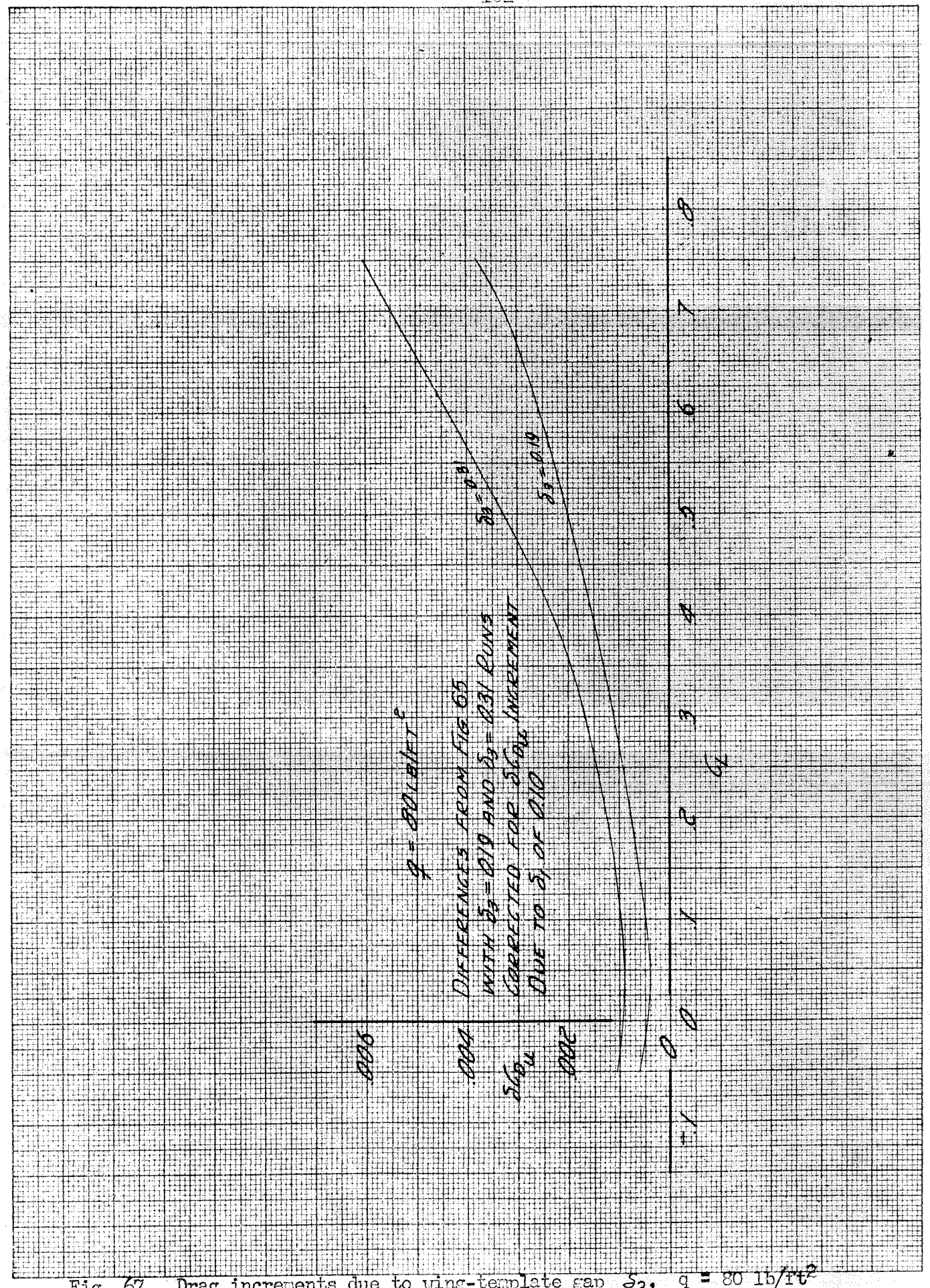

Fig. 67. Drag increments due to wing-template gap δ_3, q = 80 lb/ft^2

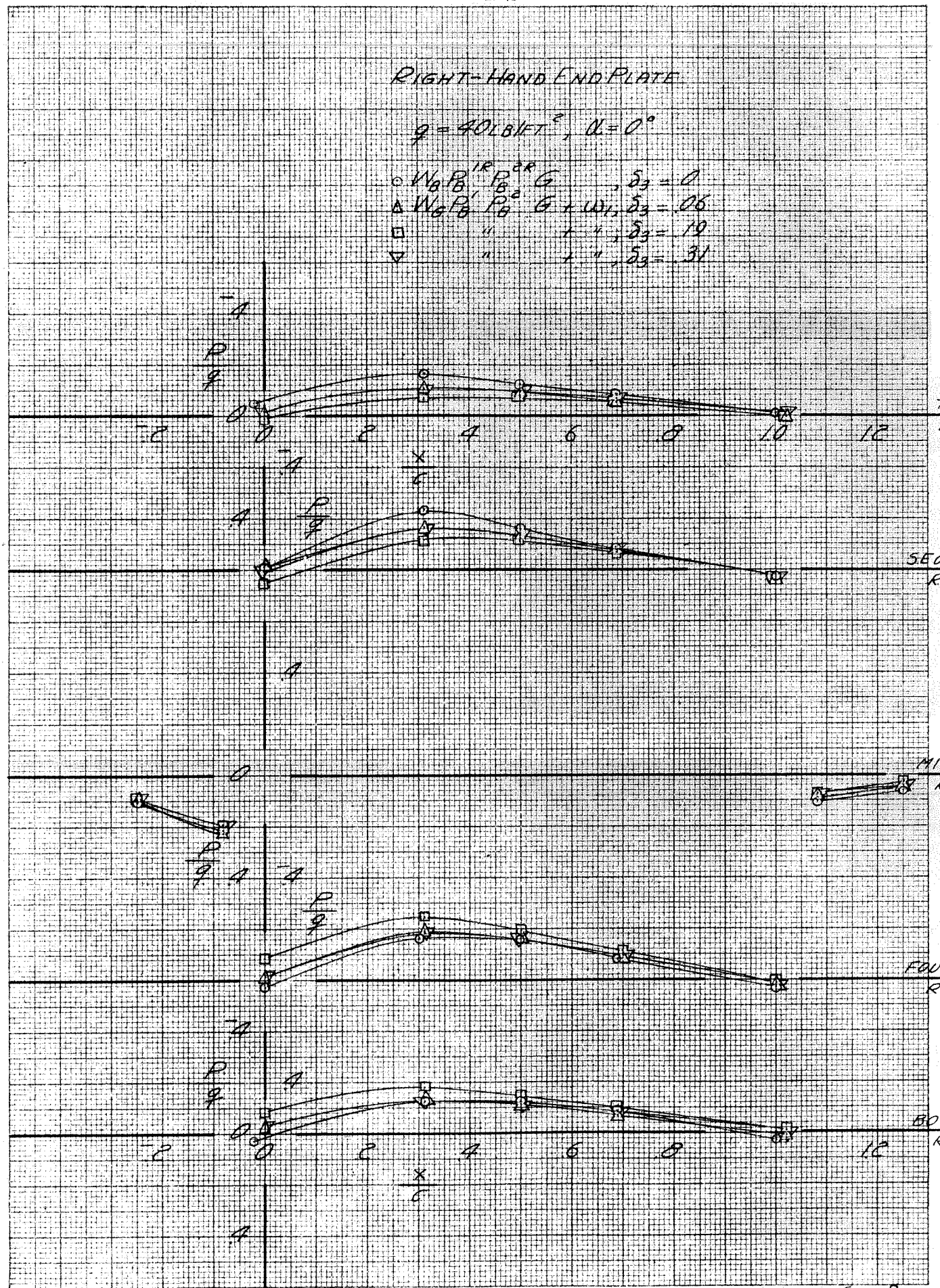

Fig. 68. Effects of wing-template gap on end plate static pressures; $\alpha = 0^{\circ}$, $q = 40$ lb/ft^2

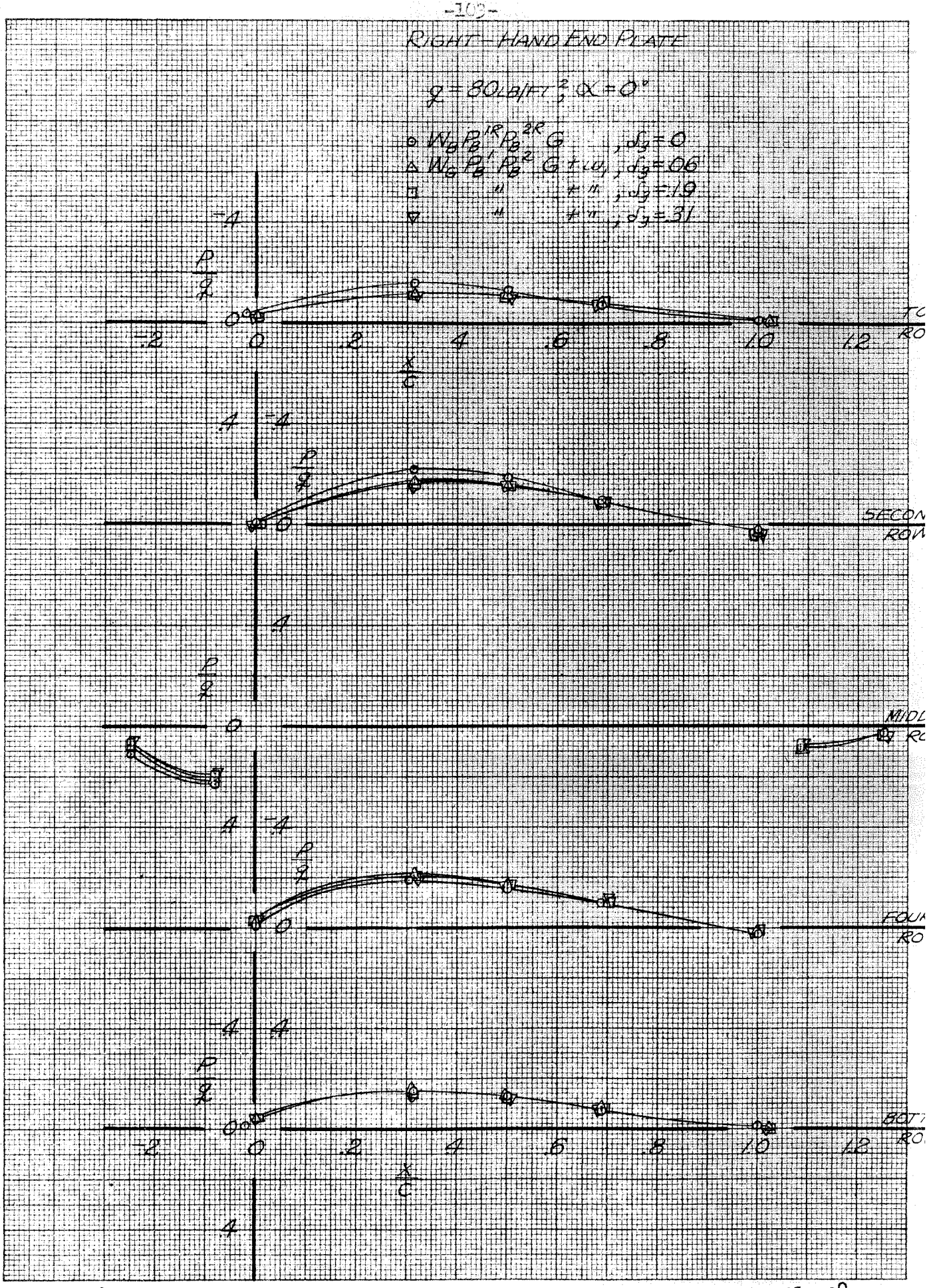

Fig. 69. Effects of wing-template gap on end plate static pressures; $\alpha = 0^{\circ}$, $q = 80$ lb/ft^2

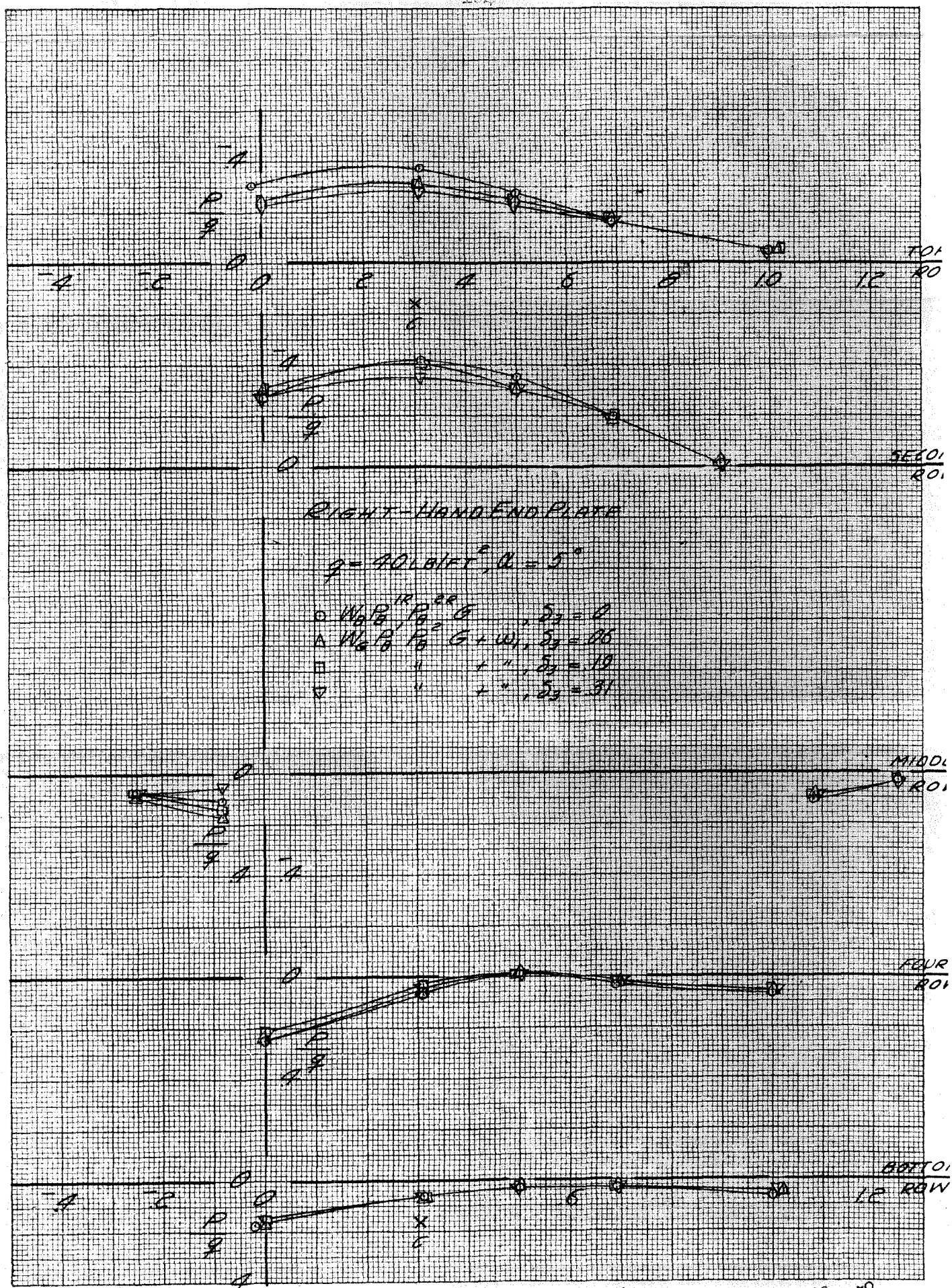

Fig. 70. Effects of wing-template gap on end plate static pressures; $\alpha = 5^{\circ}$, $q = 40$ lb/ft^2

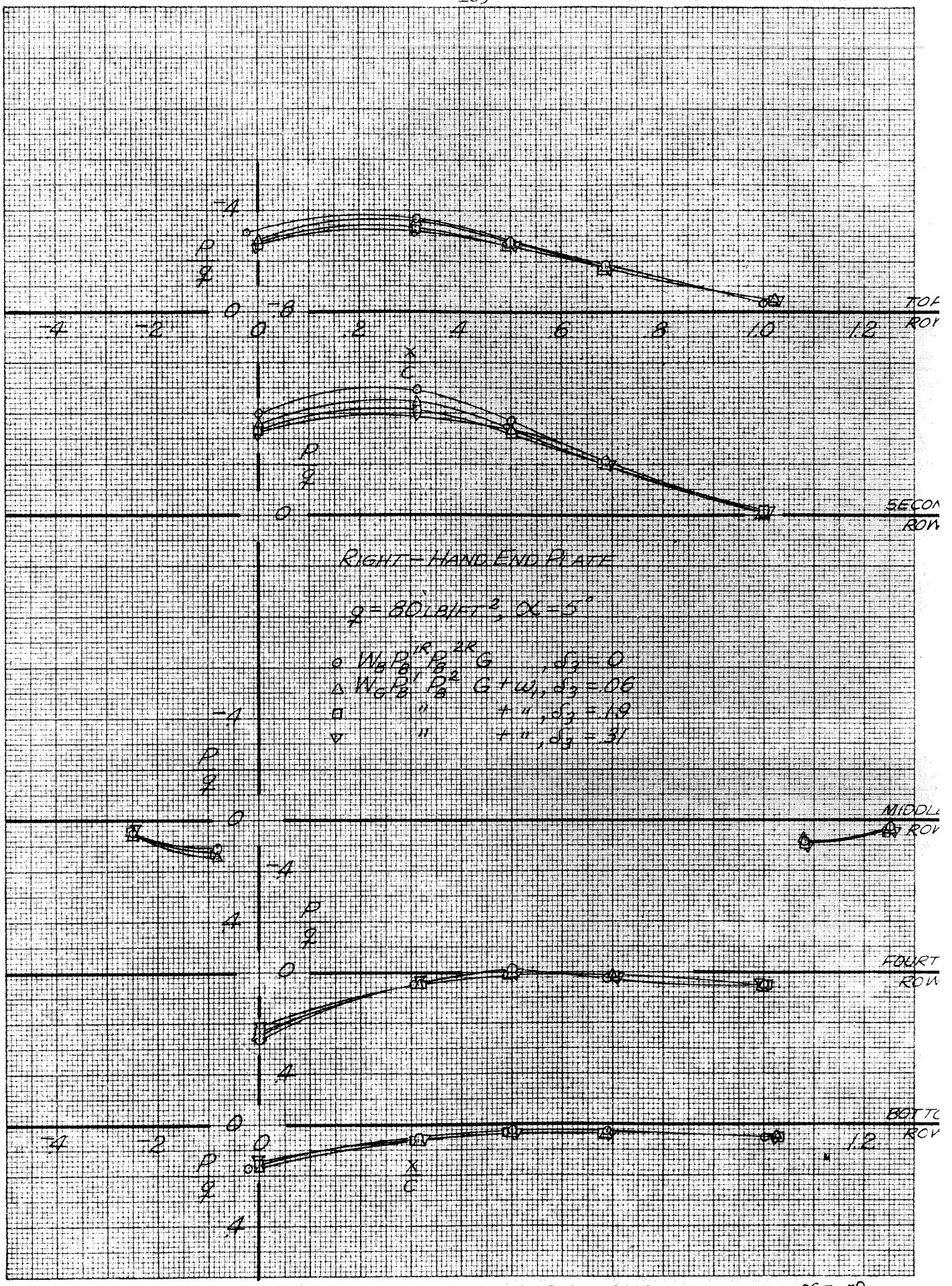

Fig. 71. Effects of wing-template gap on end plate static pressures; $\alpha = 5^{\circ}$, $q = 80$ lb/ft^2

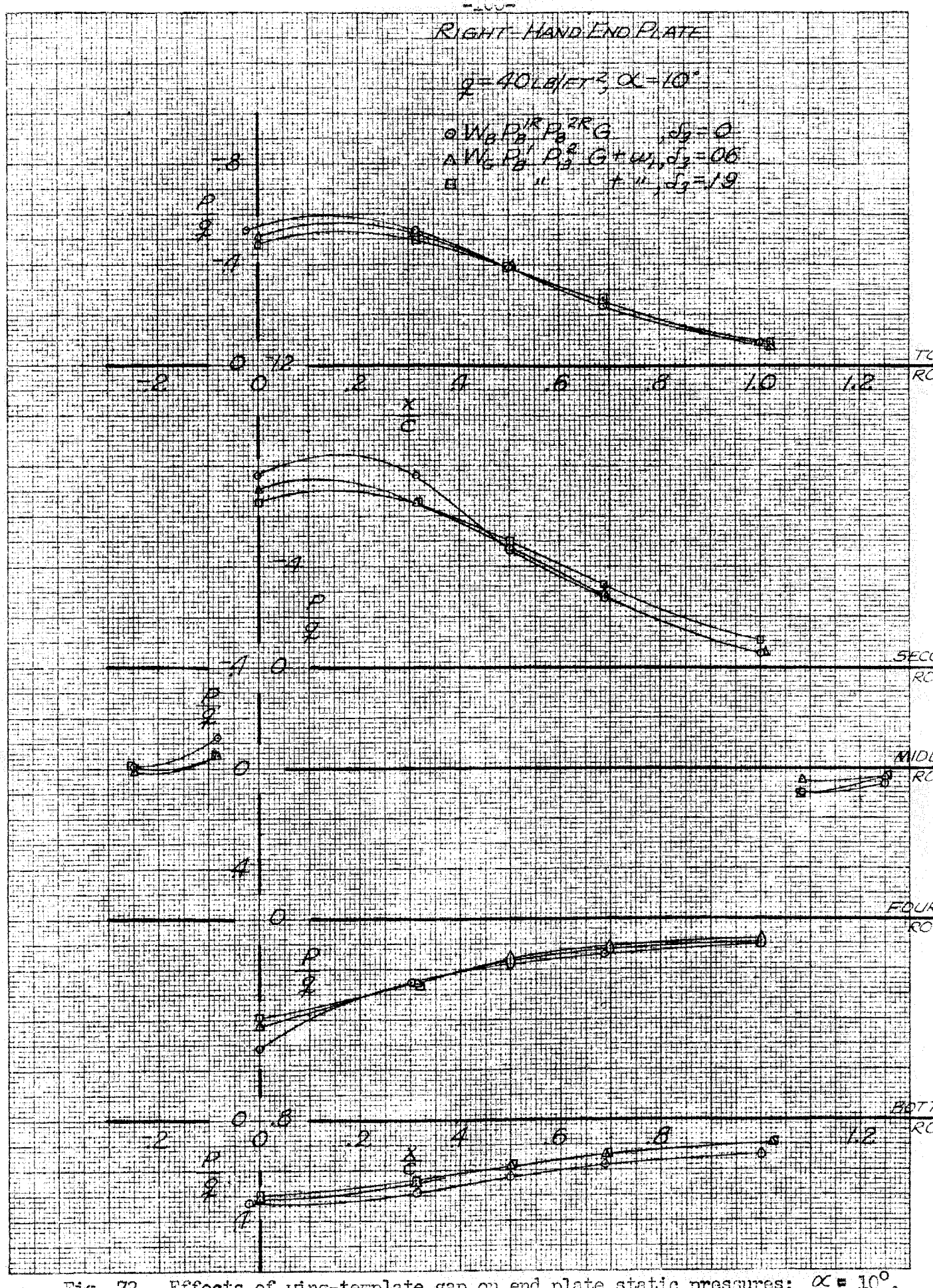

Fig. 72. Effects of wing-template gap on end plate static pressures; $\alpha = 10^{\circ}$, $q = 40$ lb/ft^2

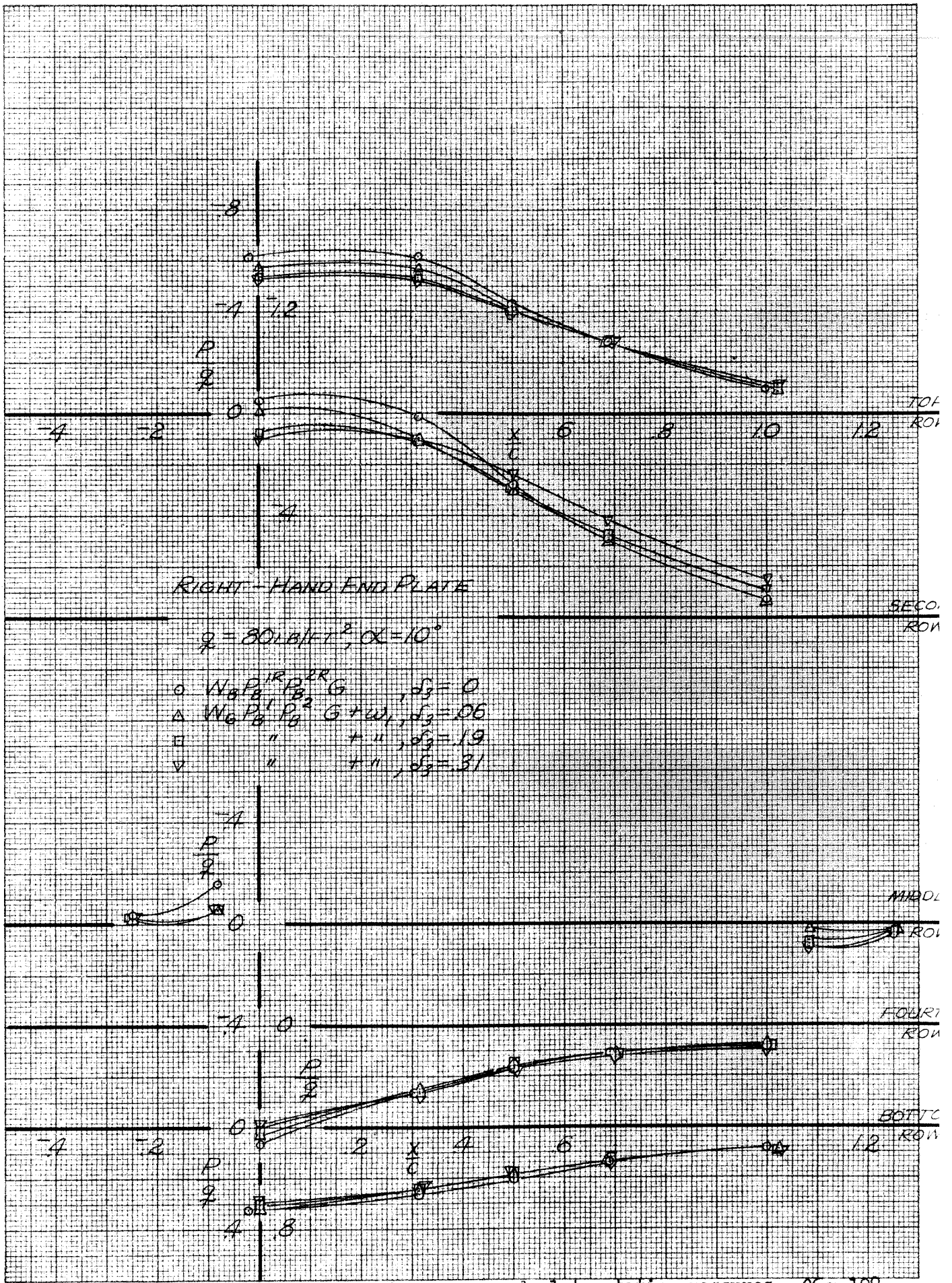

Fig. 73. Effects of wing-template gap on end plate static pressures; $\alpha = 10°$, $q = 80$ lb/ft^2

D. Forces on End Plates

The forces on the end plates are presented on Figs. 74 to 77 and in Table I. There was no variation in the forces on the end plates over the range of angles tested. The lift and pitching moment forces on the end plates were zero when the wing was not present in the tunnel.

The forces induced on the end plates by the wing were measured directly by mounting the wing in the tunnel in its normal position and supported by the grounded pitching mechanism. A very small lift which increased linearly with angle of attack was induced on the end plates by the wing. The wing also induced a stable pitching moment of very small magnitude on the end plates at the lower dynamic pressure while no change was induced at the higher dynamic pressure.

The drag induced on the end plate by the wing was very small at $q = 40$ lb/ft^2; the greatest change was of the order of four drag points. At $q = 80$ lb/ft^2, however, the effect is twice as large as this (amounts to 10% change in drag) and extends over a greater angle range.

Included in the tests was an investigation of the effects of end plate mis-alignment, of the effects of roughness strips on the walls ahead of the end plates and of the effects of sealing the gap around the end plates. The results of these tests are tabulated in the following tables.

TABLE I

RESULTS OBTAINED FOR VARIOUS END PLATE CONFIGURATIONS

Configuration	q = 40 lb/ft^2			q = 80 lb/ft^2		
	C_{D_u}	$C_{m_{c/4}}$	C_L	C_{D_u}	$C_{m_{c/4}}$	C_L
$P_B^1P_B^2G$	.0072	-.0008	.001	.0071	-.0007	-.001
" + Tr	.0075	-.0002	.000	.0072	-.0003	.000
$P_B^1P_B^2G_s$	.0118	-.0007	.000	.0129	-.0007	.000
" + Tr	.0119	-.0009	.000	.0127	-.0008	.000
$P_B^1P_B^2G^O$	.0054	-.0004	.000	.0051	-.0003	.000
$P_B^1P_B^2G^I$	.0090	-.0003	.000	---	---	---
$P_B^1P_B^2G^{I-1}$	.0088	-.0002	.001	.0087	-.0003	.000
$P_B^1P_B^2G^{I-2}$	.0078	-.0003	.000	.0074	-.0003	.000
$P_B^1P_B^2G^{I-3}$	.0080	-.0002	.000	.0078	-.0003	.000
$P_B^1P_B^2G^{I-4}$	.0078	-.0003	.000	.0075	-.0003	.000

TABLE IA

DRAG INCREMENTS DUE TO VARIOUS MODIFICATIONS

Modification	q=40 lb/ft^2	q=80 lb/ft^2
	δC_{D_u}	δC_{D_u}
Roughness strips ahead of both end plates with end plate gap open	.0003	.0001
Roughness strips ahead of both end plates with end plate gaps sealed	.0001	-.0002
Sealing end plate gap	.0046	.0056
Both end plates out of the tunnel 0.10 inch	-.0018	-.0020
" " " in to " " 0.05 "	.0013	No Data
" " " " " " 0.04 "	.0016	.0016
One " " " " " 0.05 " at the top	.0006	.0003
One end plate in to the tunnel 0.05 inch at the front	.0008	.0007
One end plate in to the tunnel 0.05 inch at the rear	.0006	.0004

It can be seen from these results that the alignment of the end plate is very critical if good drag results are to be obtained. It is also to be noted that although the roughness strips increased the boundary layer thickness by over one-half inch, the drag of the end plates remained unchanged. On the other hand, the mis-alignment of the end plate changed the boundary layer thickness and the boundary layer profile to a considerably smaller extend and yet there is an appreciable change in drag. This would indicate that for these changes the viscous forces exerted a negligible influence on the end plate as compared with the pressure forces.

The large increase in drag due to sealing the end plate gap is thought to be due to the change in flow around the end plate gap. With the gap open, there was a small flow of air out of the tunnel in the upstream portion of the end plate gap and a small flow of air into the downstream portion of the gap. When the gap was sealed, the air which formerly came out at the front of the end plate was restricted by the seal to flow around the space between the end plate and the tunnel wall and back out of this gap at the downstream end of the end plate. This change of flow, it is felt, increased the drag by increasing the viscous drag on the periphery of the end plate and possibly by increasing the pressure drag by increasing the pressure in the gap ahead of the plate and reducing it in the gap at the trailing edge; either or both.

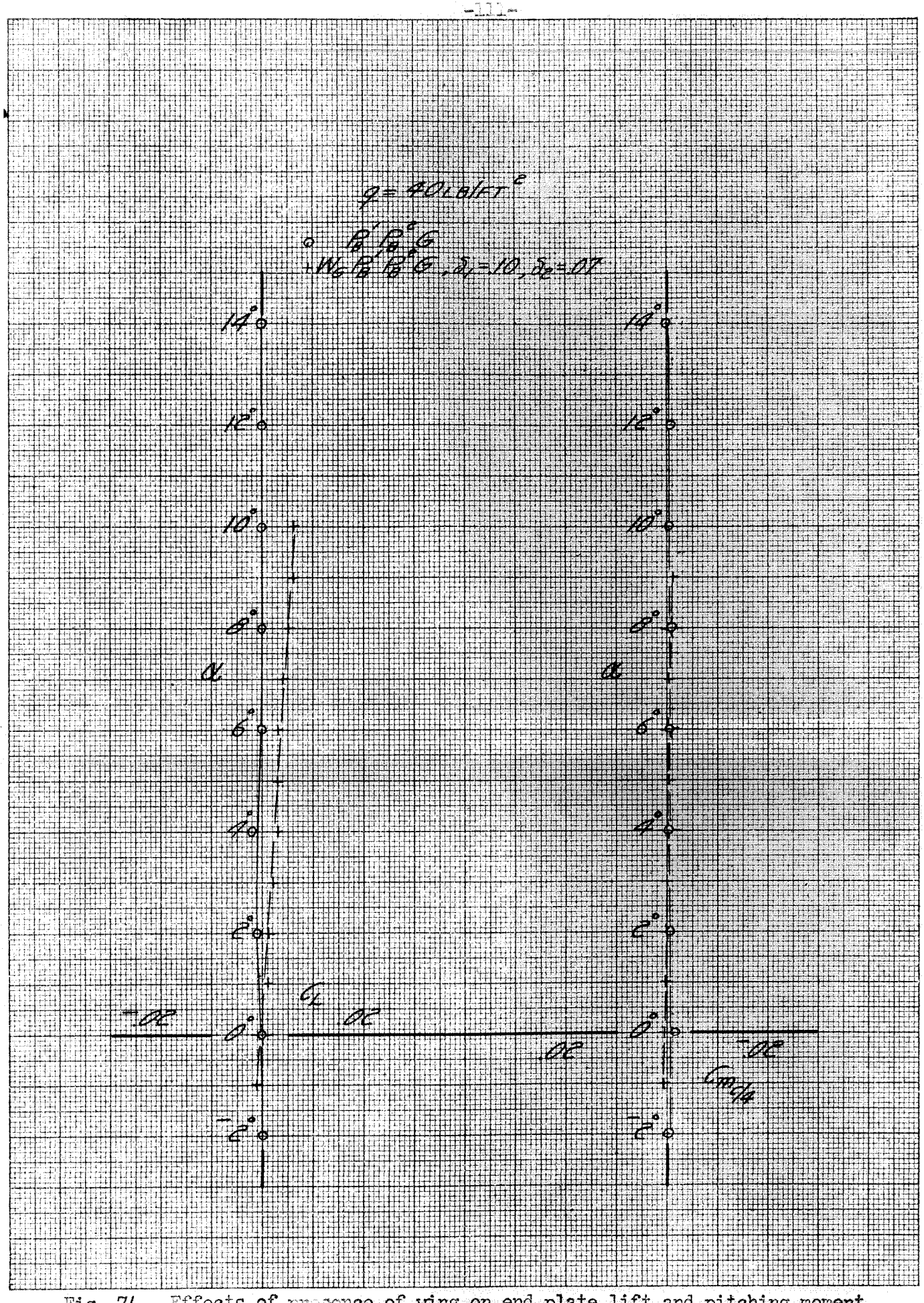

Fig. 74. Effects of presence of wing on end plate lift and pitching moment results, q = 40 lb/ft^2

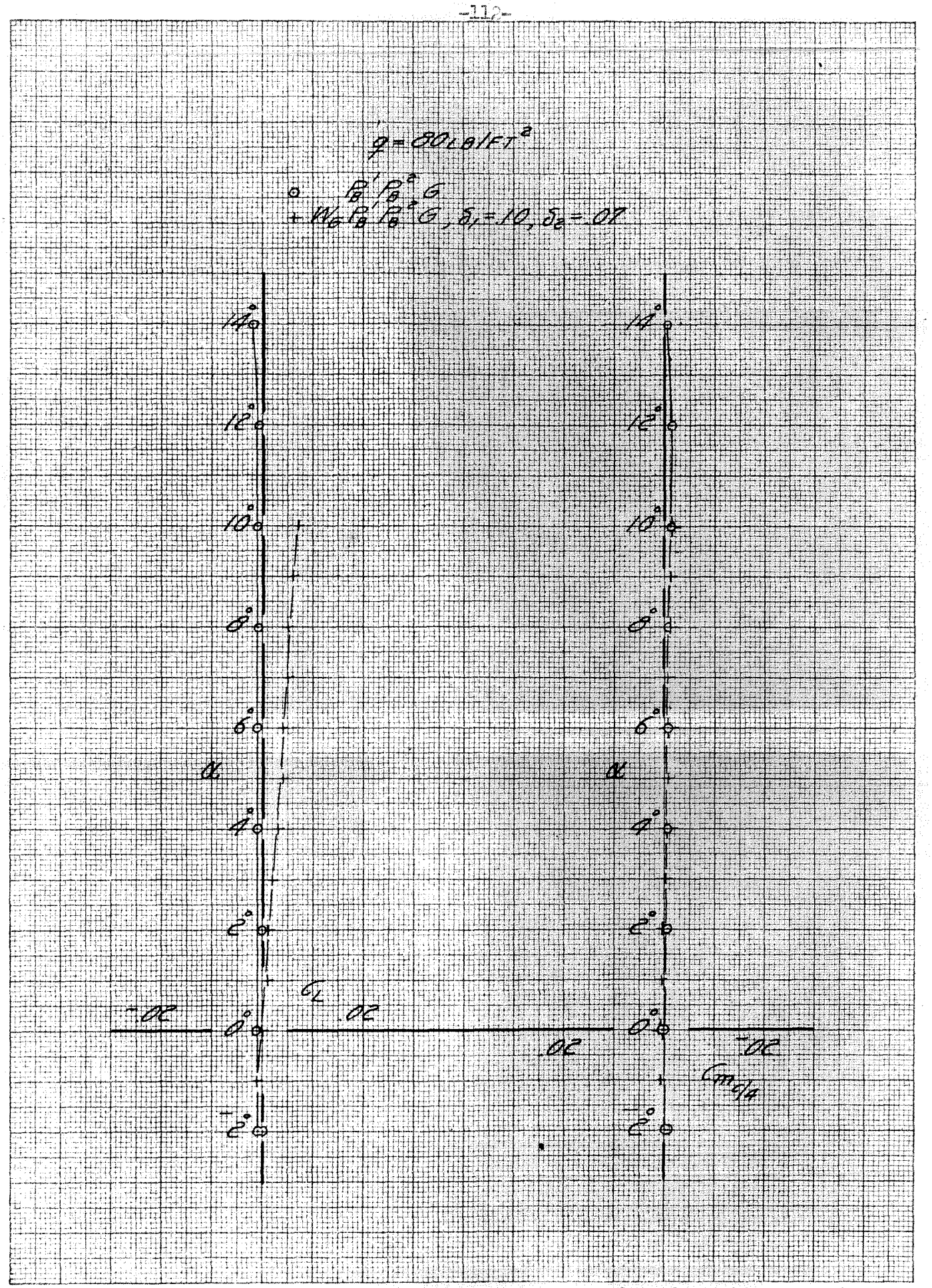

Fig. 75. Effects of presence of wing on end plate lift and pitching moment results, q = 80 lb/ft^2

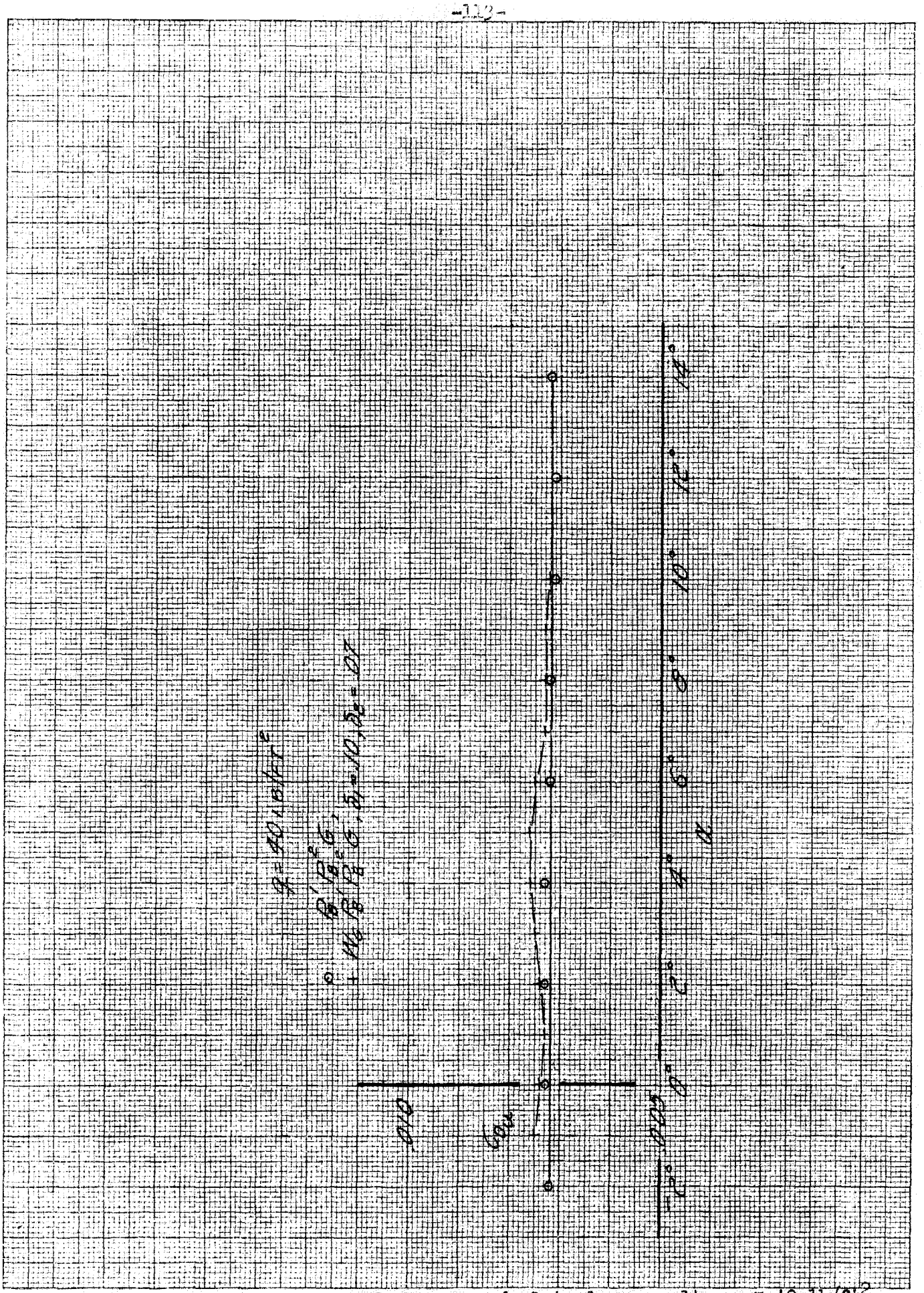

Fig. 76. Effects of presence of wing on end plate drag results, q = 40 lb/ft^2

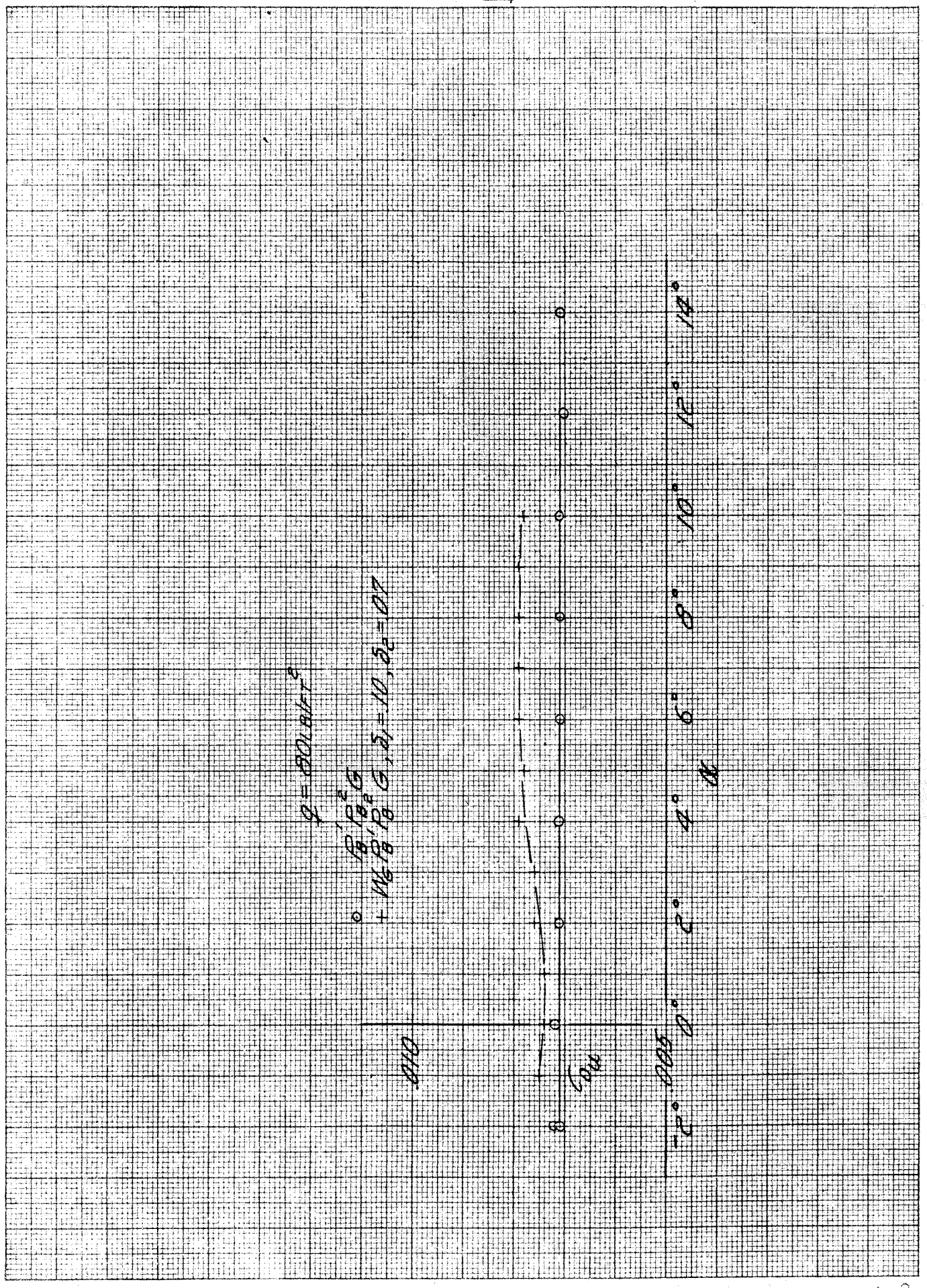

Fig. 77. Effects of presence of wing on end plate drag results, q = 80 lb/ft^2

VI SUMMARY OF RESULTS

The more important results of the test are summarized below.

1. Portion of the wing in the boundary layer carried within 3-7% of the lift carried by a like portion of the wing in the free stream. The lift developed on the portion of the wing in the boundary layer is due to the lift developed by the main portion of the wing carrying across through the boundary layer. The lift developed by the wing will carry across relatively large gaps to the portion of the wing in the boundary layer.

2. Gaps between wing and end plate cause a slight change in lift and pitching moment and an increase in drag. The change in drag increases rapidly with increasing lift. This increase in drag with increasing lift can be decreased by sealing the gap around the end plates.

3. End plate alignment is extremely critical if the end plate is metrical and good drag results are desired. Mis-alignment of only 0.05 inch of one end plate (41 inch diameter) can increase the drag by as much as eight points (based on wing panel area of six square feet).

4. Interference effects of end plate on wing are small if plate is smooth.

5. Interference effects of wing on end plates are small for lift and pitching moment but may be large for drag.

6. If gap seals are used on metrical portions of the test installation, care must be exercised to prevent the introduction of erroneous forces due to the seal.

7. Roughness strips on tunnel walls ahead of end plates which caused a large change in the boundary layer thickness and profile did not change the forces on the end plate.

VII. FUTURE TESTS

The results described in this report have described some of the factors which must be known to interpret results obtained from tests of reflection-plane models. Much remains to be done before these results may be accurately interpreted; the following list contains some of the more important investigations which should be made.

1. Test with wing protruding through end plate; vary gap between wing and end plate.

2. Check effect of angle of wing sweep.

3. Test bodies of revolution mounted at center of wing panel and as reflection-plane models.

4. Extend investigations to three-dimensional tests.

5. Extend results to higher Mach numbers.

REFERENCES

1) C. B. Millikan and A. L. Klein, Description and Calibration of 10-foot Wind Tunnel at California Institute of Technology, presented at the Berkeley meeting, Aeronautical Section of the A.S.M.E., June 1932.

2) Arthur L, Klein, Peter V. H. Serrell, and Clark B. Millikan, A New Two-Parameter Model Suspension System for the GALCIT 10-foot Wind Tunnel, Jour. Aero. Sci., Vol. 9 (No. 8), p. 302, June 1942

3) Cambridge University Aeronautics Laboratory, Measurement of Profile Drag by the Momentum Method, R. and M. No. 1688, British A.R.C., 1936.

4) Young, A. D. and J. N. Mass, The Behavior of a Pitot Tube in a Transverse Total-Pressure Gradient, R. and M. No. 1770, British A.R.C., 1937.

5) Robert A. Mendelsohn and Josephine F. Polhamus, Effect of the Tunnel-Wall Boundary Layer on Test Results of a Wing Protruding From a Tunnel Wall, NACA TN 1244, April 1947

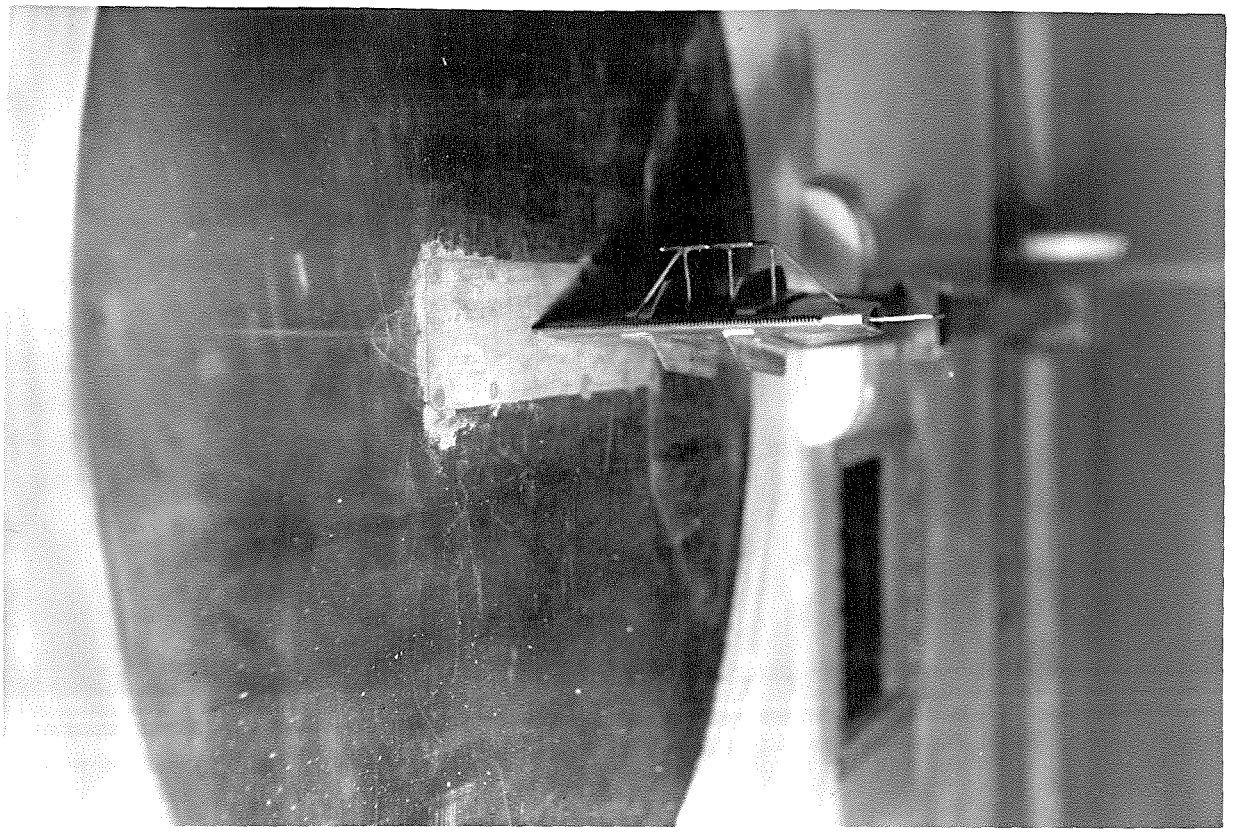

Photo 1. Front view showing wake rake mounted on end plate.

Photo 2. Front view showing roughness strip mounted ahead of end plate.

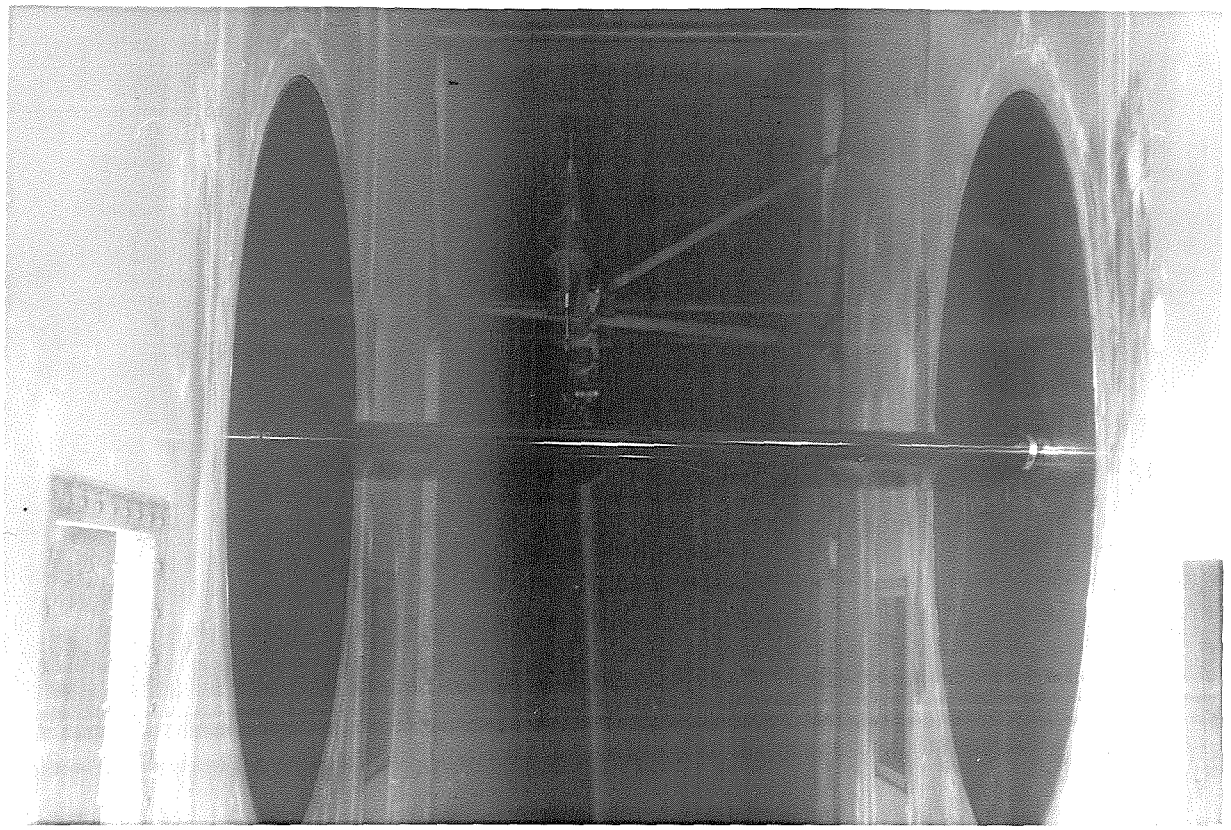

Photo 3. Front view showing wing and end plates (Drag wake rake can be seen in background).

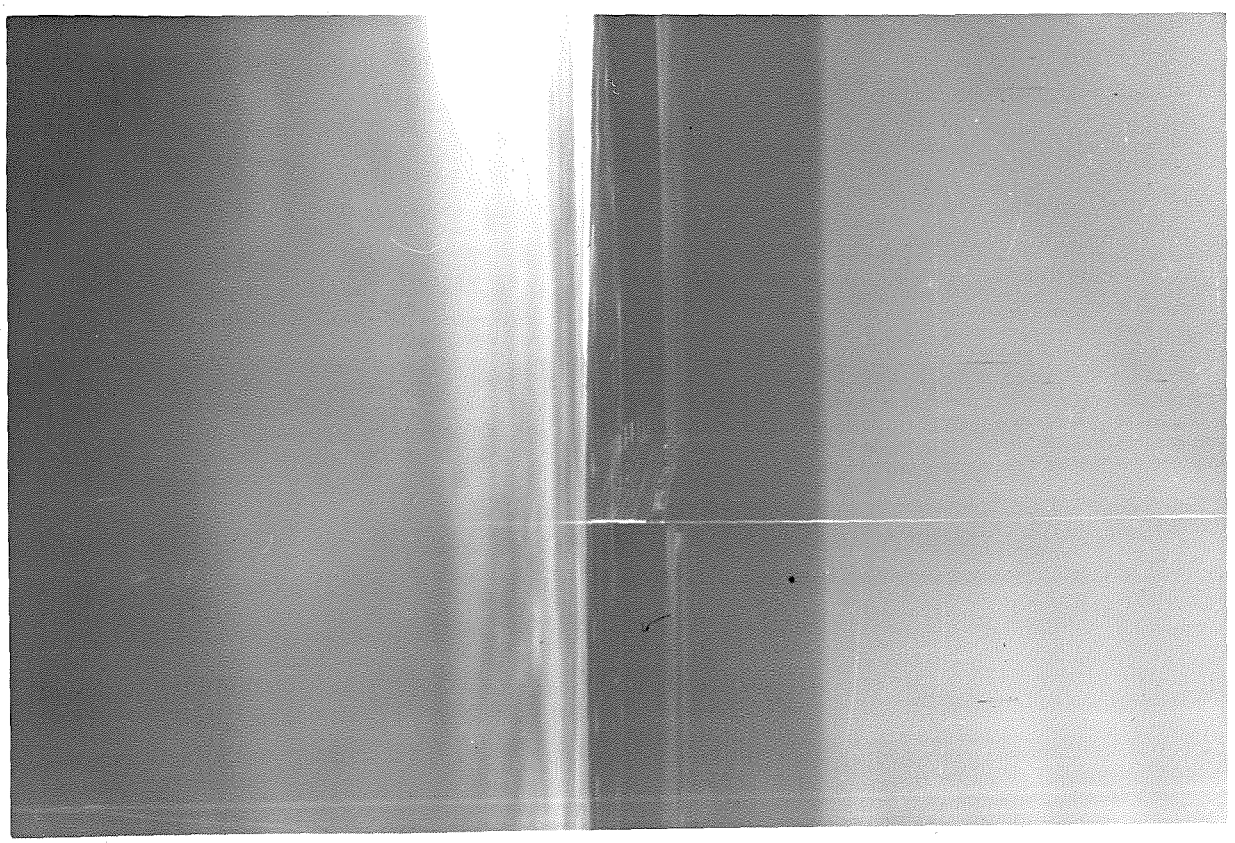

Photo 4. Rear view showing template W and gap δ_3.

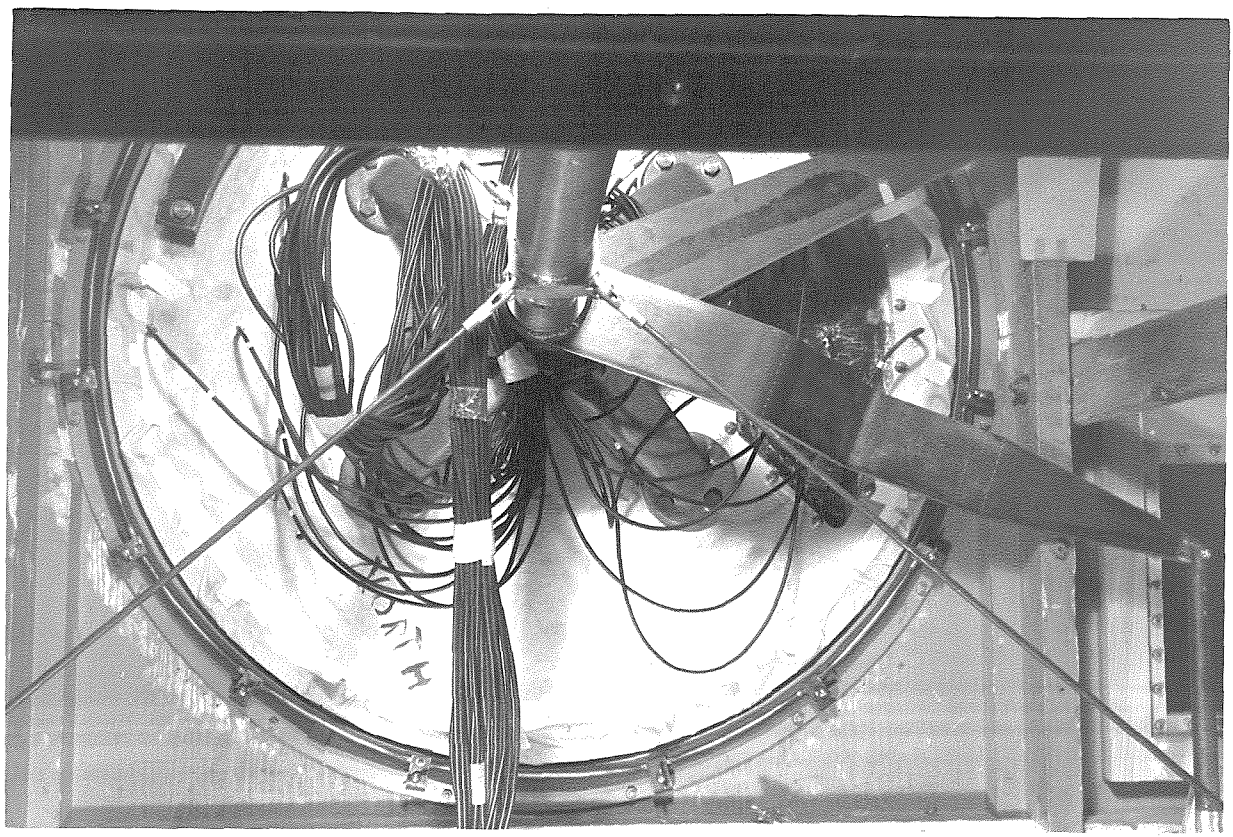

Photo 5. Lower side view showing auxiliary support for wing.

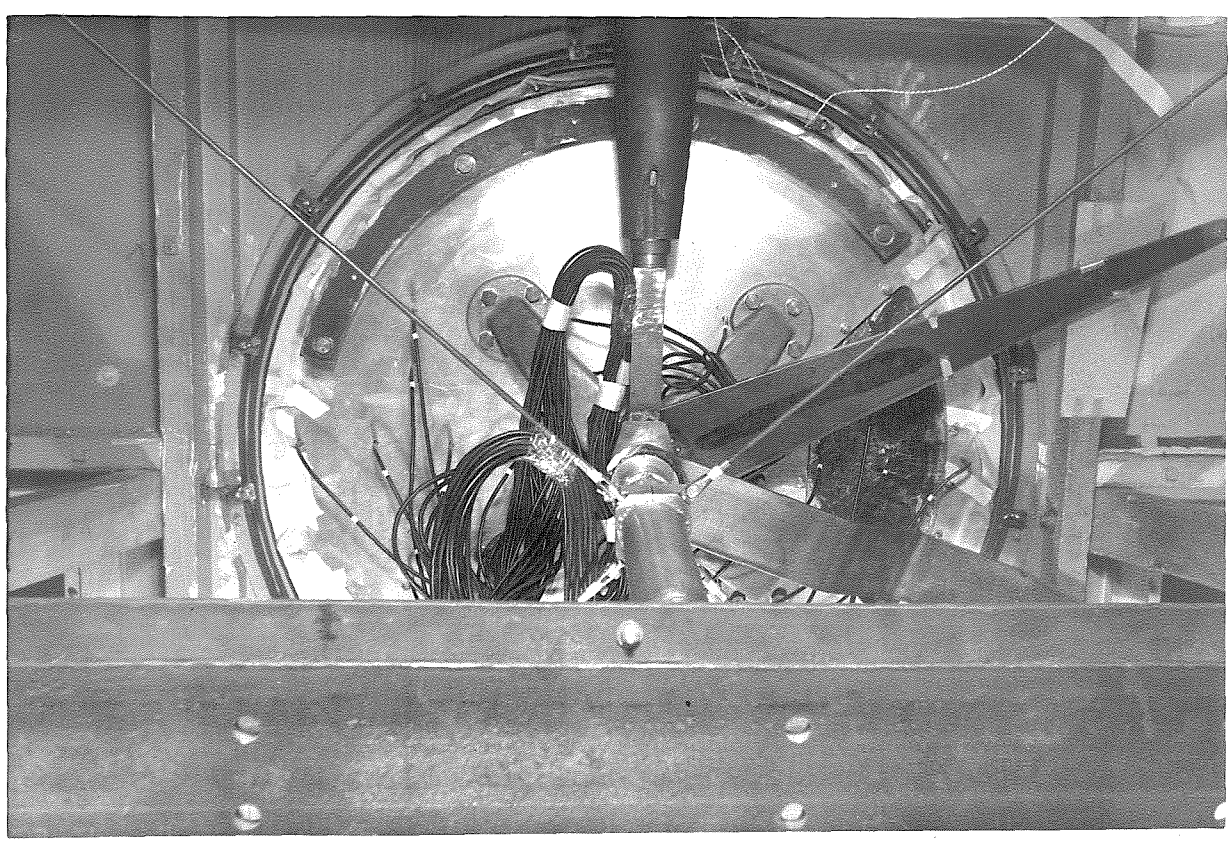

Photo 6. Upper side view showing auxiliary support for wing.

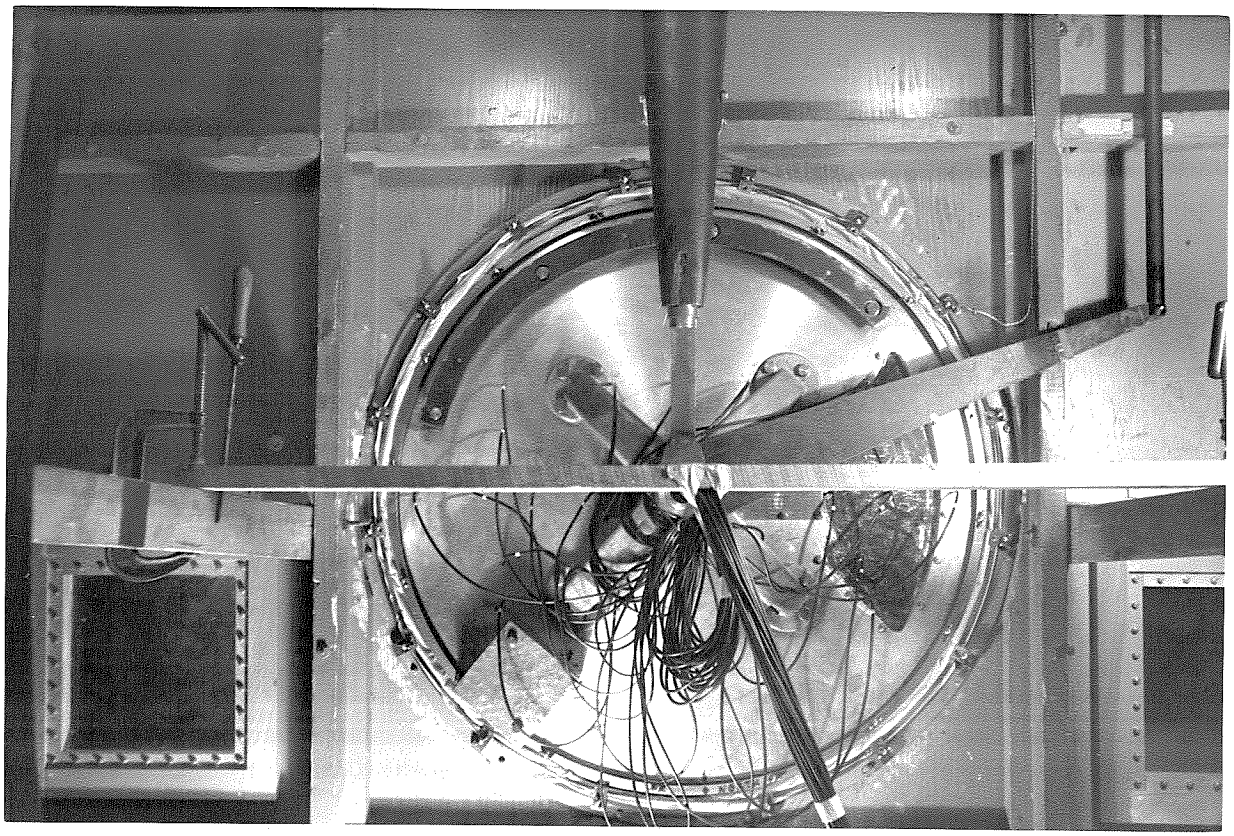

Photo 7. Side view showing normal wing and end plate support, pressure leads to end plate and end plate gap seal.